TAMPEREEN TEKNILLINEN YLIOPISTO
TAMPERE UNIVERSITY OF TECHNOLOGY

ATTE KEKONEN

BIOIMPEDANCE MEASUREMENT DEVICE FOR CHRONIC WOUND HEALING MONITORING

Master of Science Thesis

Examiners and topic approved by the
Faculty Council of the Faculty of Computing
and Electrical Engineering on May 5st 2010.

Examiner:
Professor Jari Hyttinen

ABSTRACT

TAMPERE UNIVERSITY OF TECHNOLOGY
Master's Degree Programme in Electrical Engineering
KEKONEN, ATTE: Bioimpedance Measurement Device for Chronic Wound Healing Monitoring.
Master of Science Thesis, 132 pages, 6 Appendix pages
May 2013
Major subject: Medical electronics
Examiner: Professor Jari Hyttinen
Supervisor: Ph.D. Pasi Kauppinen
Keywords: Bioimpedance, device, measurement, tetrapolar, extracellular fluid, chronic wound, triangular wave, voltage to current converter, amplifier

A chronic wound is loosely defined as a wound that fails to heal within a time period of a few months. Elderly bedridden people and people suffering from certain underlying medical conditions, such as vascular diseases and type 2 diabetes, are particularly prone to develop chronic wound. The group of people exposed is increasing in numbers. Treatment of a chronic ulceration is very costly and the monitoring of healing is often based on visual inspection by medical professionals. There exists a need for objective and non-intrusive method for assessment of chronic wound healing.

In this Master of Science Thesis a prototype of a bioimpedance device for monitoring of chronic wound healing was designed, constructed and tested. The device works from an indicator basis and measures the changes in the tissue impedance. The direction of the change correlates with the change in the volume and in the conductivity of the tissue, consequently in the swelling around the inflamed wound. Decrease in extracellular fluid can be detected as increasing low frequency impedance. The device measures impedance at 5kHz and 100kHz frequency by using triangular excitation. The emphasis of the design was on the simplicity of the device to provide a possibility for downscaling in the future. Ultimately the device would be integrated on a patch type platform together with a drug delivery system.

The test measurements with the bioimpedance device were fairly extensive. The measurements were performed with a purely resistive load and a 2R-1C circuit. For 5kHz excitation the results for both load circuits did show only a slight mean error with a fairly small standard deviation. For 100kHz excitation the results did show larger mean error with a small standard deviation. Small standard deviation points to a systematic error. However, the 100kHz results are somewhat controversial since the difference between mean error for the purely resistive load and for the 2R-1C is fairly large. Restricted in vivo measurements were also performed. The in-vivo measurements did show large error compared to the reference measurements. Due to the limited nature of the measurements solid conclusions from these measurements cannot be made. All in all, the test measurements indicate the potential of simplified design. The accuracy of the device can be increased remarkably with certain improvements made to the design.

TIIVISTELMÄ

TAMPEREEN TEKNILLINEN YLIOPISTO
Sähkötekniikan koulutusohjelma
KEKONEN, ATTE: Bioimpedanssimittaukseen perustuva laite kroonisten haavojen paranemisen seurantaan.
Diplomityö, 132 sivua, 6 liitesivua
Toukokuu 2013
Pääaine: Lääketieteellinen elektroniikka
Työn tarkastaja: Professori Jari Hyttinen
Työn ohjaaja: TkT Pasi Kauppinen
Avainsanat: Bioimpedanssi, laite, mittaus, solunulkoinen neste, krooninen haava, kolmioaalto, jännitevirtamuunnin, operaatiovahvistin

Avoin haava voidaan määritellä krooniseksi, jos se ei ole parantunut muutaman kuukauden sisällä aktiivisesta haavanhoidosta huolimatta. Haavojen kroonistumiselle ovat alttiita erityisesti potilaat, jotka kärsivät laskimovajaatoiminnasta tai diabeteksesta sekä ikääntyneet vuodepotilaat. Tämä riskiryhmä kasvaa jatkuvasti. Kroonisten haavojen hoito on kallista, ja niiden paranemisen seuranta pohjautuu hoitohenkilökunnan subjektiiviseen arvioon. Kroonisten haavojen seurantaan tarvitaan objektiivinen, kvantitatiivinen ja paranemista häiritsemätön menetelmä.

Tässä diplomityössä suunniteltiin, rakennettiin ja testattiin bioimpedanssimenetelmään pohjautuva mittalaite kroonisten haavojen paranemisen seurantaa varten. Laitteella seurataan haavakudoksen impedanssin muutosta, ja erityisesti muutoksen suuntaa. Haavakudoksen impedanssin muutoksen suunta riippuu muutoksesta haavakudoksen tilavuudessa ja kudoksen sähkönjohtavuudessa, toisin sanoen tulehdukseen liittyvästä turvotuksesta.

Solun ulkoisen nesteen määrän väheneminen nostaa mitattua impedanssia matalalla taajuudella. Laite mittaa impedanssia 5kHz ja 100kHz taajuuksilla käyttäen kolmioaaltoeksitaatiota. Suunnittelun lähtökohtana oli yksinkertainen toteutus, jotta laite olisi mahdollista miniaturisoida tulevaisuudessa. Tarkoitus on integroida impedanssilaite ja lääkkeenluovutusmekanismi laastarityyppiselle alustalle.

Laitteella suoritettiin varsin laajoja testimittauksia. Testimittauksia tehtiin sekä resistiivisellä kuormalla että käyttäen 2R-1C –testikytkentää. Kummankin testipiirin 5kHz tulokset osoittivat vain pientä virhettä tulosten keskiarvossa, ja keskihajonta oli hyvin pieni. 100kHz:n tulokset osoittivat suurempaa virhettä keskiarvossa, mutta keskihajonta oli pieni. Pieni keskihajonta viittaa systemaattiseen virheeseen. In-vivo mittauksia suoritettiin hyvin rajallisesti. In-vivo mittausten tulokset osoittivat paljon suurempaa virhettä kuin testimittaukset, mutta in-vivo mittausten vähyydestä johtuen pitäviä johtopäätöksiä ei näistä tuloksista voitu tehdä. Kaiken kaikkiaan testimittaukset kuitenkin osoittivat, että yksinkertaistetulla laitteella on mahdollista saavuttaa riittävät tarkkuus haavan paranemisen seuraamiseksi. Laitteen tarkkuutta voidaan olennaisesti lisätä tietyillä muutoksilla laitteen suunnittelussa sekä komponentti valinnoilla.

PREFACE

This Master of Science Thesis was conducted in the Department of Biomedical Engineering, Tampere University of Technology, Finland. This work was done for a TEKES funded project PEPSecond (Printed Enzymatic Power Source with Embedded Capacitor on Next Generation Devices).

I want to express my gratitude to the supervisors and examiners of my thesis, Professor Jari Hyttinen and Ph.D. Pasi Kauppinen. Thank you for providing your experience and guidance in problem situations. I also want to thank Ph.D. Timo Vuorela for discussions and valuable help with circuit design issues.

I want to thank my dear girlfriend Hanna for encouragement and final push for finalizing the thesis. I also want to thank my father Ahti, his wife Laila and my sister Annu for just being there

Tampere, 10th of May 2013

Atte Kekonen

TABLE OF CONTENTS

ABBREVIATIONS

AC	Alternating current
ADC	Analog to digital converter
BIA	Bioimpedance analysis
BIS	Bioimpedance spectroscopy
BJT	Bipolar junction transistor
CMRR	Common mode rejection ratio
CPU	Central processing unit
CRP	C-reactive protein
CTC	Clear timer on compare
CVI	Chronic venous insufficiency
DAC	Digital to analog converter
DC	Direct current
DDS	Direct digital synthesis
DMA	Digital memory access
DRC	Design rule checking
ECF	Extracellular fluid
ECM	Extracellular matrix
ECW	Extracellular water
EEPROM	Electronically erasable programmable read-only memory
EMI	Electromagnetic interference
GBW	Gain bandwidth
HF	High frequency
IA	Instrumentation amplifier
IC	Integrated circuit
ICF	Intra cellular fluid
ICW	Intracellular water
IES	Interelectrode space
ISR	Interrupt service routine
LF	Low frequency
LSB	Least significant bit
LSE	Living skin substitute
MF-BIA	Multifrequency bioimpedance analysis
MMP	Matrix metalloproteinases
MRSA	Methicillin-resistant Staphylococcus Aureus
MSB	Most significant bit
NCO	Numerically controlled oscillator
NSAID	Non-steroidal anti-inflammatory drug
OCR	Output compare register

PCB	Printed circuit board
PLL	Phase locked loop
POR	Power on reset
PWM	Pulse width modulation
RF	Radio frequency
RMS, rms	Root means square
SMD	Surface mounted device
SNR	Signal to noise ratio
SF-BIA	Single frequency bioimpedance analysis
SPI	Serial peripheral interface
SR	Slew rate
SPDT	Single pole double throw
SRAM	Static random access memory
TBF	Total body fluid
TBW	Total body water
TCNT	Timer counter register
TGF- β	Transforming growth factor β
TIMP	Tissue inhibitor of metalloproteinases
TWI	Two wire interface
UART	Universal asynchronous receiver transmitter
USART	Universal synchronous asynchronous receiver transmitter
USB	Universal serial bus

SYMBOLS

A	Area; Area of a plate of a parallel plate capacitor
A_1	The amplitude of a wave at the fundamental frequency
A_N	Amplitude at a given harmonic number
C	Capasitance
C_M	Cellular membrane capacitance
d	Separation between the plates of a parallel plate capacitor
$\boldsymbol{E_E}$	External electric field vector
E_{hc}	Half-cell potential
$\boldsymbol{E_I}$	Internal electric field vector
f_C	Center frequency, mid-frequency, characterictic frequency
G	Gain
h_{fe}	DC current gain
I	Current
I_B	BJT base current
I_{rms}	Root means square current
I_Z	Zener current
j	Imaginary number
J_V	Net fluid flux
K_f	Filtration coefficient
l	Length
N	Harmonic number; Number of bits
P_c	Capillary hydrostatic pressure
P_i	Interstitial hydrostatic pressure
R	Resistance
R_0	Resistance at zero frequency
R_∞	Resistance at infinite frequency
R_E	Extracellular resistance
R_I	Intracellular resistance
R_{WA}	Wiper resistance of a digital potentiometer
T	Periodic time
V	Voltage, volume
V_{BE}	BJT base-emitter voltage
V_{cc}	Supply voltage
V_{ref}	Reference voltage
V_{out}	Output voltage
V_Z	Zener voltage
$\boldsymbol{X}$	Reactance
$\boldsymbol{X_C}$	Capacitive reactance

$\boldsymbol{Z}$	Impedance
Z_{5kHz}	Impedance at 5kHz excitation frequency
Z_{100kHz}	Impedance at 100kHz excitation frequency
$\boldsymbol{Z_C}$	Purely capacitive impedance
Z_R	Purely resistive impedance, resistance
Δv	Change in the volume
ΔR	Change in the resistance
$\Delta \sigma$	Change in the conductivity
ε_o	Permittivity in vacuum, permittivity of free space, electric constant
ε_r	Relative permittivity of a material
π_c	Capillary oncotic pressure
π_i	Interstitial oncotic pressure
ρ	Resistivity
σ	Conductivity, reflection coefficient
τ	RC filter time constant
θ	Phase angle
ω	Angular frequency

1 Introduction

The intention of this Master of Science thesis was to evaluate a possibility to assess chronic wound healing by utilizing the bioimpedance method. For this purpose a prototype of a bioimpedance meter was developed. The device's primary function is to work as an indicator of the progression of the healing process. The later prototypes of the device are to be integrated on an active medical skin patch which is attached to a patient on the site of wound. Therefore, a small physical size of the device, a minimal complexity of the core design and a reliable functionality are essential. The device should be able to take measurements for an extended period of time, for this reason the power consumption of the device should be minimized.

This Master of Science thesis is divided into three main sections. Firstly, the medical basis of a chronic wound is investigated, the theoretical basis of bioimpedance is clarified and different ways to implement the critical functional blocks of the bioimpedance device are evaluated. Secondly, the design process of the bioimpedance device with the chosen approach is brought forward. The functional hardware and software blocks of the device are discussed in detail. Thirdly, the developed bioimpedance device is tested first by a functional blocks and then with a complete system in use. Very limited in-vivo measurements were also performed.

A chronic wound is not unambiguously defined, however often a wound that fails to heal within months is considered to be chronic (Shai & Maibach 2005, p. 1). Very often behind a chronic wound exists systemic factors which expose the subject for developing chronic ulceration. These systemic factors include certain medical conditions. People suffering from chronic venous or arterial insufficiency or type 2 diabetes are highly exposed to develop a chronic wound. Also, elderly bedridden patients are prone to chronic wounds. Additionally, antibiotic resistive strains of bacteria are gaining ground. The number of people suffering from these conditions is increasing alarmingly. (Hietanen et al. 2003, pp. 35-48; Nwomeh et al. 1998, pp. 341-345) Often the prognosis of a chronic wound is rather dim. Generally, it takes months or even years to chronic wound to heal properly. Getting the chronic wound in control takes significant efforts and intensive medical treatment. (Panuncialman & Falanga 2007, p. 621) Obviously the costs are extremely high. Monitoring of the healing process is usually based on visual assessment by the medical professionals or on laboratory tests of the wound bed composition. There exists a need for objective and simple method for assessing chronic wound healing without interfering the delicate healing process itself.

Bioimpedance refers to the ability of a biological tissue to oppose an alternating current. Bioimpedance in an exogenic measure; the tissue volume in concern has to be stimulated externally in order to determine the impedance. The measurement routine is indirect and goes as follows; a small AC current is fed into tissue, the voltage induced by the current is measured differentially and by using the extended Ohm's law the bioimpedance can be determined. The electrical properties of biological tissue are characterised by the duality of a volume conductor and a dielectric. Biological tissue is strongly frequency dependent and contains capacitive elements in addition to resistive. (Grimnes & Martinsen 2008, p. 1) The electrical behavior of biological tissue is largely governed by three variables. The amount of extracellular fluid (ECF, R_E), the amount of intracellular fluid (ICF, R_I) and the membrane capacitance of cells (C_M). Often used electrical tissue equivalent is a circuit of R_E in parallel with C_M and R_I. Low frequency current is effectively blocked by the capacitive membranes of cells and flows through the purely resistive path of R_E. As the frequency increases, the current gradually starts to penetrate the capacitive cell membrane and the amount of current passing through ICF increases. Finally, at very high frequencies the effect of the capacitive reactance diminishes and the impedance can be considered to be formed purely by a parallel combination of resistive R_E and R_I. (Holder 2004, pp. 416-418)

The fundamental basis of the measurement concept lies on the pathology of a typical chronic wound. A chronic wound is trapped in an ongoing inflammation phase of a wound healing process. (Shai & Maibach 2005, p. 13; Nwomeh et al. 1998, p. 341) During the inflammation plasma starts leaking into the extracellular compartment from the intravascular space as a result of vasodilatation of precapillary arterioles. Swelling on the site of the wound can be observed. The accumulation of the fluid into the extracellular space can be detected as a decrease in extracellular resistance (R_E). (Jensen et al. 2007)

The bioimpedance device proposed in this Master of Science thesis obtains information about fluid changes in the extracellular space. The actual interest is not in the absolute impedance values but rather focused on the change and in particular the direction of the change. The device measures the bioimpedance of the wound tissue on command. A low frequency 5kHz excitation current is fed into tissue via electrodes and the induced voltage is measured by the device. Similarly, the voltage is measured with electrodes for the high frequency 100kHz excitation. The impedance (Z_{5kHz}, Z_{100kHz}) for each frequency can be determined from this data. The low frequency impedance correlates mainly with the amount of ECF and the high frequency impedance with both ECF and ICF. In addition to this, the impedance especially at 100kHz incorporates capacitive reactance. The ECF information containing LF impedance is accompanied with HF impedance for calculating the ratio of $\frac{Z_{5kHz}}{Z_{100kHz}}$. By determining the ratio, the possibility of false indications can be reduced. (Bourne 1996, p. 408) The device does not measure the phase shift, only the impedance modulus and therefore the reactance part of the HF impedance data cannot be distinguished. Consequently, the effect of ICF

cannot be separated from ECF. However, with certain premises applied it is possible to conclude that the change in the ratio of $\frac{Z_{5kHz}}{Z_{100kHz}}$ reflects the change in the ECF.

As an excitation waveform, the bioimpedance device applies triangular wave derived from the microcontroller timer output by low pass filtering the square wave. A voltage to current converter is utilized to generate the current of 115μA_{rms}. The voltage induced by the excitation current is measured differentially with an instrumentation amplifier. The voltage is then amplified and half-wave rectified. Finally, a low pass filter is applied to stabilise the voltage into a moving average. This voltage is then analog to digital converted and stored into the EEPROM memory of the microcontroller. The data can be uploaded into a PC terminal program via USB. In the terminal program's user interface the raw data is presented in mV. The rms voltage over the tissue volume can be calculated from this raw data. With the known rms current, the impedance modulus is possible to be determined.

The test measurements included tests for the current feeding circuit to obtain information about the stability of the current in changing load situation. In addition, the performance of the standalone voltage measurement circuit was evaluated by feeding a test circuit with a function generator. The system tests were performed by utilizing a purely resistive test circuit and a 2R-1C circuit. Finally, constricted in vivo measurements with a test subject were performed and the results were compared with the reference measurements.

2 Medical background

Wound healing is a complex process with multiple overlapping stages. Considering this Master of Science thesis particularly interesting are the changes in the fluids associated with the wound and its healing process. The surroundings of the wound gathers fluid and the vascular activity in the area changes. The increased amount of highly conductive fluid changes the electrical properties of the tissue and the changes can be detected by using the bioimpedance method.

The healing process of a chronic would is interesting since its careful treatment and monitoring is crucial. Chronically inflamed wound can be very difficult to treat and might take months or even years to heal properly. It is obvious that expenses accumulate. The number of people in Finland suffering from a chronic wound is estimated to be around 34 000. The cost of the treatment of a patient with a chronic ulcer is estimated to average around 5000-7000 euros a year and the total costs related to chronic wounds in Finland are 190-270 million euros per year. (Seppänen & Hjerppe 2008, p. 6) Therefore improving the existing and developing new diagnostic, treatment and monitoring methods is essential.

Clinically, wounds can be categorized in acute and chronic wounds based on the time that it takes to heal (Nwomeh et al. 1998, p. 341). A Chronic wound (A chronic cutaneous ulcer) refers to an injury that fails to heal within a reasonable time. If acute wound refuses to show signs of healing within a month, a significant risk of wound becoming chronic exists. The classification for the chronic wound has not been unambiguously defined, but if the wound fails to heal within 3-4 months it is generally considered to be chronic (Shai & Maibach 2005, p. 1). Also wounds resulting from cancer, cancer treatment or erysipelas infection can be categorized as chronic since healing of these wounds is known to be problematic and long term. (Hietanen et al. 2003, p. 22) Ulcer refers to skin area from which the whole epidermis and at least the upper part of the dermis have been lost. Ulceration may also reach into the subcutaneous fat and the bone tissue. (Shai & Maibach 2005, p. 1) The cross section of the skin and the anatomical structures are shown in the Figure 2.1.

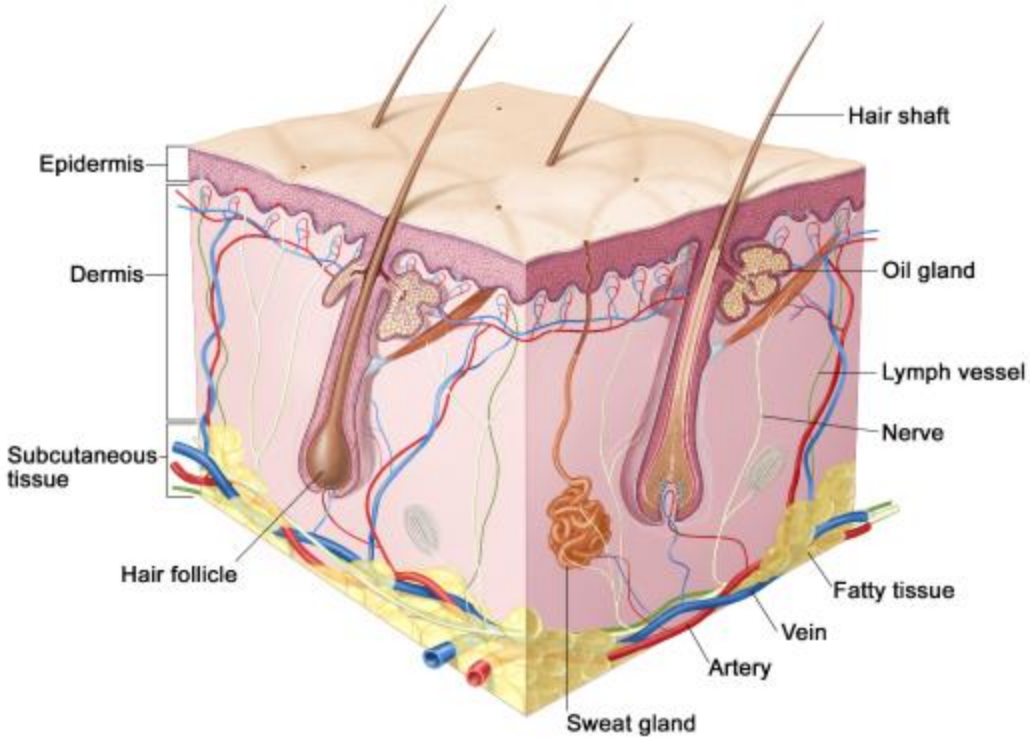

Figure 2.1 *The cross section of the skin and the anatomical structures (Memorial Hospital of South Bend 2011).*

Although the wound healing is an extremely complicated chain of events with various interconnecting processes, the healing of an acute wound is rather well known unlike the healing of a chronic wound (Hietanen et al. 2003, p. 33). The acute wound healing process can be divided into three phases but despite of the division, the phases are overlapping (Figure 2.2). However, for practical reasons they are presented in a linear order (Myers et al. 2007, p. 607; Monaco & Lawrence 2003, p. 1). The normal response to a tissue injury is highly predictable and proceeds till the restoration of anatomic and functional integrity is obtained, in contrast the chronic wound is trapped into an ongoing inflammation phase (Shai & Maibach 2005, p. 13; Nwomeh et al. 1998, p. 341).

Chronic wounds are often associated with systemic factors. The systemic factors include certain underlying medical conditions in which the blood circulation is somehow disrupted and the inflammatory response is deteriorated (Hietanen et al. 2003, p. 35, 41). Diabetes, chronic venous or arterial insufficiency and pressure necrosis are responsible for approximately 70% of all chronic wounds (Nwomeh et al. 1998, p. 341). It is necessary have these medical conditions under control to obtain a complete and permanent therapy outcome. In many cases the chronic wounds appear into the lower extremities or in case of pressure wounds to site of bony prominences. Reduced sensation of pain is a major contributor particularly for diabetic chronic wounds. (Hietanen et al. 2003, p. 35; Nwomeh et al. 1998, pp. 343-345) Infection is the most

common complication in a healing wound. Infection extends the inflammation phase in the wound, causes tissue destruction and delays the collagen synthesis. Inflammation related swelling in the wound area disturbs the adequate blood circulation, thus affecting the oxygen and nutrient delivery into the tissue. Patient's age, lifestyle, general health condition, drugs and nutrition have also a significant effect on the wound healing. (Hietanen et al. 2003, pp. 38-48) In addition to things mentioned above many other factors affect the healing of a chronic wound, both local and systemic.

2.1 Normal wound healing

Normal wound healing is divided into three phases. Often wound healing phases are overlapping.

2.1.1 Inflammation phase

The inflammation sequence starts immediately after an injury. Vascular injury is instantly followed by hemostasis. The main contributors to hemostasis include vasoconstriction, platelet aggregation and fibrin deposition resulting from coagulation cascade. The end product of hemostasis is a fibrin clot, which prevents blood leaking from the injured vessels. Any process that removes fibrin from the site of the injury will disrupt the formation of extracellular matrix and may delay the healing of the wound. Hemostasis has to be accomplished before the healing process may continue. The formation of fibrin clot launches the inflammatory response. (Shai & Maibach 2005, pp. 8-9; Monaco & Lawrence 2003, pp. 1-2; Myers et al. 2007, p. 608)

The classic signs of an inflammation are redness, edema, heat and pain (Monaco & Lawrence 2003, p. 2). Tissue level characteristics are increased vascular permeability and migration of white blood cells (leukocytes) into the extracellular space. One of the prime functions of the inflammation is to bring inflammatory cells (neutrophils, macrophages, monocytes, eosinophils, basophils) to the injured site, which then destroy the bacteria and debride the necrotic tissue, so that the repair processes may continue. (Monaco & Lawrence 2003, p. 2; Shai & Maibach 2005, p. 9)

Heat and redness of the skin develop soon after the injury resulting from vasodilatation. Vasodilatation follows the vasoconstriction, which lasts around 15 minutes. Vasodilatation occurs as a result of endothelial cells of capillaries creating gaps between each other in the area of injury, this leads to plasma leaking into the extracellular compartment from the intravascular space. Accumulation of the fluid leads to an edema and further contributes to the sensation of pain. Vasodilatation lasts about an hour. (Monaco & Lawrence 2003, p. 3; Shai & Maibach 2005, p. 9)

A complex chain of events results in an influx of white blood cells through the pores in the capillaries in the area of injury (Shai & Maibach 2005, p. 9). The migrating monocytes transform into macrophages as they entry into the extracellular space. After activation, neutrophils and macrophages start the cellular wound debriding by

phagocytosing bacteria and foreign material. In addition to phagocytosis, macrophages are the primary source of cytokines, for example various growth factors, which mediate the later phases of the healing process like angiogenesis, fibroblast migration and proliferation. (Monaco & Lawrence 2003, pp. 3-4) Macrophages also release nitric oxide, which may have a significant role in a normal wound healing process; much research has been done to determine their effects in detail (Shai & Maibach 2005, p. 9). Other inflammatory cell types present in inflammation phase include eosinophils and basophils (Monaco & Lawrence 2003, p. 5).

The presence of leukocytes in the area of the injury declines gradually in few days (Shai & Maibach 2005, p. 9). The neutrophils are the first inflammatory cells to undergo apoptosis and are then phagocytosed by macrophages. Macrophages and lymphocytes are present in the wound about a week (Monaco & Lawrence 2003, p. 5). In the normal wound healing process the inflammation phase lasts usually 4-6 days.

2.1.2 Proliferation phase

Proliferation phase, also known as tissue formation or regeneration phase, begins about 4-5 day from the injury and lasts about a week thereafter. The most important processes during the proliferative phase are angiogenesis and granulation tissue formation, re-epithelialization and formation of the extracellular matrix. (Shai & Maibach 2005, p. 9) The granulation tissue is a newly formed highly vascular loose connective tissue (Työterveyskirjasto 2011).

The cellular environment in the vicinity of the site of injury changes drastically during the first week of healing. As the initial fibrin-fibronectin is characterized by large quantities of inflammatory cells, the further phases of healing is predominantly dominated by fibroblasts and endothelial cells. Release of cytokines play a big role in this phase since it contributes to fibroplasia, re-epithelialization and angiogenesis. Additional fibroblasts are needed in the site of injury because the native cells are lost or damaged. Fibroblast accumulate in the site of injury as they migrate from the nearby tissues or through proliferation of cells, also some undifferentiated cells may transform in fibroblasts under the influence of cytokines. (Monaco & Lawrence 2003, p. 5) The increase in fibroblasts results in the formation of the extracellular matrix of the granulation tissue (Shai & Maibach 2005, p. 10). The fibroblast migration is stimulated by fibronectin and a various growth factors which comprise a large number of different wound healing related cytokines. One very important growth factor worth mentioning influencing a variety of processes in the wound healing is a transforming growth factor β (TGF-β). It has a particularly important role in the formation of the granulation tissue. (Monaco & Lawrence 2003, pp. 5-6; Shai & Maibach 2005, p. 10) The angiogenic process activates two days after the injury. The primary motive for this is a decreased oxygen tension in the injured tissue; this is because of the damaged vascular capillaries and the increased oxygen demand originating from the cells in the site of injury. The proliferating cells have up to five times higher oxygen consumption than the cells in a

resting phase. In angiogenesis endothelial sprouts derive from undamaged capillaries to wound periphery, the sprouts grow through the cell migration and proliferation, finally they interconnect with the sprouts originating from the different capillaries and form a new capillary. When the area of the injury becomes re-vascularized the amount of certain angiogenesis contributing cytokines starts to decrease. (Monaco & Lawrence 2003, p. 6)

Reconstruction of the injured epithelium starts almost immediately after the injury. The re-epithelialization is achieved in 24 to 48 hours after the injury. If the wound site is larger, obviously the generation of a neoepithelium takes a longer time. (Monaco & Lawrence 2003, p. 6) The overall purpose is to complete the healing of ulcer by covering it with a layer of epithelium (Shai & Maibach 2005, p. 11). First the basal cells start to migrate over the unfold wound surface forming a monolayer. Then the basal cells begin to proliferate providing more cell to the healing monolayer. At the same time the epithelial cells start to migrate from the edges of the wound, when the epithelial cells overlap with other epithelial cells from different directions the migration ceases. As the epithelial cells migrate they regenerate a new epidermal basement membrane over the damaged one. The further proliferation of epithelium cells create a multilaminated neo-epidermis followed by the influx of keratinocytes and fibroblasts. (Shai & Maibach 2005, p. 11; Myers et al. 2007, p. 608; Monaco & Lawrence 2003, pp. 6-7) The neo-epidermis resembles the native epidermis but it is a bit thinner, basement membrane is flatter and it lacks the rete pegs which normally penetrate to the underlying dermis (Shai & Maibach 2005, p. 11; Monaco & Lawrence 2003, pp. 6-7).

The synthesis and deposition of proteins and wound contraction start to predominate 4 to 5 days after the injury. The quality and quantity of matrix deposited during this phase has a major role in the strength of the scar. More than 50% of scar tissue is formed of collagen, thus its production is very important to proper healing of the wound. Fibroblasts synthesize collagen and other proteins like proteoglycans during the repair process. Collagen synthesis is also affected by different growth factors and characteristics of the patient and the wound. As the synthesis of proteins continues, the original wound matrix made of fibrin and fibronectin will be replaced by collagen and other proteins as the main constituent of the matrix. The collagen synthesis lasts 2 to 4 weeks and then begins to slow down. Elastin provides elasticity to normal skin, but it is absent in scar tissue, for this reason the scar tissue has increased stiffness and decreased elasticity compared to the normal skin. (Monaco & Lawrence 2003, pp. 7-8)

Wound contraction is an important part of wound healing process. It does not involve formation of new tissues; instead it is based on the movement of healthy tissues from the outskirts of the site of the injury. (Shai & Maibach 2005, pp. 11-12) Wound contraction begins four to five days after the injury and the process lasts about two weeks. The wounds, which are still open after two weeks time, this process could take a much longer time. The contraction of the wound is much dependent on the patient's general and nutritional state, the shape of the wound and the location of the injury, but the average rate is approximately 0.6 to 0.7mm per day. (Shai & Maibach 2005, p. 12;

Monaco & Lawrence 2003, p. 8) Modified fibroblasts called myofibroblast are responsible of the contraction effect. They resemble smooth muscle cells and they can induce contractile forces towards the center of the wound. After 2 to 3 weeks myofibroblasts disappear from the site of the wound presumably via apoptosis. (Shai & Maibach 2005, p. 12; Monaco & Lawrence 2003, p. 8)

2.1.3 Tissue remodeling phase

Tissue remodeling phase may take up to two years. It is characterized by the synthesis of a new type of collagen and disintegration of the old. During the first two weeks, type III collagen is replaced by more stable and thicker type I collagen. The new collagen fibers are arranged in parallel to skin stresses, also cross-linking within and between the molecules increases. The collagen matrix becomes less cellular as the cells involved in the healing process undergo apoptosis, also proteoglycans diminish and water content decreases. Because of these processes, the strength of the tissue gradually increases. (Shai & Maibach 2005, p. 12; Monaco & Lawrence 2003, pp. 8-9) After two weeks from injury the wound site has about 5% of its original strength and after one month about 40%. The new tissue will never regain more than 80% of its original strength. (Shai & Maibach 2005, p. 12)

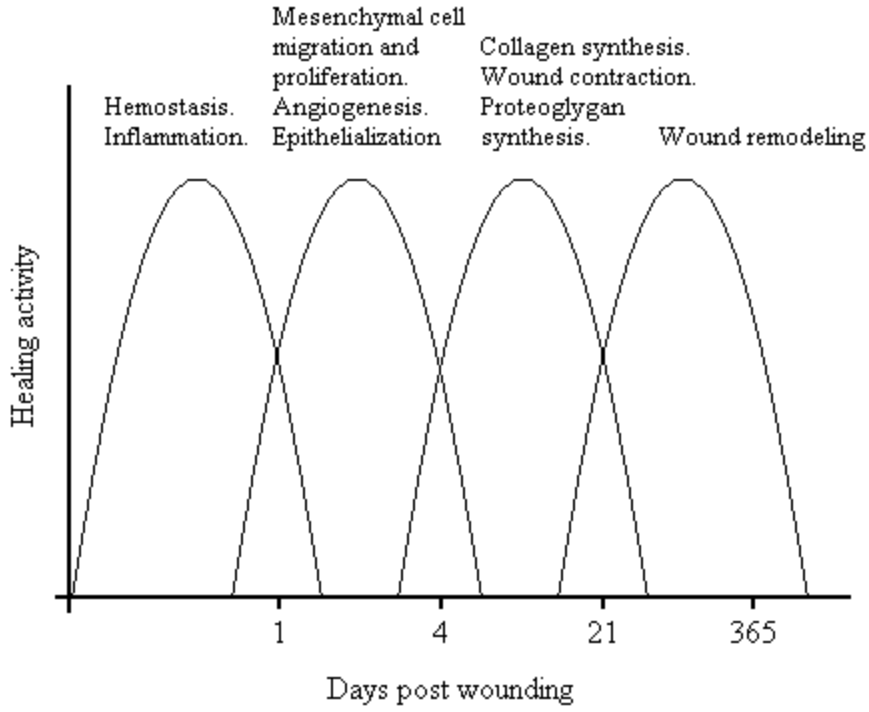

Figure 2.2 *The phases of wound healing process (Modified from Lawrence 1998, p. 323).*

2.2 Impaired wound healing: Chronic wound

Wound healing is a complex process, in which many interconnected processes form a network of events. Impairment of one or more of these processes may lead to a non-healing wound. (Ramasastry 1998, pp. 368-369) As mentioned before, a chronic wound can be considered to be trapped to an ongoing inflammation phase. This is a situation where the normal wound healing mechanisms are overwhelmed and the wound does not heal as supposed. The appearance of the wound area tends to be fibrotic, it may contain necrotic debris and exudates, also infection might be evident and the wound area is often swollen. (Shai & Maibach 2005, p. 13; Panuncialman & Falanga 2007, p. 622)

Studies have shown certain abnormalities in the chronic wound bed compared to bed of a normally healing wound. Chronic wounds are shown to have increased activity of matrix metalloproteinases, reduced response to growth factors and cellular senescence. (Shai & Maibach 2005, p. 13) The sequence of events leading to a chronic wound versus normal wound healing is represented in the Figure 2.3.

Degradation of the old extracellular matrix (ECM) and formation of a new ECM is an essential step in a proper wound healing process, this promotes angiogenesis, keratinocyte migration, re-epithelialization and remodeling of the provisional matrix (Panuncialman & Falanga 2007, pp. 626-627). Matrix metalloproteinases (MMP) are enzymes that are present in the ECM. MMPs are capable to break down the components in the ECM and degrade the growth factors. (Shai & Maibach 2005, p. 13) The MMP production and activation is governed by the inflammatory cytokines, growth factors and proteinases. The activity of MMP is constraint by tissue inhibitors of metalloproteinases (TIMP) and plasma α macroglobulin. MMPs have an important role in normal wound healing process. However, it has been shown that in chronic wounds MMPs are present excessively with lowered levels of TIMPs. The imbalance contributes to the prolonged inflammation and excessive degradation of the ECM and growth factors. (Panuncialman & Falanga 2007, pp. 626-627)

As mentioned before, cytokines like growth factors have an important role in wound healing. They regulate various cellular processes, for example the cell division, growth, proliferation, differentiation and migration. Growth factors also degrade and reform the ECM and attract leukocytes into the site of injury. (Hietanen et al. 2003, p. 33) It has been noticed that either growth factors or their receptors are reduced in a chronic wound at the same time the amount of MMPs has increased (Shai & Maibach 2005, p. 13; Panuncialman & Falanga 2007, pp. 627-628).

Cellular senescence refers to the aging of a cell. Aging cells have a reduced proliferative capacity. Each human cell may undergo certain limited amount of cellular divisions. Replication of cells in the wound is crucial for proper healing. (Shai & Maibach 2005, p. 14) Recent studies suggest that cells in the chronic wound get prematurely old and exhibit senescense. The senescent cells have decreased response to growth factors. For example fibroblasts in a chronic wound have been noticed to be in senescent or in near-senescent condition. They are shown to produce elevate levels of

MMPs and decreased amounts of TIMPs. (Panuncialman & Falanga 2007, p. 628) Possible explanations for the cell senescence have been suggested, although definite causes remain uncovered. One suggestion is that the cells in the chronic wound are under constant stimulus to proliferate since the wound remains open. The cells undergo many ineffectual divisions and eventually lose their ability to proliferate. Another assumption is that the chronic wound fluid and the ulcer microenvironment contain components that lead to cellular senescense; these components may involve inflammation cytokines, bacterial toxins and reactive oxygen species. When the population of the senescent cells accumulates and exceeds critical level the wound healing ceases and even with optimal care successful wound healing is unlikely to occur. (Shai & Maibach 2005, p. 14; Panuncialman & Falanga 2007, p. 628)

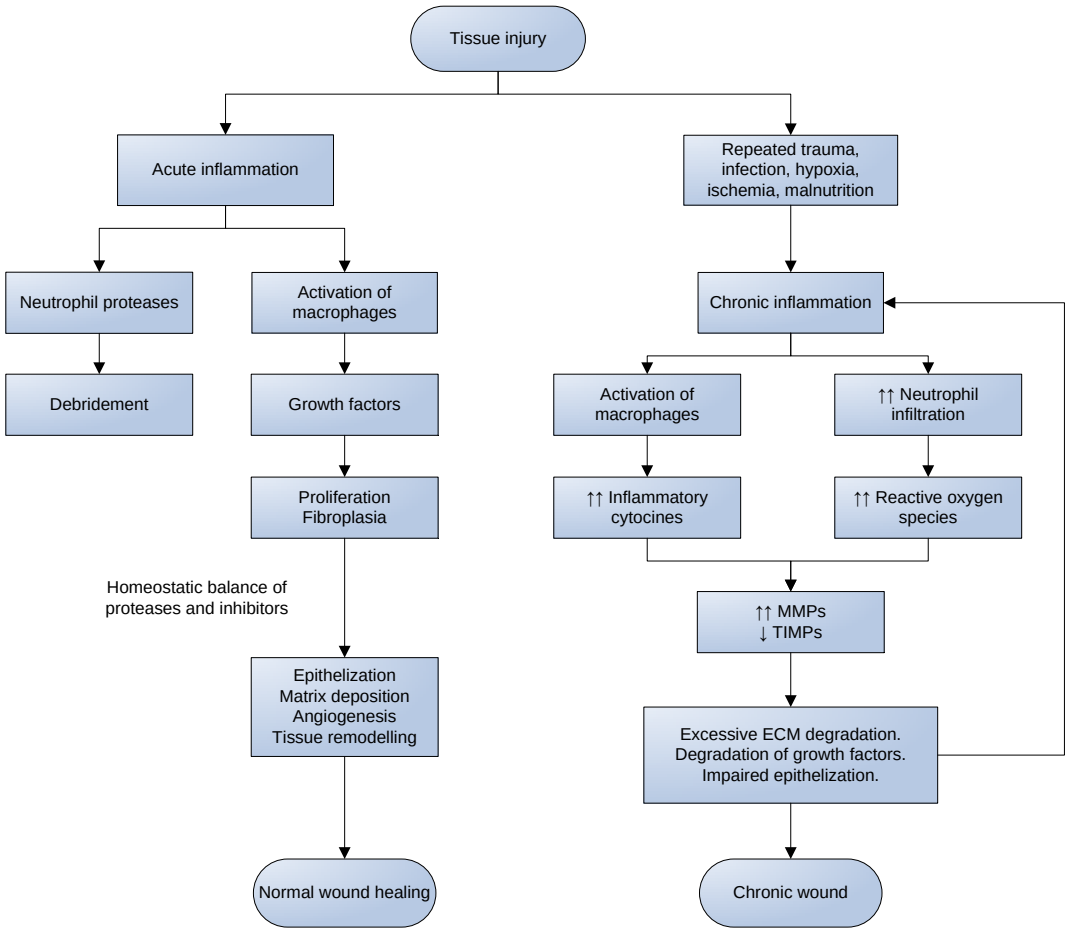

Figure 2.3 *The final common pathway in the pathophysiology of a chronic wound (Modified from Nwomeh et al. 1998, p. 352).*

Numerous important factors contributing to impaired wound healing have been identified. These factors are divided into two categories; local and systemic. (Myers et al. 2007, p. 608) The local factors relate directly to the wound itself. The systemic factors are factors that have local effects on the wound healing response. In many cases several systemic and local factors affect a non-healing wound, these factors should be

identified and controlled before a proper healing can be expected (Ramasastry 1998, p. 368). The local and systemic factors are listed in the Table 2.1. Some of these factors are discussed in the sections 2.2.1 and 2.2.2 in more detail.

Table 2.1 *Factors detrimental to wound healing (Hietanen et al. 2003, p. 34; Ramasastry 1998, p. 368)*

Local factors	*Systemic factors*
Wound size, shape and location	Aging
Ischemia	Malnutrition
Edema	Medication
Infection	Diabetes
Necrosis	Smoking
Radiation	Steroids
Repeated trauma	Stress
Cancer	
Local toxins	

2.2.1 Local factors

Wound size, shape and location

Tissue loss and depth of the wound have a weakening effect on the healing. Therefore correctional surgical operations are often needed. A wound extending to muscle or bone takes a longer time to heal than a surface wound. Also the location of the injury has a major role in the healing process. For example wounds in the scalp or in mucosa heal faster because of the good blood circulation. Wounds located in the site of tension or constant movement, for example close to joint, are prone to tearing. At a site of stress, pressure distracts blood circulation and exposes the skin to ulceration. A wound becomes easily infected in an area of incontinence if not treated appropriately. (Hietanen et al. 2003, p. 36)

Ischemia

Transport of oxygen and nutrients via vascular system is extremely important to a proper wound healing. Local short-term hypoxia supports the wound healing. Immediately after injury partial oxygen pressure decreases, this launches the activation macrophages and promotes angiogenesis. Formation of new blood vessels in the area of injury enhances blood circulation and therefore increases the oxygen concentration in the tissue. (Hietanen et al. 2003, p. 37) However, prolonged hypoxia in tissue decreases

the number of leucocytes and the ability for phagocytosis so that the risk for infection increases. Also the growth factor and collagen formation is affected. Tissue hypoxia is a common problem in especially patients who suffer from arterial, venous, diabetic or pressure ulcers (Myers et al. 2007, p. 610; Hietanen et al. 2003, p. 37).

Edema

Under normal circumstances, continual movement of fluid from the intravascular compartment to the extravascular space occurs. Fluid from extravascular space is cleared by lymphatics and returned to circulation. This fluid transport can be described partly by the Starling's law. (Rubin & Farber 1999, p. 41) Starling's hypothesis states that the pressure gradient through the vascular wall depends on both the hydrostatic and the oncotic pressure differentials between the intravascular and extravascular compartment. The equation 1 presents the Starling's equation. In the equation J_V represents the net fluid flux, K_f is a filtration coefficient, P_c is a capillary hydrostatic pressure, P_i is an interstitial hydrostatic pressure, σ is a reflection coefficient, π_c is a capillary oncotic pressure and π_i is an interstitial oncotic pressure. If J_V is positive, the fluid escapes from the capillary. (Starling's Hypothesis 2011)

$$J_V = K_f\left(\left(P_c - P_i\right) - \sigma\left(\pi_c - \pi_i\right)\right) \quad (1)$$

Non-inflammatory edema refers to a situation in which the movement of fluid to the extracellular space exceeds the clearance ability of the lymphatic system. This ultimately results in the accumulation of fluid into the extracellular space and therefore swelling. This can be a result of various medical conditions. When fluid is accumulated in the tissues as a result of damage to the lymphatic system the edema is referred as lymphedema. (Rubin & Farber 1999, p. 41) The main cause for lymphedema is venous insufficiency (Shai & Maibach 2005, p. 98).

Inflammatory edema is the immediate response to tissue injury. The inflammatory edema starts to develop from the vasoconstriction of arterioles in the site of injury. Shortly after the vasodilatation of the precapillary arterioles increases blood flow to the tissue. The increase in the permeability of the endothelial cell barrier leads to the leakage of fluid into the extracellular compartment. (Rubin & Farber 1999, p. 41) Inflammation related swelling in the area of injury disrupts blood circulation and therefore interferes the flow of oxygen and nutrients to the site. Prolonged swelling delays the healing process. (Hietanen et al. 2003, p. 39)

Infection

A reasonably mild injury may turn into a serious chronic wound when infected by bacteria, virus, fungus or parasite. The most common wound infection sources are bacteria such as Staphylococci or Streptococci. These bacteria cause infections such as erysipelas and cellulitis. Particularly susceptible to infections are patients with venous insufficiency, peripheral arterial disease or diabetes related ulcers, the other factors

include malnutrition and steroid use. (Shai & Maibach 2005, pp. 37-38; Nwomeh et al. 1998, p. 346) Bacterial concentration, virulence and growth characteristics as well as a weakened host resistance and the presence of necrotic tissue expose a patient to the emergence of wound infection. Infection increases tissue damage as a result of bacterial toxins, prolongs inflammation and can also alter the protease and cytokine repertoire so that the wound healing process is endangered (Hietanen et al. 2003, p. 229; Nwomeh et al. 1998, p. 346). Inflammation and mild infection have similar symptoms. These include a sensation of heat, redness of skin and swelling. Sometimes it is difficult to distinguish an inflammation from an infection. However, in normal wound healing process the inflammation phase starts to ease after 4 to 5 days as a classic wound infection shows up after 5 to 7 days. Also in the case of infection the redness of skin reaches wider a area than in inflammation and fever may occur. Eventually, the wound starts exude bad smelling pus. (Tuuliranta 2007, pp. 24-25; Hietanen et al. 2003, p. 230) In a chronic wound, distinguishing an infection may be even more difficult, but increasing ulcer size, increased exudate and fragile granulation tissue may refer to an infection (Panuncialman & Falanga 2007, p. 624). Also C-reactive protein (CRP) laboratory test is a common diagnostic tool when infection is suspected (Hietanen et al. 2003, p. 231)**.** Methicillin-resistant Staphylococcus Aureus (MRSA) is a serious bacterial infection. MRSA is resistant to a large group of antibiotics. It is present especially in hospitals where surgeries are performed. The most susceptible to MRSA infection are elderly patients and patients whose general condition is poor and chronic open wounds (Hospital District of Helsinki and Uusimaa (HUS) 2007). According to the Finland's National Institute for Health and Welfare (THL) the yearly number of MRSA infections in Finland has been around 1300 since year 2005 and the number has been worryingly increasing in the recent years (Finland's National Institute for Health and Welfare (THL) 2011).

2.2.2 Systemic factors

Aging

Aging has been noticed to have a weakening effect on the inflammatory response, proliferation and angiogenesis. Collagen formation and re-epithelialization are delayed. (Pukki 2006, p. 10) Aging leads to various structural changes in the skin tissue, which may result in functional changes of the skin. Due to these changes the nutrient delivery into the skin tissue is decreased, also the elasticity and the water content is affected. Therefore the skin of aged people often feels dry and fragile. Decreased inflammatory response and weakened blood circulation combined with the factors mentioned above predisposes aged people to wound infections. (Hietanen et al. 2003, pp. 40-41)

Malnutrition

Dietary optimization creates a basis for proper wound healing. Especially hospitalized elderly people and unconscious bedridden patients are in an endangered position to inadequate nutrition supply. Carbohydrates are the main energy source of the body. Carbohydrates are converted to glucose which is then used in cellular metabolism, for example inflammatory cells use glucose as a primary energy source. Adequate supply of carbohydrates ensures that protein is used for tissue formation, not as an energy source. (Hietanen et al. 2003, p. 45) Proteins are composed of amino acids. Amino acids have an important role in wound healing as it is a key factor in angiogenesis and fibroblast proliferation. Therefore protein depletion impairs collagen production. Amino acids are also important for the formation of antibodies and leucocytes. (Burns et al. 2003, p. 48; Hietanen et al. 2003, p. 45) Certain vitamins like A, C, E and K are known to contribute to the wound healing process. The most important for this purpose are A and K. Lack of vitamins A and K leads to a decreased production and formation of collagen and susceptibility to infection. Minerals like copper, magnesium, iron and zinc are also important providers in a wound healing process. (Myers et al. 2007, p. 615)

Medication

Certain medications are known to have an adverse effect on the wound healing. Particularly harmful are non-steroidal anti-inflammatory drugs (NSAIDs), steroids and chemotherapeutic agents. NSAIDs include some common pain relievers like aspirin and ibuprofen. In general, NSAIDs decrease the collagen production and in addition aspirin has been observed to have anticoagulant properties. However, in ischemic wounds NSAIDs may limit necrosis and in fact improve wound healing. (Myers et al. 2007, p. 615; Burns et al. 2003, p. 52) Steroids disturb the epithelialization process and wound contraction as fibroblast proliferation and therefore collagen synthesis is decreased. Also granulation tissue and ECM formation is decreased. Chemotherapeutic agents used in cancer treatments to reduce tumor growth also interfere wound healing process since these drugs target the rapidly dividing cells (Burns et al. 2003, p. 51).

2.2.3 Chronic wound types

Determining the etiology of a chronic ulcer is a complicated task. The exact reason for ulceration in many cases remains uncovered, as the ulcer may be a result of many complex overlapping mechanisms (Shai & Maibach 2005, p. 31). However, most of the chronic wounds are associated to a small number of medical conditions. Chronic venous stasis, diabetes mellitus and pressure necrosis are responsible for about 70 to 90% of all chronic wounds. In many cases these conditions are overlapping and patients are usually over 60 years old. These patients are affected by many of the local and systemic factors mentioned in the Table 2.1. (Nwomeh et al. 1998, p. 341; Hietanen et al. 2003, p. 137) In this section, the most common types of ulcers are presented and described briefly.

Venous ulcers

Over 70% of all leg ulcers are of venous origin. In many cases the actual trigger for ulceration is an external physical injury. As healthy person recovers from physical injury rather swiftly, a person with venous insufficiency is in a much higher risk for developing ulceration. (Shai & Maibach 2005, p. 41)

The chronic venous insufficiency (CVI) is characterized by a prolonged venous hypertension, increased venous blood pressure. Most frequently high venous pressure is a result of incompetent valves, but also deep vein thrombosis or calf muscle dysfunction might have a part in it (Nwomeh et al. 1998, p. 344). The mechanism of the tissue damage related to CVI remains uncertain. Blood pressure peaks characterize the CVI and occur when muscles are contracted. These pressure peaks are then transmitted to skin capillaries. It has been proposed that the skin capillaries and subcutaneous tissue may suffer gradual and progressive damage caused by the pressure peaks. (Shai & Maibach 2005, p. 41) Localized edema is characteristic to venous ulcers. Although, microvascular changes in venous ulcers are not exactly known, the leakage of fluids from the capillaries into the interstitium of dermis and subcutaneous tissues causes edema. Edema has adverse effects on the quality of skin. It causes sclerotic changes in the subcutaneous tissue and therefore interferes metabolic and gas exchange. Edema also causes fibrotic changes in lymphatic vessels and their valves. These changes causes reduction in the lymphatic functions and in the removal of fluids, this worsens edema even further. (Hietanen et al. 2003, p. 142; Shai & Maibach 2005, p. 41) It has been also suggested that the microvascular obstruction by thrombosis or leukocyte adhesion could have a part in the ulcer formation. The latter suggestion states that leukocytes release certain enzymes and reactive oxygen species, which could damage the capillaries and increase the permeability and tissue damage. In addition to above it has been proposed that certain macromolecules leaking into the dermis trap the growth factors, which then become unavailable and cannot participate in the tissue repair. (Nwomeh et al. 1998, p. 344; Shai & Maibach 2005, p. 42)

Venous pressure is maximal in distal parts of the body. Venous ulcers are usually located in the lower calf just above the ankle. The leg is often eczematous; the skin is dry and flaking and edema is present. The skin surrounding the wound is sclerotic, painful and seems brownish-red in color. The wound bed itself looks yellowish because of the fibrous tissue. (Hietanen et al. 2003, p. 146)

Arterial ulcers

Arterial ulcers tend to occur to elderly people, usually over 70 years old, who suffer from peripheral arterial disease. In the western world population ages and lives longer and therefore the cases of arterial ulcers are increasing in number. In addition to peripheral arterial disease, many patients also suffer from venous disease or diabetes. (Hietanen et al. 2003, p. 164)

Peripheral arterial disease is characterized by a poor tissue oxygenation as the blood circulation in the lower extremities has been compromised. Ulceration tends to initiate

from a reasonably mild injury, which would heal with no problems in the case of a healthy person. However, in case of a person exposed to poor tissue vascularization, the healing is more complicated and the site of injury becomes a portal of entry for infectious agents. Ischemia increases significantly the risk of infection. Arterial ulcers may also appear without physical injury, in that case ischemia has reached the critical level and necrosis has been developed. Atherosclerosis blocking the large arteries is a key factor contributing to the critical limb ischemia. Also anemia and low blood pressure might promote the progressing ischemia. Sometimes amputation is inevitable. (Shai & Maibach 2005, pp. 42-43; Hietanen et al. 2003, p. 161,164)

As mentioned before, arterial ulceration in many cases initiates from an injury in the lower extremities. Therefore, arterial ulcer may basically develop anywhere on the lower calves. In the case of a critical limb ischemia, it is common that necrosis appear in the toes or forefoot. (Hietanen et al. 2003, p. 43)

Diabetic ulcer

Type 2 diabetes is increasing to epidemic levels especially in the western world. It has been estimated that over 360 million people will be affected by type 2 diabetes by 2030 (Wallace 2007, p. 731). In Finland about 300 000 people are diagnosed with diabetes and approximately 200 000 people have undiagnosed diabetes (Suomen Diabetesliitto 2010). It is obvious that costs are immense. About 15% of people with diabetes will suffer from a diabetic ulcer at some point of their life and about 15% of these will undergo an amputation. A diabetic has around 10 times higher risk for amputation compared a non-diabetic person. The risk of an amputation is higher than in any other chronic wound. (Hietanen et al. 2003, p. 168) Several factors contribute to the formation of diabetic ulcer. Atherosclerosis or kidney failure is common among diabetic patients. Neuropathy is a major contributor to the ulceration. Diabetic patients are also prone to infections. Certain metabolic, cellular and biochemical alterations are common among diabetic patients as well (Greenhalgh 2003, p. 38).

People with diabetes are predisposed to macro- and microvascular diseases. Macrovascular problems such as atherosclerosis are common amongst the diabetic patients. Wound problems are quite often related to vascular occlusion and insufficient local oxygen delivery. Microvascular problems occur as the capillary level vessels develop a thickened perivascular membrane. This results into an altered delivery of nutrients and oxygen and also increased capillary permeability. Edema is a common feature in diabetes as in venous insufficiency. Diabetic patients are prone to uremia as a result of kidney failure. Uremia further exposes the diabetic patient to edema. (Greenhalgh 2003, p. 38; Shai & Maibach 2005, p. 46)

Neuropathy is a major contributor to the diabetic ulceration. Around 50% of diabetics suffer from a clinically significant neuropathy. People with diabetes are predisposed to develop neuropathy in the lower extremities. The major underlying factor for the development of neuropathy is hyperglycemia. Sensory neuropathy reduces sensation pain and therefore protective reflexes are compromised and injury might not

be felt. Diabetics tend to lose the normal position of the arc of the foot as a result of motor neuropathy. Combined with the loss of sensation, pressure necrosis occurs often on the sole. Autonomic neuropathy is associated with a dry skin with no sweating. Lack of moisture results in cracking of the skin and predisposes to an infection. (Hietanen et al. 2003, p. 169; Shai & Maibach 2005, p. 45)

Various factors contribute to a reduced resistance to infection amongst the diabetic patients. Cracking skin and loss of sensation makes a perfect site for infection. Lack of sweating may also alter the bacterial flora. Loss of glucose control increases the risk of an infection. Hyperglycemia may increase available nutrients for bacteria and it may also have an impairing effect on the local defenses. Leukocytes do not function properly under hyperglycemia, also tissue ischemia may contribute to the improper leukocyte function. (Greenhalgh 2003, p. 39; Hietanen et al. 2003, pp. 170-171)

Usually diabetic ulcer appears on the sole or toes. However, as multiple detrimental factors contribute to a diabetic ulceration it is possible that ulcer occur anywhere on the lower leg. (Shai & Maibach 2005, p. 47)

Pressure ulcer

Elderly, bedridden or otherwise immobilized patients are in particularly prone to develop a pressure ulcer. For example patients admitted to hospital following a spinal cord injury, the prevalence after 1-5 years from the initial injury is between 20-30%. (Shai & Maibach 2005, p. 37) Pressure ulcers tend to appear over bony prominences where soft tissue is compressed against the bone and an external object. Pressure ulcers are characterized by deep tissue necrosis and a loss of volume much greater that the overlying affected skin would suggest. (Nwomeh et al. 1998, p. 343).

When the external pressure exceeds the capillary pressure the blood flow and lymphatic functions are disrupted. This results in a tissue ischemia and as a consequence the toxic metabolites accumulate into the tissue spaces. A healthy individual with no neurological obstructions would sense pain in this case. The muscle tissue and subcutaneous tissues are more susceptible to the pressure induced injury than the epidermis. A cone shaped pressure gradient is created over bony prominences and therefore the skin in the affected area may seem intact, but the necrosis is gaining underneath. (Nwomeh et al. 1998, p. 343; Shai & Maibach 2005, p. 37)

2.3 Treatment of a chronic wound

Conservative wound management is consisted of the local wound care and compression therapy when necessary. The purpose of local wound care is to alter wound environment favorable to healing process. The operative wound management refers to use of more laborious surgical means to enhance the healing process. This often includes a vascular reconstruction. (Hietanen et al. 2003, p. 148)

Before a chronic wound can be expected to heal, the systemic factors have to be under control. For example chronic edema has to be dealt in patients with a leg ulcer. Diabetic patients must obey a tight glycemic control. For a patient with neuropathy the use off-loading footwear is necessary. Patient's nutritional status has to be inspected and smoking has to be ceased (Panuncialman & Falanga 2007, p. 621).

Sometimes surgical methods are necessary to provide permanent wound healing. For a patient with venous ulcer it might be beneficial to undergo venous valve reconstruction or venovenous bypass to improve peripheral blood circulation. For an arterial ulcer or a diabetic ulcer patient an arterial bypass or angioplasty can be helpful. In extreme cases the only solution might be amputation of the affected limb (Ramasastry 1998, pp. 378-379; Hietanen et al. 2003, p. 149, 169,182).

As mentioned before, the most of the chronic wounds are possessed by necrotic or devitalized tissue or are under an infection risk because of the high bacterial burden. These issues impair the wound healing. Therefore a debridement of the wound bed is often necessary. The goal of the debridement procedure is to transform a chronic wound into an acute one. (Myers et al. 2007, p. 608) Various methods for the debridement include the classic surgical debridement, however it is a harsh and unselective method since it removes viable tissue as well. Mechanical debridement includes for example wet to dry dressings, hydrotherapy and irrigation. This method is fast, but also unselective and painful. Autolytic debridement is based on the body's own proteolytic enzymes and phagocytic cells to clean up the wound bed. The autolytic debridement may take weeks to finish. One interesting method is to use larvae for debridement of a chronic wound. The maggots digest necrotic tissue and secrete bactericidal enzymes. This method has been reported being effective against the MRSA and beta-hemolytic streptococcus, it is also selective and takes around two days to finish. It can be done at home under a nurse's supervision. (Panuncialman & Falanga 2007, pp. 622-623) After suitable steps mentioned above are taken, skin grafts, skin substitutes or dressings can be inserted and management of wound can be moved forward to the local wound care level and finally the patient might be taken into home care.

Antibiotics and antiseptics are traditionally used in wound management to reduce the risk of bacteria in the wound bed to provoke an infection further compromising the healing process. Antibiotics target the bacteria via a specific mechanism that is unique to each class of antibiotic. Antiseptics instead act via non-selective toxicity and therefore the damage is also done to the non-pathogenic microorganisms as well. (Shai & Maibach 2005, pp. 136-137)

Realization that a moist environment is beneficial to a non-healing wound and that occlusive dressings do not increase the risk for infection has been a major advance in wound treatment practices. As a result of this discovery a wide variety of dressings providing a moist healing environment, pain relief and drainage has entered the market. An ideal dressing for a chronic ulcer would provide a moist environment, absorb exudates, prevent the maceration of surrounding tissue, is impermeable to bacteria, would not cause re-injury upon removal and would be cost effective. Unfortunately, any

single dressing does not provide all of these features and therefore the choice of the dressing has to be done according to the wound type and wound bed characteristics at a given time. (Panuncialman & Falanga 2007, p. 625)

The current areas of research have paid a lot of attention for development of selective MMP inhibitors. As mentioned earlier the MMPs are excessive in non-healing wounds and do lead to a persistent inflammation and degradation of the ECM and growth factors. There exists great deal of scientific interest towards the growth factors. The growth factors have many remarkable roles in the wound healing and closure and the amount of growth factors is decreased in the non-healing wounds. Impaired function of one growth factor likely affects several growth factors and other cytokines. Positive clinical results have been obtained with the platelet-derived growth factors (PDFG) and with certain other growth factors. However, many other have failed show any significant improving effect. The current focus of research is on the improving the delivery systems to provide high concentrations of growth factors to the wound bed or a more intimate relationship with the target cells. In the future, the best results are expected to be obtained by using several growth factors specific for different stages of wound healing. (Panuncialman & Falanga 2007, pp. 626-628)

Figure 2.4 *Chronic non-healing ulcer on thigh. a) After debridement. b) Five weeks after application of a living skin substitute (LSE). c) Five months after LSE application. The ulcer has completely closed. (Medscape 2011).*

3 Technical background

3.1 Bioimpedance theory

Bioimpedance describes the ability of living tissue to oppose alternating current flow. Biological tissues have strong frequency dependency and contain capacitive features in addition to resistance. Therefore, instead of resistance it is reasonable to talk about impedance. Bioimpedance is an exogenic measure and the measurement of bioimpedance is indirect. The tissue has to be stimulated or excited externally. The voltage induced by the excitation current is measured, and by using extended Ohm's law the impedance can be determined. (Grimnes & Martinsen 2008, p. 1)

3.1.1 Impedance and bioimpedance

The fundamental Ohm's law deals with the relationship between voltage and current in an ideal conductor. The relationship states that the potential difference over the ideal conductor is proportional to the current through it. The proportionality is called resistance (Eq. 2) (University of Guelph, Department of Physics 2008).

$$R = \frac{V}{I} \tag{2}$$

Ohm's law applies only to purely resistive circuits. If the circuit contains capacitive or inductive elements and is exposed to alternating current, resistance has to be replaced by impedance (Eq. 3). Impedance is a vector quantity. In addition to a magnitude it also holds a direction.

$$\bar{Z} = \frac{\bar{V}}{\bar{I}} \tag{3}$$

Impedance is a measure of a total opposition to an alternating current. Impedance takes account the frequency dependency of the opposition to applied current. Resistance is actually a special case of impedance, since purely resistive circuits have no frequency dependency or does not induce phase shift between the applied current and the voltage. However, if an AC circuit contains capacitive or inductive elements phase shift between

applied current and voltage can be observed. The general Cartesian form of impedance can be defined as in the equation 4.

$$\bar{Z} = R + j \cdot X \tag{4}$$

With a capacitive element.

$$\bar{Z} = R - j \cdot X_C = R + \frac{1}{j \cdot \omega \cdot C} \tag{5}$$

, where resistance R refers to the real part of the impedance and reactance X refers to the phase sensitive imaginary part of the impedance.

Reactance may be either inductive, capacitive or both. In context of biological tissue capacitive effects are important. When alternating current is applied to a capacitor, the positive half cycle of the current gradually charges the capacitor and voltage increases over the capacitor. During the negative half cycle the voltage decreases accordingly. The voltage lags the applied alternating current by 90° (θ = -90°). The resistive part of the impedance for purely capacitive circuit is zero (Eq. 6). The negative sign on the equation 6 indicates the voltage lagging the current. X_C refers to capacitive reactance.

$$\bar{Z}_C = 0 + (-j \cdot X_C) = -j \cdot X_C = -\frac{1}{\omega \cdot C} \cdot j = \frac{1}{j \cdot \omega \cdot C} \tag{6}$$

$$X_C = \frac{1}{\omega \cdot C} = \frac{1}{2\pi \cdot f \cdot C} \tag{7}$$

The magnitude and the phase of the impedance can be calculated from equation 8 and equation 9 accordingly.

$$\left|\bar{Z}\right| = \sqrt{R^2 + X_C^2} = \sqrt{R^2 + \left(-\frac{1}{2\pi \cdot f \cdot C}\right)^2} \tag{8}$$

$$\theta = \arctan\frac{X_C}{R} \tag{9}$$

For purely resistive circuit which does not contain phase shift (θ=0), impedance equals resistance (Eq. 10).

$$Z_R = R + j \cdot 0 = R \tag{10}$$

3.1.2 Change in a tissue volume and conductivity

As mentioned earlier, chronic wounds are often stuck into inflammatory phase. This means that the permeability of capillaries is increased due to damage caused to endothelial cell barrier. The increased blood pressure forces leakage of relatively conductive fluid into the extracellular space. Therefore swelling around the site of wound occur. The volume of the tissue segment is changed.

We may simplify the situation by portraying the tissue segment by a cylinder model to describe the effect of the volume change into the impedance of the tissue. The volume (V) of the cylinder in Figure 3.1 is the area (A) of the base of the cylinder times the length (l) of the cylinder (Eq. 11).

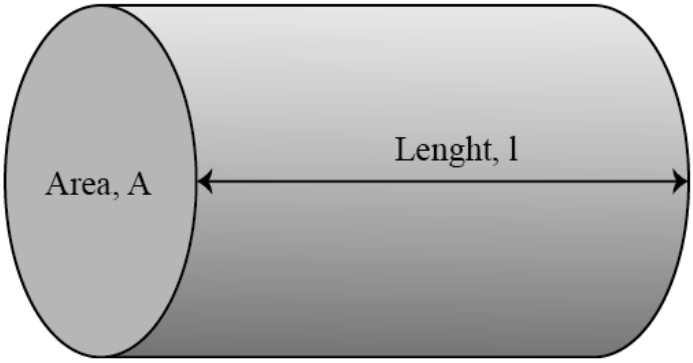

Figure 3.1 *Cylinder with base area A and length l.*

$$V = A \cdot l \tag{11}$$

If we consider this cylinder as a uniform volume conductor with a resistivity ρ or conductivity σ, we are able to determine the resistance of the cylinder (Eq. 12).

$$R = \rho \cdot \frac{l}{A} = \frac{1}{\sigma} \cdot \frac{l}{A} \tag{12}$$

By combining the equation 11 and the equation 12 we can draw a relationship between the volume and the resistance of the cylinder. In the equation 13, the resistivity ρ is replaced by the conductivity σ.

$$V = \frac{1}{R} \cdot \frac{l^2}{\sigma} \tag{13}$$

If the volume of the cylinder increases by amount of ΔV and we assume that the volume increase comes only from transverse increase of the cylinder (l= constant), we may express the new volume as in the equation 14.

$$V+\Delta v=\frac{1}{R+\Delta R}\cdot\frac{l^2}{\sigma}\Rightarrow\Delta v=\frac{1}{R+\Delta R}\cdot\frac{l^2}{\sigma}-V\Rightarrow\Delta v=\frac{1}{R+\Delta R}\cdot\frac{l^2}{\sigma}-\frac{1}{R}\cdot\frac{l^2}{\sigma}$$
$$\Rightarrow\Delta v=\left(\frac{1}{R+\Delta R}-\frac{1}{R}\right)\cdot\frac{l^2}{\sigma}=-\frac{\Delta R}{R}\cdot\frac{1}{R+\Delta R}\cdot\frac{l^2}{\sigma} \quad (14)$$

If we assume that $R>>\Delta R$, then we can write

$$\Delta v=-\frac{\Delta R}{R}\cdot\frac{1}{R+\Delta R}\cdot\frac{l^2}{\sigma}\Rightarrow\Delta v=-\frac{\Delta R}{R}\cdot\frac{1}{R}\cdot\frac{l^2}{\sigma}=-\Delta R\cdot\frac{1}{\sigma}\cdot\left(\frac{l}{R}\right)^2 \quad (15)$$

From the equation 14 we see that there is a negative correlation between the increase in volume and change in the resistance. Therefore, increase in the volume of the tissue due to swelling results in decrease in the measured impedance. Not so surprisingly, we can find similar negative correlation between increasing conductivity and change in the resistance (Eq. 16). It is also worth noticing that the determination of ΔV does not have to involve information about the absolute volume (Grimnes & Martinsen 2008, pp. 348-349).

$$R+\Delta R=\frac{1}{\sigma+\Delta\sigma}\cdot\frac{l}{A}$$
$$\Rightarrow\ldots\Rightarrow \quad (16)$$
$$\Delta\sigma=-\frac{\Delta R}{R}\cdot\frac{1}{R+\Delta R}\cdot\frac{l}{A}$$

If we assume $R>>\Delta R$, then we can write

$$\Delta\sigma=-\frac{\Delta R}{R}\cdot\frac{1}{R+\Delta R}\cdot\frac{l}{A}=-\frac{\Delta R}{R}\cdot\frac{1}{R}\cdot\frac{l}{A}=-\Delta R\cdot\frac{l}{A\cdot R^2} \quad (17)$$

The fluid leaking into extracellular space is mostly water with ionic solutes and can be estimated to possess the conductivity of 0.9% saline (Table 3.1). It is highly conductive in relation to surrounding tissue material. Therefore, the total conductivity tissue can be expected to increase when tissue is swollen due to inflammatory response. Both phenomena in the sustaining chronic wound, the increase in volume and the increase in conductivity, decrease the impedance compared to a healthy tissue. Contrary to this, healing of chronic wound can be perceived as increasing impedance.

Table 3.1 *Tissue conductivities at low frequency and at high frequency (Grimnes & Martinsen 2008, p. 103).*

Tissue	***σ (S/m)*** *1Hz – 10kHz*	***σ (S/m)*** *~ 10Mhz*	***Anisotrophy***
Saline, 0.9%, 37°C	2	2	
Human skin, dry	10^{-7}	10^{-4}	?
Human skin, wet	10^{-5}	10^{-4}	?
Fat	0.02 – 0.05	0.02 – 0.05	Small
Muscle	0.05 – 0.4	0.6	Strong
Bone	0.005 – 0.06		Strong
Whole blood	0.7	0.7	Flow dependent

In reality, tissues are not homogenous or even isotropic. Different tissue types have different frequency dependent conductivities as can be seen from Table 3.1 in addition to this the electrical properties of tissue are also direction dependent. The direction dependency of the conductivity is called anisotropy. (Grimnes & Martinsen 2008, p. 124)

3.1.3 Biological tissue models and their interpretation

In section 3.1.2, biological tissue was depicted by a simplistic model of a uniform volume conductor. This is not a sufficiently accurate model to describe the electrical behavior of the tissue.

Electrons are charge carriers in metals. Charge carriers in biological tissues are ions. An electrode is the site of a charge carrier shift from electrons to ions. (Grimnes & Martinsen 2008, p. 8) The most important charge carrying electrolytes in biological tissue are Na^+, Cl^- and K^+ ions (Grimnes & Martinsen 2008, p. 24). Table 3.2 lists the most important electrolytes in body liquids and their concentrations.

Table 3.2 *Concentrations of electrolytes in body liquids (Grimnes & Martinsen 2008, p. 24).*

Cations (meq/L)		
	Extracellular	***Intracellular***
Na^+	142	10
K^+	4	140
Ca^{2+}	5	10^{-4}
Mg^{2+}	2	30
H^+	4×10^{-5}	4×10^{-5}
Sum	153	180

Anions (meq/L)		
	Extracellular	***Intracellular***
Cl^-	103	4
HCO_3^-	24	10
$Protein^-$	16	36
$HPO_4^- + SO_4^-$ + organic acids	10	130
Sum	153	180

Tissues are formed from cells and extracellular media. Cells are enclosed in a cellular membrane that controls the exchange of ions and molecules between the intracellular and extracellular media. Both extra- and intracellular media are highly conductive due to their high ion concentration. The basic structure of the cell membrane is consisted of the lipid bilayer with transmembrane proteins embedded in it (Figure 3.2). The lipid bilayer does allow ions to diffuse through the cell membrane. Ions are selectively exchanged between intracellular and extracellular media by the transmembrane protein channels creating a composite structure of different permittivities. Therefore the cell membrane can be treated as a dielectric interface and represented as a two conductive plates of a capacitor. (Bourne 2001, p. 272-273)

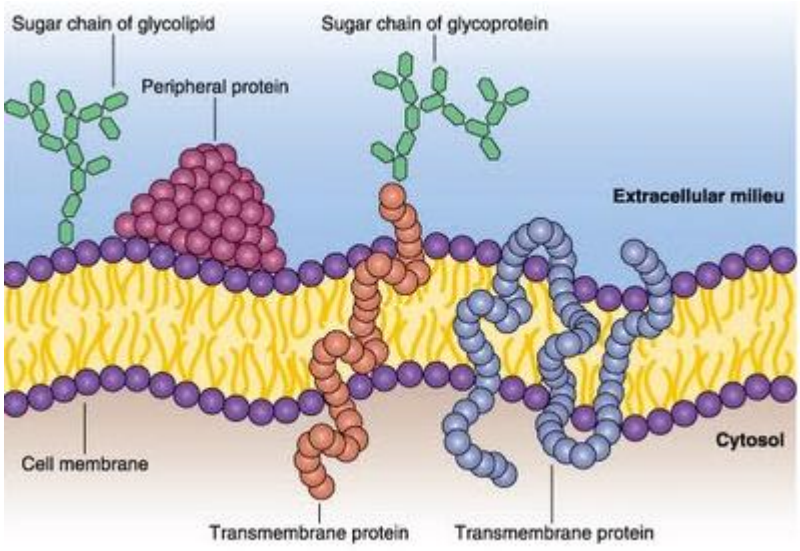

Figure 3.2 *The cross section of a cellular membrane with the membrane proteins (Modified from Jungueira & Carneiro 1997).*

Various electrical equivalents have been proposed to describe the behaviour of biological tissues. The most widely used electrical equivalents are three component models consisted of two resistors and one capacitor. These are arranged either in series or in parallel form (Figure 3.3). The series model is often used for a skin electrical equivalent whereas parallel version describes cells and living tissue in a more general way.

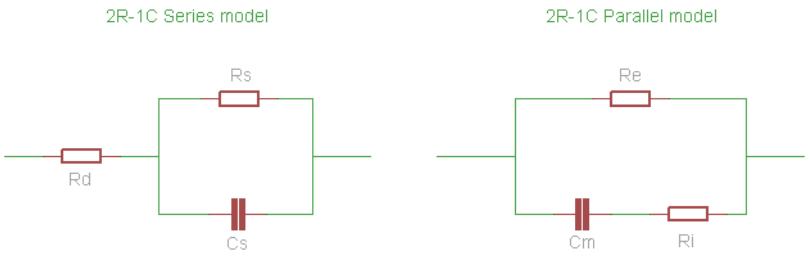

Figure 3.3 *Three component models of biological tissue aka. 2R-1C model. The 2R-1C series model (left) is used for describing the electrical behaviour of the skin. The parallel model (right) describes the electrical behavior of the deeper tissue segments (Modified from Grimnes & Martinsen 2008, p. 303).*

The total impedance of the parallel 2R-1C model

$$\begin{aligned}\bar{Z} &= \frac{R_E \cdot (R_I - j \cdot X_C)}{R_E + R_I - j \cdot X_C} = \frac{R_E \cdot (R_I - j \cdot X_C)}{R_E + R_I - j \cdot X_C} \cdot \frac{R_E + R_I + j \cdot X_C}{R_E + R_I + j \cdot X_C} \\ &= \frac{(R_E \cdot R_I - j \cdot R_E \cdot X_C) \cdot (R_E + R_I + j \cdot X_C)}{{R_E}^2 + R_E R_I + j \cdot R_E \cdot X_C + R_E \cdot R_I + {R_I}^2 + j \cdot R_I \cdot X_C - j \cdot R_E \cdot X_C - j \cdot R_I \cdot X_C - j^2 \cdot {X_C}^2} \\ &= \frac{{R_E}^2 \cdot R_I + R_E \cdot {R_I}^2 + j \cdot R_E \cdot R_I \cdot X_C - j \cdot {R_E}^2 \cdot X_C - j \cdot R_E \cdot R_I \cdot X_C - j^2 \cdot R_E \cdot {X_C}^2}{{R_E}^2 + 2R_E \cdot R_I + {R_I}^2 + {X_C}^2} \\ &= \frac{{R_E}^2 \cdot R_I + R_E \cdot {R_I}^2 - j \cdot {R_E}^2 \cdot X_C + R_E \cdot {X_C}^2}{{R_E}^2 + 2R_E \cdot R_I + {R_I}^2 + {X_C}^2} \\ &= \frac{{R_E}^2 \cdot R_I + R_E \cdot {R_I}^2 + R_E \cdot {X_C}^2}{{R_E}^2 + 2R_E \cdot R_I + {R_I}^2 + {X_C}^2} - j \cdot \frac{{R_E}^2 \cdot X_C}{{R_E}^2 + 2R_E \cdot R_I + {R_I}^2 + {X_C}^2}\end{aligned} \tag{18}$$

The modulus of the parallel 2R-1C model

$$\left|\bar{Z}\right| = \sqrt{\left(\frac{{R_E}^2 \cdot R_I + R_E \cdot {R_I}^2 + R_E \cdot {X_C}^2}{{R_E}^2 + 2R_E \cdot R_I + {R_I}^2 + {X_C}^2}\right)^2 + \left(\frac{{R_E}^2 \cdot X_C}{{R_E}^2 + 2R_E \cdot R_I + {R_I}^2 + {X_C}^2}\right)^2} \tag{19}$$

The phase angle of the parallel 2R-1C model

$$\begin{aligned}\theta &= \arctan \frac{\dfrac{{R_E}^2 \cdot X_C}{{R_E}^2 + 2R_E \cdot R_I + {R_I}^2 + {X_C}^2}}{\dfrac{{R_E}^2 \cdot R_I + R_E \cdot {R_I}^2 + R_E \cdot {X_C}^2}{{R_E}^2 + 2R_E \cdot R_I + {R_I}^2 + {X_C}^2}} \\ &= \arctan \frac{\left({R_E}^2 \cdot X_C\right) \cdot \left({R_E}^2 + 2R_E \cdot R_I + {R_I}^2 + {X_C}^2\right)}{\left({R_E}^2 + 2R_E \cdot R_I + {R_I}^2 + {X_C}^2\right) \cdot \left({R_E}^2 \cdot R_I + R_E \cdot {R_I}^2 + R_E \cdot {X_C}^2\right)}\end{aligned} \tag{20}$$

In the skin electrical equivalent the parallel combination of C_S and R_S refers to the outermost layer of the skin, the stratum corneum, and to the conductance created by the sweat ducts. The resistor R_D represents the deeper layer series resistance. (Grimnes & Martinsen 2006, p. 6)

The parallel version of tissue electrical equivalent introduces the resistor R_E which represents the resistance of extracellular fluid. The capacitor C_M describes the cellular membrane and R_I is used for describing the resistance of intracellular fluid. At low frequencies the cell membrane prevents the current entering into the intracellular space. Therefore, at lower frequencies almost all of the current flows through the extracellular media, the total impedance measured is largely resistive and contributed by R_E. The parallel model circuit (Figure 3.3) is reduced to R_E. For a healthy person, extracellular medium comprises around 20% of the total tissue volume and thus the resulting

impedance is relatively high. At higher frequencies, the current can make its way through the capacitance of the cell membrane and enter the intracellular medium as well as the extracellular medium. Therefore, the total impedance at higher frequencies is lower than at low frequencies. (Holder 2004, p. 416) If the frequency is gradually increased and the behaviour of the capacitor is investigated, we may notice that the phase angle increases and the reactance decreases, more current is diverted away from extracellular resistance. Finally, at high frequencies the reactance X_C diminishes according to equation 7 and the current encounters the parallel resistances of extra- and intracellular compartments ($R_E || R_I$). Between these extremities lies the center frequency (f_C) in which the current passing the capacitive path reaches its maximum, the maximum reactance. Occasionally, the center frequency is also called the mid-frequency or characteristic frequency. (Holder 2004, p. 416-418; Matthie 2008, pp. 240-241)

The fundamental law of solving linear equations states that if we have N unknown variables, then to find unique solutions for each of the variables we need at least N mutually independent equations. To determine the components R_E and R_I of the parallel model 2R-1C from the measurement data, we need at least three data sets with different excitation frequencies of the total impedance modulus Z and the phase θ. From the three independent measurements, we are able to generate three independent equations from which the values of R_E and R_I are possible to solve unambiguously. Obviously, we have to make an assumption that R_E and R_I remains constant between the measurements. As they are not frequency dependent that is appropriate. If we have measurement data of impedance modulus and phase only for two frequencies, then we are only able to solve the relation $\frac{R_E}{R_I}$ unambiguously, which is sometimes enough to provide the necessary information. According to Nordbotten et al. (2010) it is also possible to solve the phase angle with good accuracy from only impedance modulus data taken at four frequencies by using Kramer-Kronig equation. The downside of this approach is that it requires rather heavy calculus.

The Cole diagram is a popular way to present the bioimpedance data in a complex plane (Figure 3.4). In particular, it is used to plot data obtained from bioimpedance spectroscopy (BIS) measurement. BIS takes numerous impedance measurements gradually stepping up the frequency over a wide frequency range up to 1MHz. Also phase shift caused by the capacitive cellular membrane is measured for each data point. The phase information provides the possibility to distinguish the reactance part from the resistive part of the impedance. By using the Cole approach, resistances on zero frequency (R_0) and infinite frequency (R_∞) can be extrapolated, which would not be obtainable by using measurements. (Matthie 2008, pp. 240-241; Kyle et al. 2004a, pp. 1229-1230)

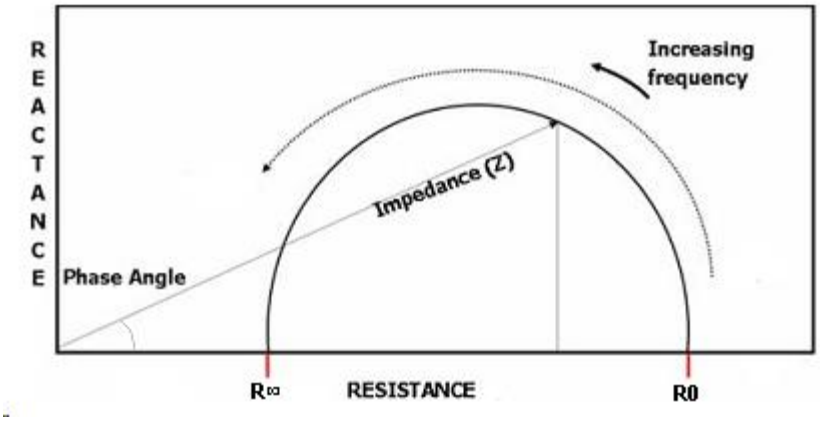

Figure 3.4 *Cole diagram visualizing the relationship between impedance (Z) and its components of resistance (R) and reactance (X_C) (Modified from York et al. 2009, p. 178).*

3.1.4 Permittivity and conductivity of biological tissue

In section 3.1.2, biological tissue was depicted by a simplistic model of a uniform volume conductor. This is not sufficiently accurate model to describe the electrical behavior of the tissue.

Permittivity is the most important measure of an electric insulator. It describes the ability of the material to oppose an externally applied electric field. When a dielectric material is placed between two conductive plates, the potential difference between the plates decreases (Figure 3.5). Therefore, also the magnitude of the external electric field must decrease between the plates. A perfect dielectric, as oppose to perfect conductor, does not contain free charge carriers. It may contain permanent dipole molecules or molecules that under an external electric field turn into electric dipole moments, thus creating an internal electric field inside the dielectric. Polarized molecules are oriented so that the internal electric field of the dielectric opposes the external electric field. This phenomenon is called dielectric polarization.

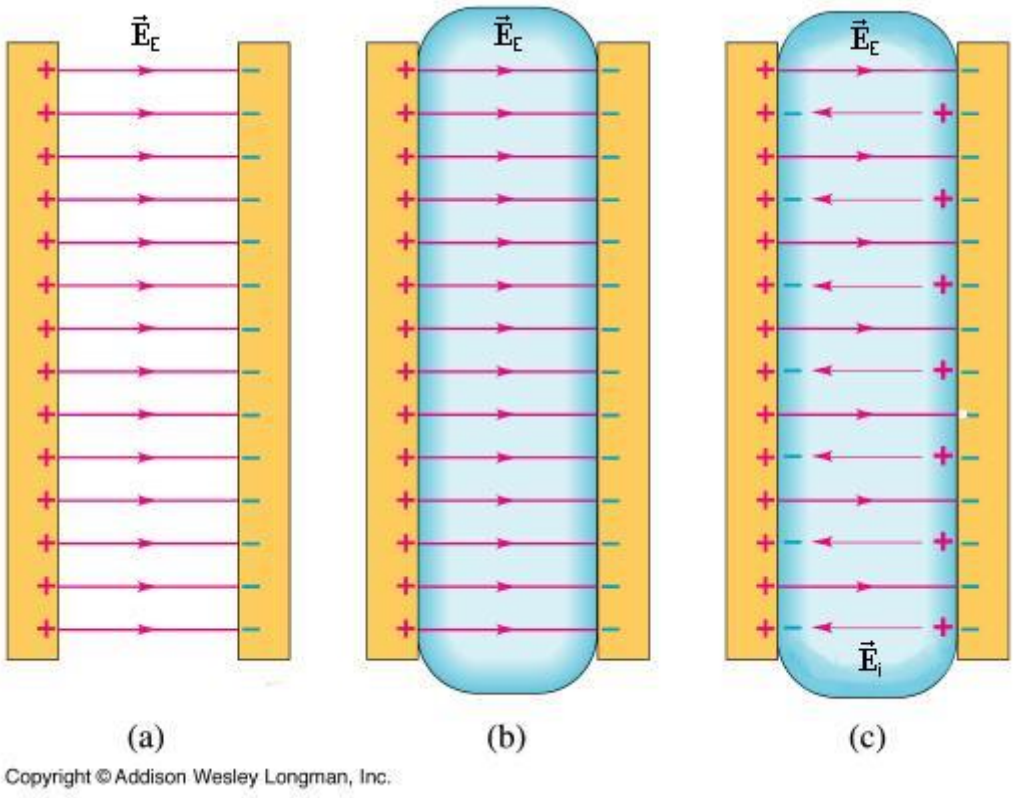

Figure 3.*5 The dielectric polarization. (a) External electric field of magnitude* $\overline{E}_E$ *between two conductive plates. (b) Dielectric is introduced. (c) Internal electric field* $\overline{E}_I$ *of the dielectric opposes the external electric field (Modified from Young & Freedman 2000).*

Good dielectric materials are easily polarizable and therefore have a high value of permittivity (Young & Freedman, pp. 782-785). Static permittivity properties of a biological tissue are exceptional. Tissues provide extraordinarily high permittivity and thereby capacitance which is up to 1000 times higher than inorganic materials, such as plastics used in capacitors. This is because the capacitance is provided by numerous and closely opposed cell membranes, each of which behaves as a tiny capacitor. (Holder 2004, p. 418; Bourne 1996, p. 274)

Equation 21 for capacitance in a static electric field is used just for describing the relationship between the permittivity and the capacitance.

$$C = \frac{\varepsilon_0 \cdot \varepsilon_r \cdot A}{d} \tag{21}$$

In an ideal matter polarization of a dielectric would happen instantaneously without any delay. However, in reality there is a delay in polarization of molecules of dielectric related to changes in applied external electric field. This is called relaxation time. In the case of biological tissue, at very low frequencies the time constant is sufficiently low to

allow the charging and discharging of the cellular membranes to take place in a single period. This shows up as a very high value of permittivity, which in turn means that the tissue capacitance is very high and the measured conductivity is then basically the conductivity of the extracellular medium. (Bourne 1996, p. 276) If the frequency of an externally applied electric field is high enough, the molecules do not have enough time to get fully polarized. This results in decrease in permittivity. The frequency dependency of permittivity is called dispersion. (Grimnes & Martinsen 2008, pp. 70-71) Losses related to relaxation are sometimes called also dielectric losses and a capacitor with dielectric losses as a lossy capacitor. Permittivity and capacitance are directly related to each other, decrease of permittivity with increasing frequency causes also capacitance to decrease with increasing frequency. The lossy capacitor has a frequency dependent capacitance. For a good dielectric, the capacitance deteriorates very slowly with frequency and in generally for example in electronics design capacitance is considered to be constant. (Johnson 2001)

In addition to dielectric losses, there exists another type of loss in capacitors related to conduction electrons. As mentioned earlier a perfect dielectric does not contain free charge carriers. However, this is not the case in reality. Due to non-idealities in dielectric medium free charges exists and displacement currents arise. This results in energy losses in capacitor. The frequency dependent conductivity can be found in dielectric. The conductivity increases with increasing frequency. (Grimnes & Martinsen 2008, pp. 66-67, 73-74)

The decrease of permittivity of tissue over increasing frequency is not linear. Non-linear behaviour of the dispersion is due to different relaxation mechanisms. From all biological tissue types, three steps of steep permittivity decrease can be distinguished, even though the magnitudes and the dispersion frequencies may vary. These are called α-, β- and γ-dispersion regions (Figure 3.6).

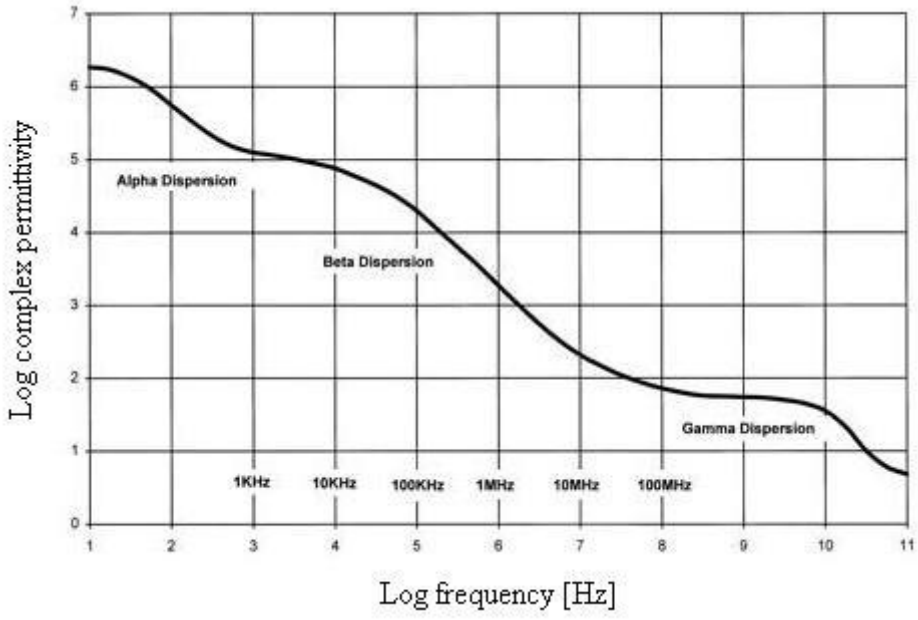

Figure 3.6 *The dispersion regions in biological tissue. The figure represents the frequency dependency of the complex permittivity of muscle tissue. (Modified from De Lorenzo et al. 1996).*

The alpha -dispersion dominates at low frequencies on a scale of mHz to kHz. It is generally considered to be associated with the diffusion processes of the ionic species, although certainty of its origins has been disputed. (Ivorra 2003, p. 17; Grimnes & Martinsen 2010) Beta -dispersion occurs at frequencies from a few kHz to some tens of MHz. Beta -dispersion is mainly due to the dielectric properties of the cell membranes and their interactions with the extracellular and intracellular electrolytes (Ivorra 2003, p. 17). When the frequency increases, the cell capacitive reactance decreases and thereby an increasing amount of current is passing through the intracellular medium thus increasing the conductivity of tissue (Bourne 1996, p. 276). Most changes between normal and pathological tissues occur in the alpha- and beta-dispersions. Gamma-dispersion dominates at very high GHz scale frequencies and is mainly due to relaxation of water molecules. (Holder 2004, p. 418) At these high frequencies, capacitances are short-circuited and reactance is effectively non-existent (Bourne 1996, p. 276).

Permittivity and conductivity are not only frequency dependent when dealing with measurements of biological tissues. Permittivity and conductivity are also dependent on the direction of the approach due to the morphological patterns in the tissue. In a living tissue the conductivity can be 10 times higher in one direction than the other. One example of strong anisotropy is lungs constantly filled and emptied with air. (Grimnes & Martinsen 2008, p. 126) Another example is muscle tissue which has a strong anisotropic nature due to cylindrical shape muscle cells (Matthie 2008, p. 255). The Figure 3.7 visualizes the effect of the anisotropy to the path of the applied electrical current.

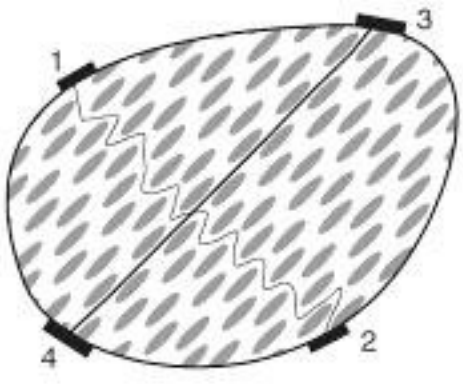

Figure 3.7 *The effect of the anisotropy to the applied current in the tissue. Each ellipse represents a cell with a cell membrane (Grimnes & Martinsen 2008, p. 127).*

3.1.5 Bioimpedance measurement methods

Interpretation of the results of bioimpedance measurements are predisposed to simplifications and approximations due to limitations of the models describing electrical behaviour of biological tissue. However, in a strictly limited framework it is possible to obtain good results related to acknowledged reference methods. Wide variety of electrical and mathematical models have been developed for different purposes to explain the measurement data. Often the phase data is also measured in addition to the impedance data.

Bioelectrical impedance analysis refers to assessment of human body composition based on the measured bioimpedance data. It can be used for estimating for example volumes or masses of whole body or different body compartments.

Terminology varies in the literature when concerning the body composition and may be confusing, sometimes articles point to the total body water (TBW), the extracellular water (ECW) and the intracellular water (ICW). Sometimes to the total body fluid (TBF), the extracellular fluid (ECF) and the intracellular fluid (ICF). Basically, these abbreviations refer to the same issue. However, to underline the fact that it is all about the volumes when using these abbreviations it is preferable to use TBF, ECF and ICF. (Matthie 2008, p. 2) Total body fluid (TBF) is divided between the intracellular and the extracellular spaces. The fluid in the extracellular space is called extracellular fluid (ECF) and the fluid in the intracellular space is referred as intracellular fluid (ICF). The ECF composes around one third of total body fluids in healthy person. The ECF itself is comprised of intravascular plasma (25%) and interstitial fluid (75%). (Cho & Atwood 2002)

A widely used method in non-scientific bioelectrical impedance analysis is 50kHz single frequency measurement (SF-BIA). It is thought to predict the total body fluid (TBF) volume as the current passes through both intra- and extracellular fluids at the

frequency of 50kHz. However, in practise it measures the weighted sum of intra- and extracellular fluids. Numerous empirical equations for different subject groups have been developed for SF-BIA to interpret the measurement results. These equations are tailored to take into account for example age, gender, health status or weight of the subject. (Kyle 2004a et al., p. 1229; Matthie 2008, p. 240)

Multifrequency bioelectrical impedance analysis (MF-BIA) determines impedances at multiple different frequencies; at low and high frequencies. Like SF-BIA it also uses empirical regression models to predict the volumes of ECF, ICF and TBF from the impedance data. It is thought to represent more accurate predictions of ECF than SF-BIA. (Kyle 2004a et al., p. 1231)

Bioimpedance spectroscopy (BIS) refers to a method in which a large number of measurements are taken over wide frequency range usually up to 1MHz. The results are then plotted in a graph called Cole –diagram (Figure 3.4) from which resistances on zero frequency (R_0) and infinite frequency (R_∞) can be extrapolated. (Kyle at al. 2004a, pp. 1229-1230; Matthie 2008, pp. 240-241) The Cole –diagram is shortly discussed in the section 3.1.3.

3.1.6 Assessment of chronic wound healing with a bioimpedance device

The bioimpedance method can be used for assessing various static or dynamic physiological events. Although, the use of bioimpedance methods in a widespread fashion in routine clinical work has been rather limited so far, the scientific interest in the area of bioimpedance has been quite intense and increasing. Nevertheless, certain applications based on bioimpedance are used in everyday clinical medicine. Plethysmography and body composition analysis are good examples of this and more recently there has been new commercial applications for lymphedema assessment as well. Scientific research have found use for bioimpedance methods for example in ischemia detection and monitoring of the function of a skin graft. Bioimpedance methods have also been used in cancer detection, tissue characterization studies and in cellular level research. All in all, the range of possible applications is wide. Bioimpedance methods in general are fairly easy to implement and relatively inexpensive. From the design point of view possibilities for miniaturization and portability are good. In addition bioimpedance can be measured non-invasively. (Kyle et al. 2004b)

This Master of Science thesis introduces a prototype of a bioimpedance device for monitoring of chronic wound healing. Basis for this usage lies on the changes in the electrical characteristics of the affected tissue segment in comparison to a healthy tissue. Usually a wound heals properly if not exposed to infection, fungus, parasite or some other exposing factor. In most cases a chronic wound is caused by a serious underlying medical condition and therefore wound healing is impaired. These conditions are various with many individual characteristics. However, it can be said that a chronic cutaneous wound is characterized by prolonged inflammation phase; for some reason

healing is delayed or suspended. The surrounding tissue of an inflammated wound is swollen as the fluids accumulate in the wound area.

Concerning inflammation related fluid accumulation into tissues in a chronic wound, two types of mechanisms can be distinguished.

Firstly, the fluids may accumulate into intracellular space as a result of ischemia. The increase in ICF can be detected as a decrease in intracellular resistance (R_I). This mechanism works so that if the blood flow into tissues is interrupted, the cell metabolism continues but in an anaerobic way. However, prolonged ischemia inevitably results in decline of metabolism. This results in the decreased activity of ion pumps, which leads to changes in ion distribution in ECF and ICF. The result is cellular edema because of the inflow of water and sodium in to the cell. The decline of ECF volume reduces the width of the electrical path of low frequency current and therefore increases the extracellular resistance. The increasing area of cellular membrane results also in the increased membrane capacitance. Severe ischemia finally results in cell necrosis. In necrosis the cellular integrity is lost and intracellular fluid leaks into the extracellular space. Necrosis is observed as a decrease in extracellular resistance (R_E). (Grimnes & Martinsen 2008, pp. 122-123; Haemmerich et al. 2002)

Secondly, the fluids may accumulate into extracellular space. The increase in ECF can be detected as a decrease in the extracellular resistance (R_E). Often related to the chronic wounds, the swelling is due to vasodilatation and the increased permeability of capillaries. As a result the fluid accumulates into the extracellular space (Jensen et al. 2007). Another possible cause for fluid accumulation into extracellular space is peripheral edema. Peripheral edema results from increased capillary permeability or impaired return of fluid by lymphatic system from interstitial space to vascular compartment. Lymphedema is a result of impaired function of the lymphatic system. Lymphedema usually occurs in the body extremities and involves abnormalities such as an enlargement of the limb. As a result of lymphedema, fluid accumulates in the extracellular space. (Abboud et al. 1995; Lauronen 2009)

Because these two mechanisms have opposite effect on the ECF, a careful diagnosis has to be made about the underlying medical conditions of the subject. In addition to this the nature of the wound itself has to be assessed explicitly. This is important for correct interpretation of the bioimpedance measurement results.

The proposed bioimpedance device is optimized in terms of simple design, component amount and current consumption. The device works on an indicator basis, the aim is to reliably indicate the direction of change in the extracellular fluid volume by measuring the impedance of the wound site. Obtaining the absolute impedance values is not necessary. It should be kept in mind that the change in the measured impedance is inversely related with the change in the volume of the tissue compartment in question as proven in the section 3.1.2. The instrumentation needed for the monitoring purpose is not complex, for example the phase angle measurement is not necessarily needed. The accuracy of the measurement results compared to the reference method is not strictly crucial, if only the direction of the change between different

measurement sets is same with the both devices. The possible systematic measurement error therefore does not hamper the reliability of the device. Basically, to estimate the change in ECF only low frequency impedance data (Z_{LF}) would be needed. However, to reduce the possibility of false indications high frequency impedance data (Z_{HF}), correlating with the TBF, is needed for calculation of Z_{LF}/Z_{HF} ratio. By using the ratio of Z_{LF}/Z_{HF}, unwanted changes in the impedance data due to movement of the limbs or electrode displacement between the measurement sets can be reduced. When a limb is bent or the electrodes are displaced, the impedance changes but the impedance ratio is unaffected, the ratio between body fluids remains same (Bourne 1996, p. 408).

To interpret the measurement results correctly, it is important to choose the most appropriate electrical equivalent to describe the tissue in question and its functionality. 2R-1C electrical tissue equivalents introduced in the section 3.1.3 are often used. The small area (the smaller the inter electrode space, the smaller the penetration depth) with relatively low frequencies (the higher the frequency, the deeper the penetration into tissue) on the surface of the body would suggest that the series model also known as the skin model would be preferred. However, chronic wounds tend to appear to have lost effectively all of the outer skin layer if not the entire skin tissue on the site. The dermis and subcutaneous tissues are exposed. Therefore, it might be better to use the parallel model since it is thought to describe the electrical behavior of tissues in a more general way.

As mentioned in section 3.1.3, at least three impedance measurement sets and the phase angle data from each is needed for separation of ECF from ICF. Now the proposed device takes two impedance measurements, one with a low frequency (Z_{5kHz}) and one with a high frequency (Z_{100kHz}), and does not measure the phase shift. The separation of the fluids cannot be made with such modest data input. Therefore, certain assumptions have to be made.

1. The capacitance of cell membranes does not change. This means that both the amount of ICF and the amount of the cells do not change. Therefore the reactance X_C and the resistance R_I remain constant regardless of the time between the measurement sets.

2. At low frequency, the current travels only through ECF or the amount of the current through the TBF branch remain constant regardless of the time between measurement sets.

These premises can be justified by the fact that usually during inflammation the fluid accumulates mainly into extracellular space of tissue. This however requires careful examination of the nature of the wound, since these assumptions close out the possibility for detection of the changes of ECF in case of ischemic tissue. By using the assumption (2) and the equation 18, equation 22 can be derived.

$$\frac{Z_{5kHz}}{Z_{100kHz}} = \frac{R_E}{\frac{R_E \cdot (R_I - j \cdot X_C)}{R_E + R_I - j \cdot X_C}} = \frac{R_E \cdot (R_E + R_I - j \cdot X_C)}{R_E \cdot (R_I - j \cdot X_C)} = \frac{R_E + R_I - j \cdot X_C}{R_I - j \cdot X_C} \quad (22)$$

By using assumption 1, we can write

$$k = R_I - jX_C = constant \quad (23)$$

$$\frac{Z_{5kHz}}{Z_{100kHz}} = \frac{R_E + k}{k} = \frac{R_E}{k} + 1 \quad (24)$$

From the equation 24, we may deduce that the change in the ratio of the 5kHz and 100kHz impedance modulus is dependent only by the change of the R_E which correlates with the amount of the ECF.

The number of patients with chronic wounds is expected to rise in numbers in the near future as contributing factors like the number of elderly people, with type 2 diabetes and infections caused by antibiotic resistive bacteria increases. There also exists a growing effort to shift the site of wound care treatment from an expensive hospital environment to a cost effective home care (Terry et al. 2009). Naturally, before home care is possible the chronic wound has to be taken into control with proper treatment including, for example debridement and medication. Nowadays the assessment of the healing of a chronic wound in home care is usually based in on the visual assessment of the wound area by visiting nursing staff. Digital photos are often taken of the wound site and used for assessment of progress. Plain visual assessment might not be the enough in case of a recovering chronic ulcer, additionally constant removal of wound dressing may hamper the delicate recovery process. There exists a need for objective and simple way for assessing the chronic wound healing without compromising the healing process. The bioimpedance method could be utilized for this purpose. Chronic ulcers are also known to have a high recurrence. Recovering chronic ulcer patients face a remarkable risk for re-ulceration and therefore a need for constant monitoring and assessment of wound healing is obvious, also for home care patients. The accumulation of fluid into tissues may precede a chronic ulceration. For example in pressure ulcers and diabetic ulcers the inflammatory changes with resultant edema may occur 3 – 10 days before skin breakdown (Jensen et al. 2007). Objective monitoring of the fluid status at wound area could give valuable time for preventing the re-ulceration. A miniature bioimpedance device could be integrated into a drug releasing patch or into simple antiseptic or antibacterial wound cover without additional inconvenience to the patient. The device could be programmed to take measurements in a certain time of a day. Then the measurement data could be sent wirelessly to a home computer and then via internet to a physician, who could evaluate the progress and in case of signs of situation worsening advise patient to meet the physician. Patients suffering from for example chronic venous disease consequently in many cases suffer also from limb

edema. This can be treated by using a compressing sock. (Hietanen et al. 2003, pp. 153-155) The effectiveness of compression treatment could be assessed by using bioimpedance measurement. Miniature bioimpedance meter attached to a compression sock would be for ideal also for this purpose.

3.2 Instrumentation theory

A bioimpedance meter is composed of two main operative blocks; the current feeding and the voltage measurement circuitry. The interface with a human body is executed using electrodes. This section represents proposals for the implementation of a miniature bioimpedance device. The proposals are critically discussed and evaluated. Various excitation current waveforms are also analyzed and evaluated. Particularly, the current feeding circuit can be implemented in various techniques. Certain methods for current feeding and voltage sensing are reviewed; their pros and cons are evaluated keeping in mind the special requirements for this type of a device. The power consumption and safety issues related to a portable bioimpedance measurement device are also briefly discussed.

3.2.1 Requirements for the device

The fundamental requirement for a patch integrated bioimpedance device is small physical size. The device proposed in this Master of Science thesis is a fully functional prototype and the possibility to further miniaturize the device in the later prototypes has been one of the key design parameters.

Equally important is the logic simplicity of the design with a minimal effect on the measurement accuracy and resolution. Therefore, one important aspect of the thesis work is evaluating the effect of design simplification to measurement accuracy. The initial requirements for measurement accuracy are not defined specifically. This bioimpedance measurement device is designed to indicate fluid changes in small tissue volumes. Therefore, the measurement range will be rather small; impedance values from few ohms to few tens of ohms are anticipated. Such low impedance values are a challenge for the measurement instrumentation. Smallest impedance values might be possible to measure with a reasonable accuracy of one decimal.

The number of components, particularly active components and ICs should be minimized as the novel manufacturing techniques like printable electronics are not yet capable of working very well with the components having a complex internal structure. The nature of bioelectrical measurements often incorporates dealing with very small differential mode signals, therefore high amplification is needed with very high input impedance so that the voltage measurement circuitry will have a minimal effect on the load and vice versa. High common mode rejection characteristics are also essential to low-level signal measurements, because of the relatively high undesired common mode

signals coupling to the inputs of an instrumentation amplifier. Common mode signals arise from various possible sources; Capacitive, inductive or electromagnetic coupling from external devices and ground loops in the instrumentation. In an ideal case only the information carrying differential signal would be amplified, in real world this is far from the truth. Practical limitations of an amplifier such as internal resistance imbalance or transistor non-idealities limit the CMRR. CMRR is also a highly frequency dependent feature and therefore working with relatively high frequencies for example 100kHz degrade the instrumentation amplifier capabilities. Instrumentation amplifiers are specifically designed to meet the requirements mentioned above and employing an instrumentation amplifier in the voltage measurement circuitry is practically mandatory. (Nilsson & Riedel 2001, pp. 203-205; Hambley 2000, pp. 112-113)

The current feeding circuitry faces a requirement for highest possible output impedance. High output impedance ensures that rapid changes in the load resulting from for example movement artifacts or imperfect electrode contacts have minimal degrading effect on the excitation current. Therefore, also current feeding circuitry requires the use of operational amplifier.

Utilization of low and high frequency excitation currents is essential in order to make a distinction between the extracellular fluid and the total fluid. The low frequency excitation is limited to 5kHz due to the safety issues. In an ideal case the high frequency signal would be in megahertz scale, however practical limitations restrict usage of such frequencies, since stray capacitances and noise coupling would decrease signal to noise ratio into unacceptably low levels. These adverse effects could be overcome with careful and highly complex design that is not tolerable in this case. Therefore, the high frequency excitation is set to 100kHz . Working with high frequencies and high gains imposes special demands for operational amplifiers. Speed and bandwidth characteristics like slew rate and gain bandwidth are the most crucial in this case. The higher requirements for SR and GBW mean accepting compromises with other characteristics like power consumption and noise characteristics. Additionally, the use of single supply limits the range of suitable amplifiers with appropriate characteristics.

As the device is a battery powered portable device, the power consumption should be minimal. However, this is not the most crucial requirement to fulfill. The purpose of the measurements is not to indicate dynamically changing events, instead changes in the tissue fluid level can be considered to output a stationary signal changing only in a matter of hours. For this reason the device is designed to take discrete measurements only few times a day, each measurement taking only a few seconds and for the rest of the time the device will be in sleep or off mode. Therefore, it is reasonable to expect a quite long operational time, regardless of the power consumption of each measurement sets.

3.2.2 Excitation current waveform

According to French mathematician Joseph Fourier any periodic waveform can be presented as a sum of sine and cosine functions in a mathematical series expansion known as the Fourier series. Fourier method reveals the frequency contents of a waveform. This approach is useful to excitation waveform analysis. A periodic waveform in frequency analysis presents a line spectrum with the fundamental frequency and its multiples called harmonic frequencies. (Nilsson & Riedel 2001, pp. 833-835) The problem associated with Fourier series presentation is that very different waveforms may give an identical frequency spectrum. The amplitude magnitude frequency spectrum does not contain all of the necessary information; the phase information is lacking. (Grimnes & Martinsen 2008, pp. 220-221)

Sinusoidal wave is the most widely used excitation waveform in bioimpedance measurements. It is a periodic waveform. In an ideal case it includes only the fundamental frequency and a possible DC level. The Figure 3.8a shows the frequency spectrum of the sine wave. Sine wave is very attractive for excitation waveform since undesirable harmonics are basically non-existent, only transients arising from the non-idealities of the circuit may exist. However, sine wave generation requires reasonably complex hardware implementation from a digital signal and sine wave generation from external analog circuit can be bulgy. Digital waveform generator ICs exist and are widely used, but the cost, complexity and power consumption are questionable.

The most straightforward solution to excitation waveform generation considering the hardware would be the square wave modified directly from the microcontroller's digital output. However, any waveform containing sharp descending or ascending parts may introduce large amplitudes of undesirable higher harmonic components. The frequency spectrum of the square wave can be seen on the Figure 3.8b. By using any non-sinusoid excitation waveform the target is excited at several frequencies simultaneously. Certain studies have made use of this feature in order to obtain rapid spectroscopy measurement with extremely low power consumption, this way even the fastest changes in the impedance can be monitored. The problem incorporated to the use of modified square wave, sine wave derivatives or pulse wave is that the spectral power density is not spread equally to all frequencies. In theory, this drawback can be overcome by shortening the pulse width to zero, increasing the pulse amplitude to infinity and keeping the product at 1. Obviously this is not obtainable in practice. Use of high pulse amplitudes also creates non-linearity problems, which are not that apparent when dealing with periodic waveforms.

Triangular wave is a compromise between accuracy and simple implementation. Triangular wave is obtained from square wave by low pass filtering. Frequency analysis in the Figure 3.8c reveals that triangular wave contains only odd harmonics which roll off much faster than in a square wave. This is easily observed from the Fourier series of triangular wave as the harmonic number is in inverse square. The amplitude of given harmonic of a square wave can be calculated according to the equation 25 and similarly

for a triangular wave according the equation 26. In which the letter N represents the integer multiple of the fundamental frequency. For square and triangular wave the N is an odd number. A_1 is the amplitude of the wave at the fundamental frequency.

$$A_N = \frac{A_1}{N} \tag{25}$$

$$A_N = \frac{A_1}{N^2} \tag{26}$$

For example, a triangle wave with fundamental frequency of 100Hz with amplitude of unity would have a harmonic at 300Hz with amplitude of 0.111 and a harmonic at 500Hz with amplitude of 0.04. The table 3.3 shows the harmonic frequencies of the triangular wave with 100kHz base frequency and the decay of the unity amplitude of the voltage.

Table 3.3 *The harmonic frequencies and the decay of amplitude of triangular wave.*

Order	***Harmonic frequency (kHz)***	***Amplitude (V)***
n = 1	100	1
n = 3	300	0.11
n = 5	500	0.04
n = 7	700	0.02
…	…	1 / (n^2)

In addition to a reasonably fast decay of amplitude in respect to harmonic frequency, higher harmonics tend to have less contribution to the impedance value due to capacitive features of tissue. As the purpose of this measurement device is not to produce precise absolute impedance values but rather work as an indicator of change in ECF, the adverse effects of harmonic frequencies are not that crucial. The bigger problem might be related to the limited bandwidth of the instrumentation amplifier.

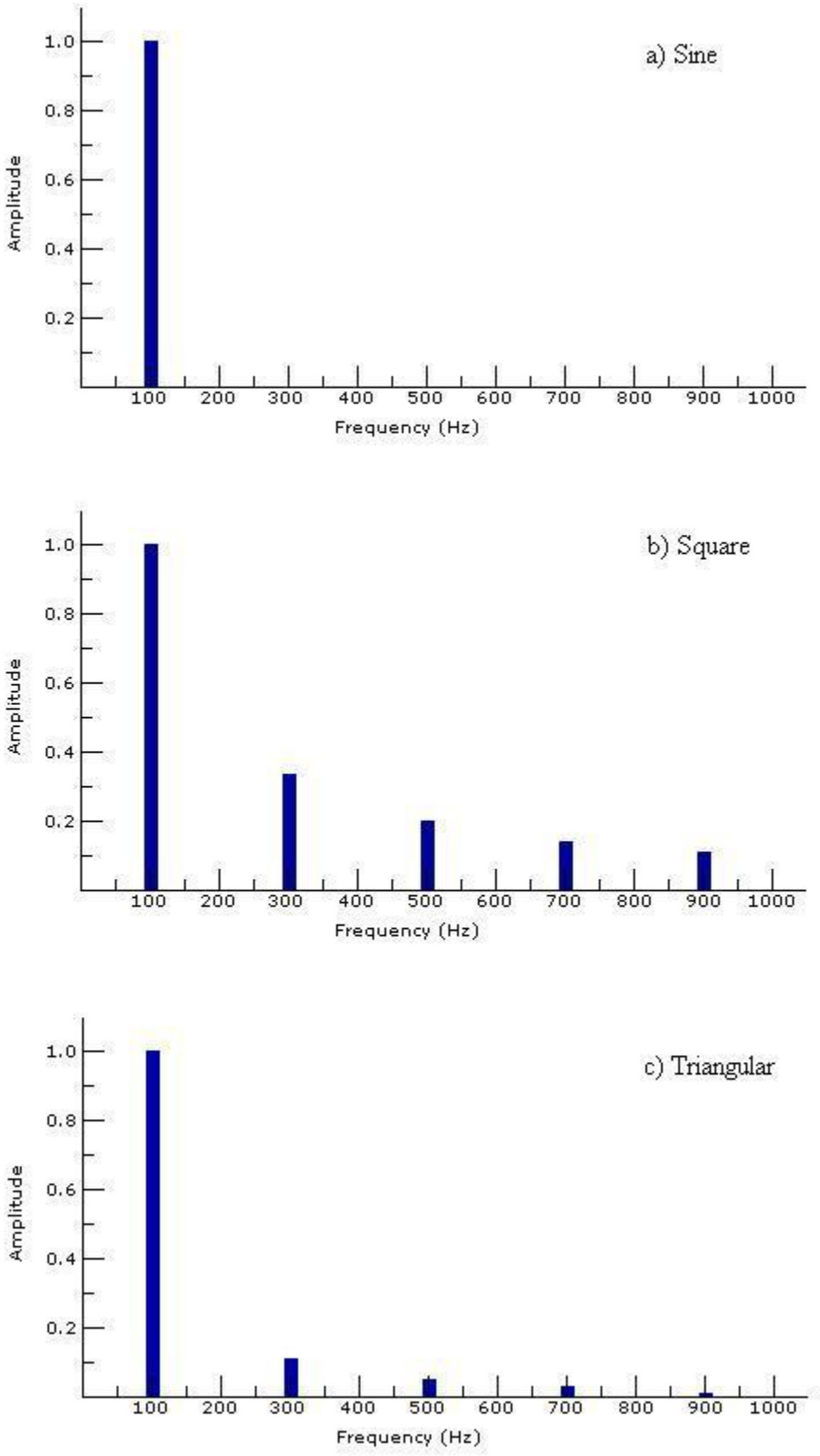

Figure 3.8 *The frequency content of a) sine b) square and c) triangular waves (Sievers 2006).*

Other proposed excitation functions found in literature include Gaussian and its derivatives, derivatives of sine function and chirp signals.

3.2.3 Excitation current source proposals

In this section some methods of generation of excitation current are introduced briefly. Their main characteristics, pros and cons are discussed.

Microcontroller PWM output

Timer/counter is an essential peripheral of a microcontroller. As the name timer/counter implies, it basically counts either time duration or a number of events. The timer/counter block provides various modes of operation. In the most basic mode of operation the timer/counter just counts upwards predetermined clock cycles and rolls over when it reaches the top value giving an interrupt request for CPU. By utilizing this feature a triangular wave can be created with a desired base frequency and a minimal number of external components. The output pin of the microcontroller incorporated with the timer/counter is set to toggle up and down in a desired frequency by manipulating the registers of the timer/counter, thus outputting a square wave with a constant 50% duty cycle. The output pin is connected to an integrator or a simple RC low pass filter which results in a triangular wave if the time constant of the low pass filter is set high enough compared to square wave input (Figure 3.9 and Figure 3.10). The RC filter does not affect to the base frequency of a triangular wave, hence to achieve a triangular signal with 100kHz frequency the square should also toggle in the frequency of 100kHz. The time constant can be chosen to be adequate by simply choosing an appropriate value for the resistor. However, a high time constant has an adverse effect on the triangular wave amplitude and thus increases the power loss. Time constant determines the rate on which the capacitor charges and discharges, thus a compromise has to be made between the amplitude of a triangular wave and its waveform quality. Excessively low time constant results in a distorted triangular waveform. Nevertheless, the overall simplicity of this method makes this option very attractive.

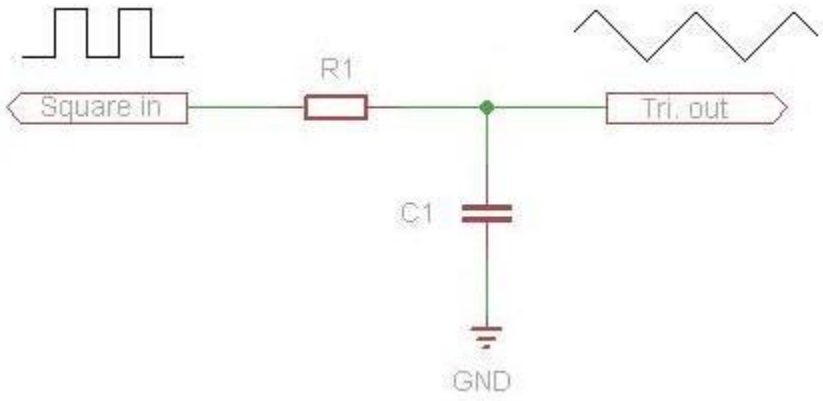

Figure 3.9 *Formation of a triangular wave from square wave input.*

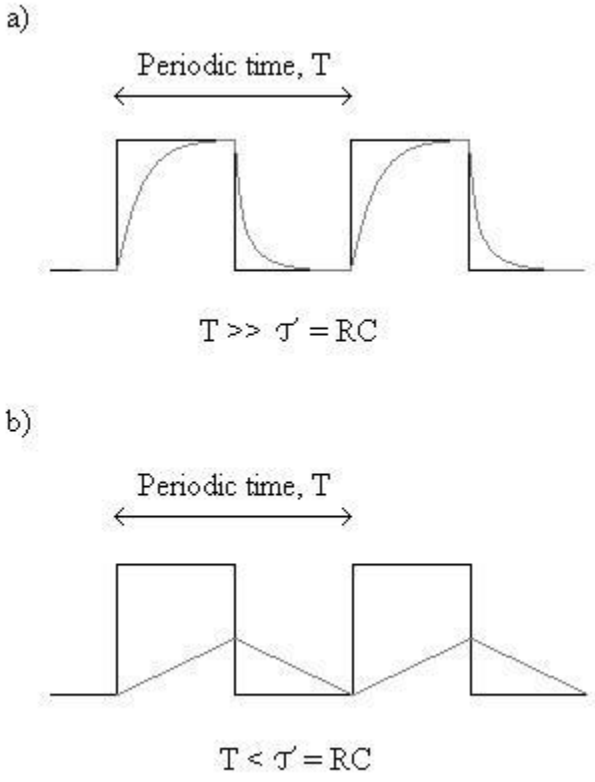

Figure 3.10 *The effect of the time constant, the resulting output waveform is marked in gray. a) The square wave period T is much larger than the RC lowpass filter time constant τ. b) The square wave period is smaller than the time constant.*

Another way to implement the microcontroller timer/counter output for waveform generation is to use its pulse width modulation -mode to generate a sine wave. This method requires a minimal amount of components as well, just a plain RC low pass filter. However, this method is a bit more complicated by the means of the code and it

also requires a much faster clock speed for the timer/counter than just the basic output pin toggle. The fundamental principle is to change the duty cycle of the output square wave steadily from 50% to 100% and opposite, then from 50% to 0% and opposite. The change of duty cycle from 50% to 100% corresponds to one quarter of output waveform that can be described as an approximation of sine wave. 50% duty cycle gives analog output with half of the supply voltage, corresponding to the angle zero of sine wave in the phase diagram representation, the starting point of sine wave so to speak. The figure 3.11 shows a sketch of the PWM input and the sinusoidal output waveform.

Each increment or decrement in the duty cycle is a sample point for the sine wave. To obtain even a very rough sine wave approximation at least 10 sample points should be included per sine wave period. However, this small number of sample points results in a barely recognizable sine wave. Thus, at least 40 sample points per sine wave period should be included. This means that the duty cycle should change in 5% steps and that the PWM frequency should be 40 times higher than the sine wave frequency; If a 100kHz sine wave with 40 sample points per period is desired, then the PWM frequency should be 4MHz. This is quite a challenging requirement for CPU but obtainable. The PWM output itself could be created by using an output compare register (OCR) which is incremented or decremented by a desired value every time the timer/counter overflow occurs. This results in a steadily varying duty cycle. It is preferable to use phase correct mode of PWM to obtain a symmetrically changing PWM output. The phase correct mode of PWM is based on the dual slope operation. This mode however reduces the maximum usable output frequency. The advantage of this method is that the timer/counter may run by itself and no processor power consuming memory operations are needed. The role of an RC low pass filter is similar to the method described above in the case of triangular wave generation with an exception that due to the changing duty cycle the charging and discharging of the capacitor is disturbed so that either charging or discharging will be left unfinished. This results in an either rising or falling edge of resultant sine wave depending on the phase of the duty cycle change.

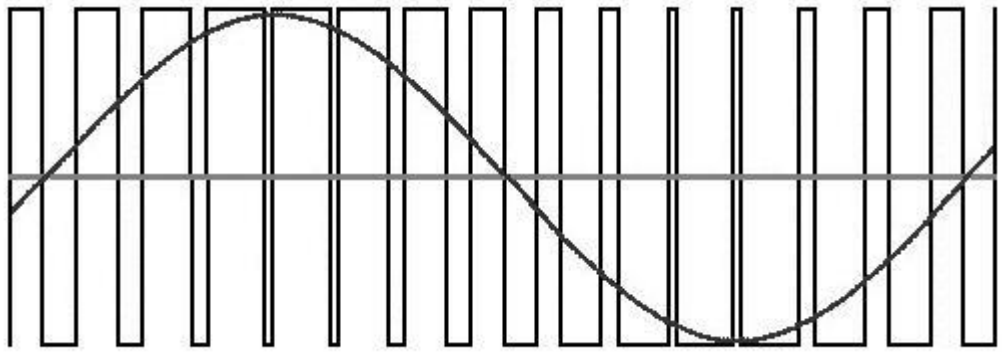

Figure 3.11 *A sketch of a sinusoidal output wave generated by PWM input and a lowpass filter. The DC voltage level is the half of the supply voltage.*

The third way of utilizing a microcontroller to create excitation waveform is to use table values stored into the program memory. This method has lot of similarities with the method described above and also outputs PWM signal with varying duty cycle. Instead of the timer/counter rolling all the time and updating output compare register automatically, this method retrieves the subsequent output compare register value from the look-up table by using an interrupt service routine (ISR) every time the overflow occurs. The larger the look-up table, the more precise sine wave approximation it generates after an appropriate filtering. However, retrieving a value from the program memory takes time and processor power. The timer/counter requires a very high clock speed. Certain 8-bit microcontrollers, like Atmel's ATtiny26A, provides a standalone up to 64MHz clock for timer/counter using phase locked loop -design. Since retrieving data from the memory requires the processor to be active in the process, it is unlikely that the processor could be able to perform other heavy duty tasks like analog to digital conversion simultaneously at such high excitation wave frequency demands. A microcontroller providing a direct memory access feature could overcome this problem. The idea of DMA is that it allows certain microcontroller blocks to access memory independently of CPU, thus conserving processor time.

Digital to analog converter methods

Implementation of digital to analog converter for waveform generation is an interesting option. A variety of DAC topologies are available for use. An external DAC IC is one option, additionally certain microcontrollers provide an internal DAC. Yet another way is to use an R-2R ladder network for a simple and cost effective digital to analog conversion. R-2R ladder requires only resistors to be used. Monolithic laser trimmed R-2R ladders are available with a high accuracy and stability (Franco 2002, pp. 570-572). For an 8-bit DAC, 16 resistors are required with only two different values (Figure 3.12). With 8-bit R-2R ladder it is possible to output 256 different voltage levels. The Figure 3.13 shows a sketch of a 3-bit R-2R ladder sine approximation output. One disadvantage in the utilization of the R-2R ladder is that it occupies a fairly large amount of output pins from the microcontroller. 8 output pins for an 8-bit ladder. In general DACs are also affected by a quantization error and non-linearities.

The operation principle is quite simple. Digital input ranges from the most significant bit (MSB) to the least significant bit (LSB) and the bits are switched to be either 0V or V_{REF}. The MSB causes the greatest change in the output and the LSB causes the smallest. Therefore it is possible to output any analog output between 0V and V_{REF} just by inputting corresponding digital input. (BI Technologies, R-2R Resistor Ladder Networks) This way the analog output will approximate the desired waveform by voltage stepping, this being a more straightforward method for generating analog waveform than varying duty cycle PWM. The output voltage can be calculated according to the equation 27 in which V_{ref} represent the output voltage of the microcontroller pin when logical 1 is written. The $VALUE_{dec}$ represent the value of the

R-2R ladder in decimals, for example an 8-bit device with 10011001 has $VALUE_{dec}$ = 153. The N is the number of the bits of the R-2R ladder network.

$$V_{out} = V_{ref} \cdot \frac{VALUE_{dec}}{2^N} \tag{27}$$

With a sufficiently high amount of sample points there will be no need for output filtering. However, low pass filtering smoothens the output signal with minimal design effort (Day & Stein 1997). The sine wave signal can be generated by implementing a look-up table stored in the program memory. This method requires CPU to constantly retrieve values from the memory, thus creating problems discussed earlier. Another way is to use a timer/counter to count up and down constantly to generate a sine wave with the desired frequency.

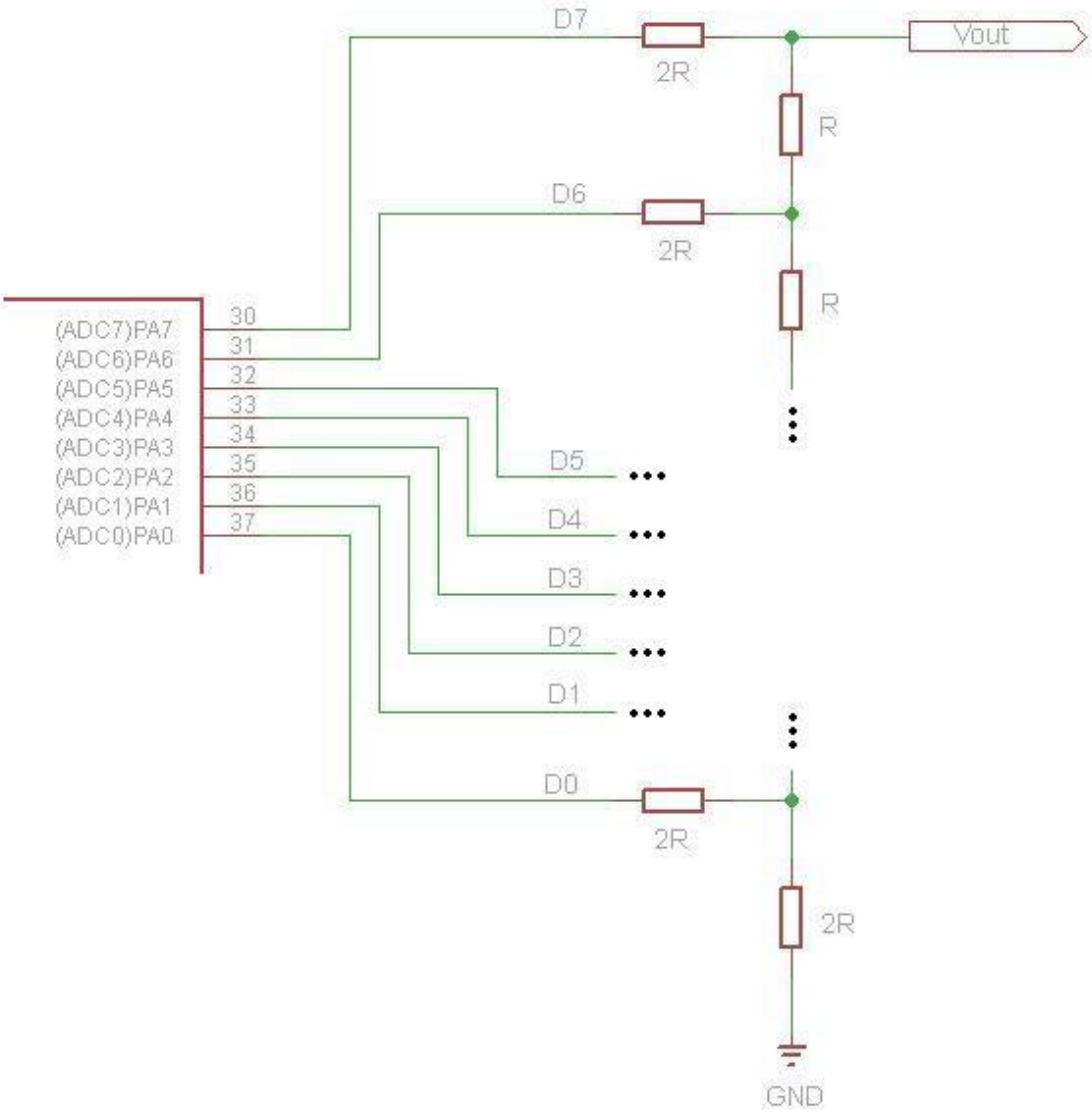

Figure 3.12 *8-bit R-2R Ladder network. D7 is the MSB and D0 the LSB.*

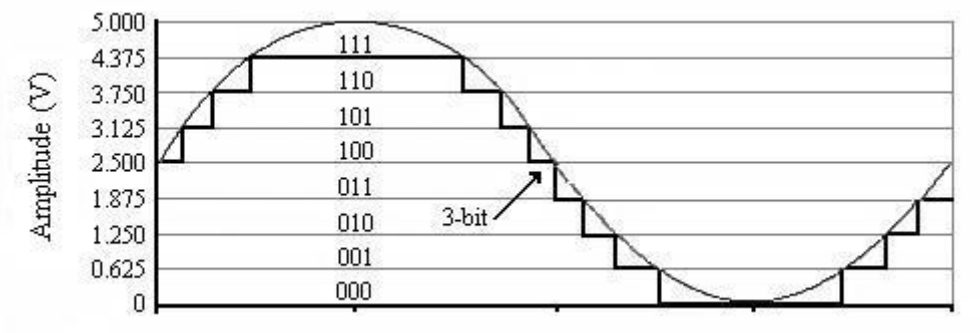

Figure 3.13 *Sketch of the output voltage of a 3-bit R-2R ladder network compared to the ideal sine waveform (BI Technologies, R-2R Resistor Ladder Networks; Day & Stein, 1997).*

External DAC ICs are also available with parallel or serial interface. Serial interface requires only one digital input. However, timing limitations this method rule out when analog output frequency requirements are high, in addition the power consumption is higher. Certain microcontrollers include internal DAC. One example is Atmel's XMEGA microcontroller -family. The XMEGA -family microcontrollers also include a DMA feature, which would allow the use of a look-up table without excessive CPU loading. Unfortunately, the XMEGA family microcontrollers are plentiful with the other features included with no use in this application, therefore being a bit too hefty for this purpose.

Hardware wave formation methods

Hardware based signal generators often yield a reasonably good quality waveforms with a wide frequency spectrum. Oscillators are able to operate without an externally applied input signal as they use some fraction of the output signal created by the feedback network as the input signal. However, they require a relatively large amount of components and amplitude or frequency adjustment can be quite tricky to accomplish. These defects make this solution out of scope for this application. The two main oscillator classes are relaxation and sinusoidal. Relaxation oscillators generate a sawtooth, triangular or some other non-sinusoidal waveform. (National Semiconductor, Inc. 2009)

A large variety of hardware based signal generation designs exist. The most popular designs of this kind are based on the Wien bridge, phase-shift or quadrature oscillator circuits. The functional component in these circuits is an operational amplifier, which is driven into an unstable state to create steady oscillation. To remove the distortion effect, some kind of amplitude control is required. Some designs use also lamps or crystals as a functional component. (Mancini & Palmer 2001)

Direct digital synthesizer

Direct digital synthesis provides a variety of waveforms, high accuracy, wide bandwidth, fine noise performance, simple tuning of both frequency and phase with a high tuning resolution in a single chip with a convenient interface to microcontroller. These features make DDS a very attractive signal generation method.

Direct digital synthesis resembles significantly to the DAC method with look-up table discussed previously. The sine wave table with amplitude information is stored into memory of a DDS chip and the table values are converted into analog form by an internal DAC. With subsequent low pass filtering the edges of steps are smoothed. An external reference clock signal is brought to the DDS chip. The core of the DDS is the numerically controlled oscillator, which provides very good frequency tuning properties for DDS. The Figure 3.14 represents a simplified block diagram of the DDS. NCO is consisted of a phase accumulator and a phase to amplitude converter, the latter being basically just a memory block containing the sine table. The phase accumulator outputs a digital sawtooth wave that is then converted to a digital sine wave by the phase amplitude converter. The phase accumulator is a certain type of a counter that increments its stored number in every reference clock pulse. The length of the word in phase accumulator (N) determines the resolution of DDS. The frequency tuning word (M) determines the actual output frequency. In fact the frequency tuning word determines the step size taken in the sawtooth output between each reference clock cycle. Finally, DAC converts the sampled sine wave to an analog form. (Stanford Research Systems, Inc. 2011; Analog Devices, Inc. 1999, pp. 5-9)

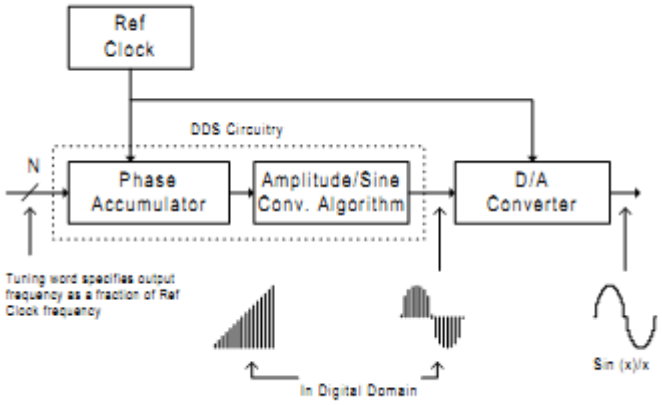

Figure 3.14 *Signal flow through the DDS architecture (Analog Devices, Inc. 1999, pp. 6-8).*

As the advantages of DDS are apparent, but some drawbacks also exist considering specific application of a bioimpedance meter with a miniaturization option. Although the interface of a DDS chip is reasonably simple, the overall design of the chip is very complicated. The complexity of the design hampers the further possibilities of

miniaturization of the bioimpedance meter and therefore should be avoided as much as possible. The power consumption of the DDS chip is also quite high. Yet another drawback is the high cost of the DDS chip.

3.2.4 Electrodes

Human body is an ion conductor and ions work as charge carriers in human body. Electrodes work as a charge carrier transducer between the metallic and non-metallic part of the circuit; the change from ion carriers to electron carriers occurs at the surface on an electrode. (Bourne 1996, p. 242)

One key feature concerning electrodes is the concept of polarization. Polarization occurs when current is able to flow in the electrode wires. The potential of an electrode will change from its equilibrium potential due to this current flow; the electrode is therefore polarized. An unpolarized electrode is in equilibrium potential and the net current flow is zero. Even though electrode is in equilibrium the electro-chemical reactions still occur, but at equal rates in both forward and reverse directions. Polarizable electrode refers to an electrode that is easily polarizable. The potential of an electrode will change significantly from its equilibrium even from a small current addition. The reason for this behavior is the slowness of the electro-chemical reactions on the electrode-electrolyte interface of the electrode and it is basically dependent on the electrode material. The rate of an electrode reaction in equilibrium can be expressed as an exchange current density; low exchange current density indicates a slow reaction, therefore a highly polarizable electrode and vice versa. A non-polarizable electrode is conversely not very sensitive to the change of current and has stable electrode potential. Closest to the perfectly non-polarizable electrode is silver-silver chloride (Ag-AgCl) electrode. Unfortunately this material is not biocompatible and cannot be used for long-term tissue contact. A platinum electrode is an example of a polarizable electrode. A platinum electrode is also biocompatible and therefore often used in implanted or invasive applications. Platinum electrodes are also often used in current feeding electrodes, since their polarization impedance is lower than of other materials. A low polarization impedance creates a smaller obstruction to the applied AC-current. A platinum electrode with black platinum coating has an even smaller polarization impedance. (Bourne 1996, p. 292)

Electrode-skin interface is a potential source for errors in biomeasurements. The outer layer of skin called stratum corneum is non-wetted and is consisted of dead cells. Therefore it has very high impedance compared to other layers of the skin and electrodes. The high impedance of stratum corneum results in a low amplitude signal and poor signal detection. Interfering signals like power line interference becomes significant and because of limited CMRR of the measurement amplifier, the interfering signals can easily hamper the measurements. Skin impedance is also highly frequency dependent, which may result in problems when implementing high frequency ranges. However, even a light abrasion of the skin surface removes very effectively dead cells

and provides direct access to the deeper layers of stratum corneum with higher water content. (Grimnes & Martinsen 2008, p. 261; Morin 2009) Another way to reduce skin impedance is to use contact electrolyte gel or paste. The purpose is to hydrate the stratum corneum and fill out spaces between the electrode and the skin for a better contact. The Figure 3.15 represents the electrical equivalent circuit of an electrode.

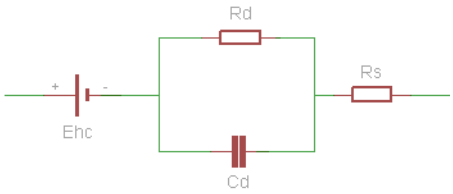

Figure 3.15 *Electrical equivalent circuit of an electrode. E_{hc} is the half-cell potential of the electrode and dependent on the electrode material. R_d and C_d refer to the impedance associated with the electrode-electrolyte interface and polarization effects. R_s is the series resistance associated with interface effects and due to resistance in the electrolyte (Morin 2009).*

Motion artifacts may greatly disturb measurements. Motion artifacts arise from two sources either from the movement of an electrode relative to the skin or the skin being stretched or deformed under the electrode. In the first case the charge distribution at the electrode-electrolyte interface is altered resulting to a change in electrode potential. This problem can be reduced by using recessed type electrodes where the contact electrolyte is contained in a sponge. This way the metal-electrolyte interface is clearly defined. In the latter case, the skin potential changes as a result of the skin stretching. This type of motion artifact can be reduced by abrasion of the skin. (Grimnes & Martinsen 2008, p. 270; Morin 2009)

In addition to the electrode material and contact electrolyte also the placement and the area of the electrodes have a great influence to the measurements. The sensitivity is proportional to the current density squared; therefore deeper layers of tissue contribute less to the result than more proximal. When the distance between electrodes, the inter electrode space, is reduced the sensitivity close to electrodes increases but the measurement depth is reduced (Figure 3.16). (Grimnes & Martinsen 2008, p. 190) Increasing the electrode area has an averaging effect on the measured signal. It also reduces the effect of the noise and provides improved frequency response. On the other hand, spatial resolution is reduced. (Grimnes & Martinsen 2008, p. 164) However, system noise altogether is dependent on the amplifier capabilities and other components on the measurement circuit as well; therefore just increasing electrode area will not necessarily improve the output substantially (Koch et al. 2002).

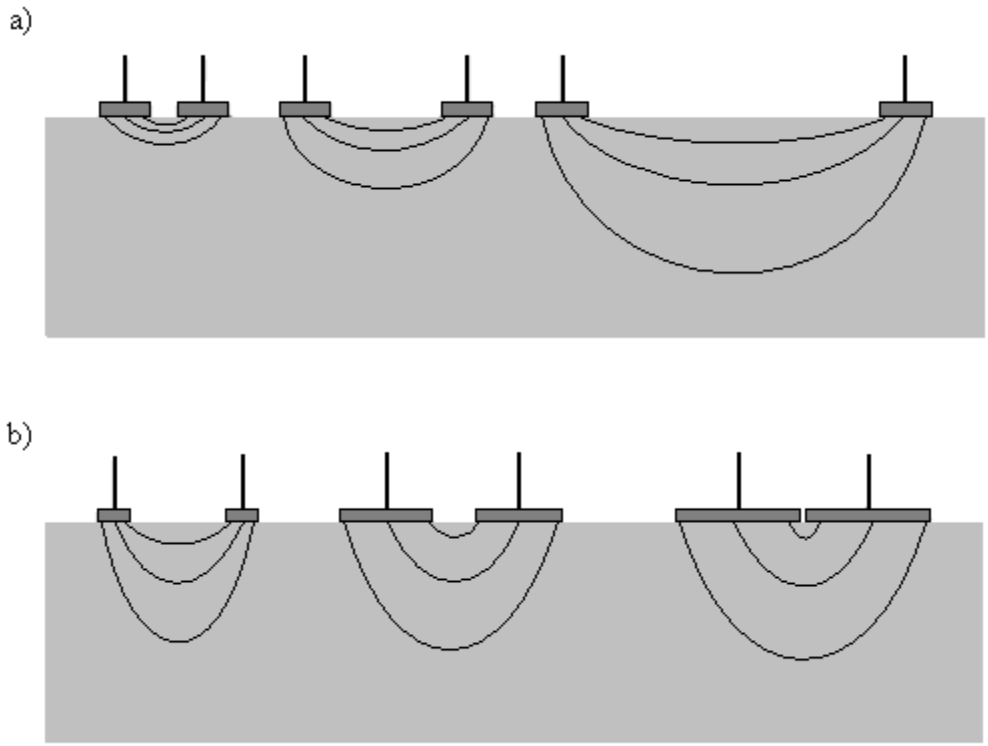

Figure 3.16 *The measurement depth. a) The measurement depth can be increased by increasing the IES. Increasing the IES also decreases the current density and therefore the sensitivity of the measurement. b) The measurement depth is not that dependent on electrode dimensions (Modified from Grimnes & Martinsen 2008, p. 190).*

3.2.5 Impedance measurement systems

The two primary electrode systems used in biomedical measurements include bipolar- and tetrapolar systems. The bipolar system utilizes one pair of electrodes. In a bioimpedance application, the same electrodes are used for both current feeding and voltage measurement. Bipolar measurements are strongly affected by the electrode impedance since the impedance of the electrodes themselves can be much higher than the impedance of the tissue. The voltage across each electrode is measured in addition to the voltage developed across the tissue. This leads to a problem of how to distinguish the tissue's impedance contribution from the electrodes. (Brown et al. 2000; Frounchi et al. 2009) A tetrapolar electrode system is consisted of four electrodes. One pair is used for excitation current injection and the other for measuring the voltage. Usually, the outer pair of an electrode is used for the current injection and the inner for the voltage measurement. However, according to reciprocity theorem current injecting and voltage measuring electrodes can be swapped without affecting to the measurement. This fact can be utilized in the quality assessment of the measurement system. (Grimnes & Martinsen 2008, p. 192, 196; Grimnes & Martinsen 2007) Tetrapolar method is by far

the most popular technique for measuring tissue impedance. The tetrapolar method with high output impedance of constant current source and high input impedance of voltage measurement circuitry compared to electrode and the underlying tissues eliminate the skin-electrode contact impedance. The reason for this action is that the current does not flow into the receiving electrodes and external polarization does not occur. Therefore tetrapolar system is insensitive to the changes in the skin-electrode impedances of both current injecting and voltage measurement electrodes. The measured impedance is ideally comprised of the impedance of the underlying tissues. Consequently, the major advantage over bipolar system is that the tetrapolar method greatly reduces electrode artifacts. (Ragheb et al. 1992; Grimnes & Martinsen 2007; Frounchi et al. 2009)

3.3 Safety issues

When electric current flows through body three kinds of reaction may occur (Webster 2008, p. 624):

1. Electric stimulation of excitable tissue
2. Resistive heating of tissue
3. Electrochemical burns and tissue damage by DC current and very high voltages

If the local current density is large enough to excite nerve endings, the subject feels a tingling sensation. This is the minimal current that induces sensation and is called a threshold of perception (Table 3.3). The threshold varies considerably among individuals and with the measurement conditions. Higher levels of current stimulate nerves and muscles so that involuntary contractions are possible. As the current increases further, involuntary contractions of muscles may prevent the subject from voluntary withdrawal. The let-go current relates to the maximal current at which the subject is able to withdraw voluntarily. Currents higher than this may lead into respiratory paralysis or ventricular fibrillation. Especially dangerous is the ventricular fibrillation since the heart does not recover from it when the current is removed. The normal heart rhythm returns only if a high current pulse from a defibrillator is applied to depolarize all the heart muscle cells simultaneously. (Webster 2008, p. 625-626)

The perception of human skin is dependent on the frequency, duration of exposure, current density, effective electrode area and skin site and condition (Grimnes & Martinsen 2008). For example frequencies lower than 10Hz increases the let-go current limit, minimal let-go currents occur at 50-60Hz frequencies and higher frequencies again increase the let-go limit. Longer exposure to current decreases the fibrillation threshold. The entry point of current also affects the threshold levels. Externally applied currents refer to macroshock which have far higher threshold level for fibrillation than

directly to heart applied microshock. High resistivity of skin has a large contribution to this protective effect. (Webster 2008, p. 627-630)

Table 3.3 *Threshold levels of perception and hazard at the frequency of 50/60Hz (Modified from Grimnes & Martinsen 2008).*

Current threshold	*Organs affected*	*Type*	*Comments*
0.3µA	Skin	Perception threshold	Electrovibration, mechanical
10µA	Heart	Microshock hazard	Myocardial excitation
1mA	Skin	Perception threshold	Nerve excitation
15mA	Muscles	Let-go limit	Loss of muscle control
50mA	Heart, lung, brain stem	Macroshock hazard	Nerve excitation

3.4 Existing functional patches

A transdermal patch is a common method for non-invasive drug delivery. The main idea is to overcome the skin's protective barrier to supply the drug into the bloodstream either by passive absorption or active penetration. A transdermal patch releases a well-defined dose of medication over a controlled time period. Transdermal drug delivery has some very distinct advantages, for example the non-invasive nature and painlessness. It is also a preferable method for drugs that have a high first pass effect, for a patient that has poor oral uptake or for a need of frequent administration. (Morrow 2004; Riordan)

Passive delivery is commonly used in nicotine patches but also in motion sickness treatments, hormone therapy and birth control. Passive delivery has certain disadvantages like that the speed of the drug absorption is dependent on the skin impedance and only limited numbers of drugs are capable of passing the protective barrier of the skin at proper rates. Because of these disadvantages major research efforts have been put into developing the active methods. (Morrow 2004; Riordan)

Active drug delivery involves addition of some sort of enhancer that increases the permeability of the skin. There exist a number of methods for this purpose for example utilization of iontophoresis, ultrasound, microneedles, lasers, chemicals including gels and electroporatic methods. Iontophoresis uses electrical charge to actively transport a drug through the skin and into the bloodstream. The device is consists of two chambers that contain oppositely charged drug molecules. The positively charged anode repels the

positively charged chemical and opposite. The electromagnetic field is therefore generated between the two chambers and will deliver the medicine through the skin in a controlled way. (Morrow 2004; Riordan) The Figure 3.17 below shows the mechanism of iontophoresis.

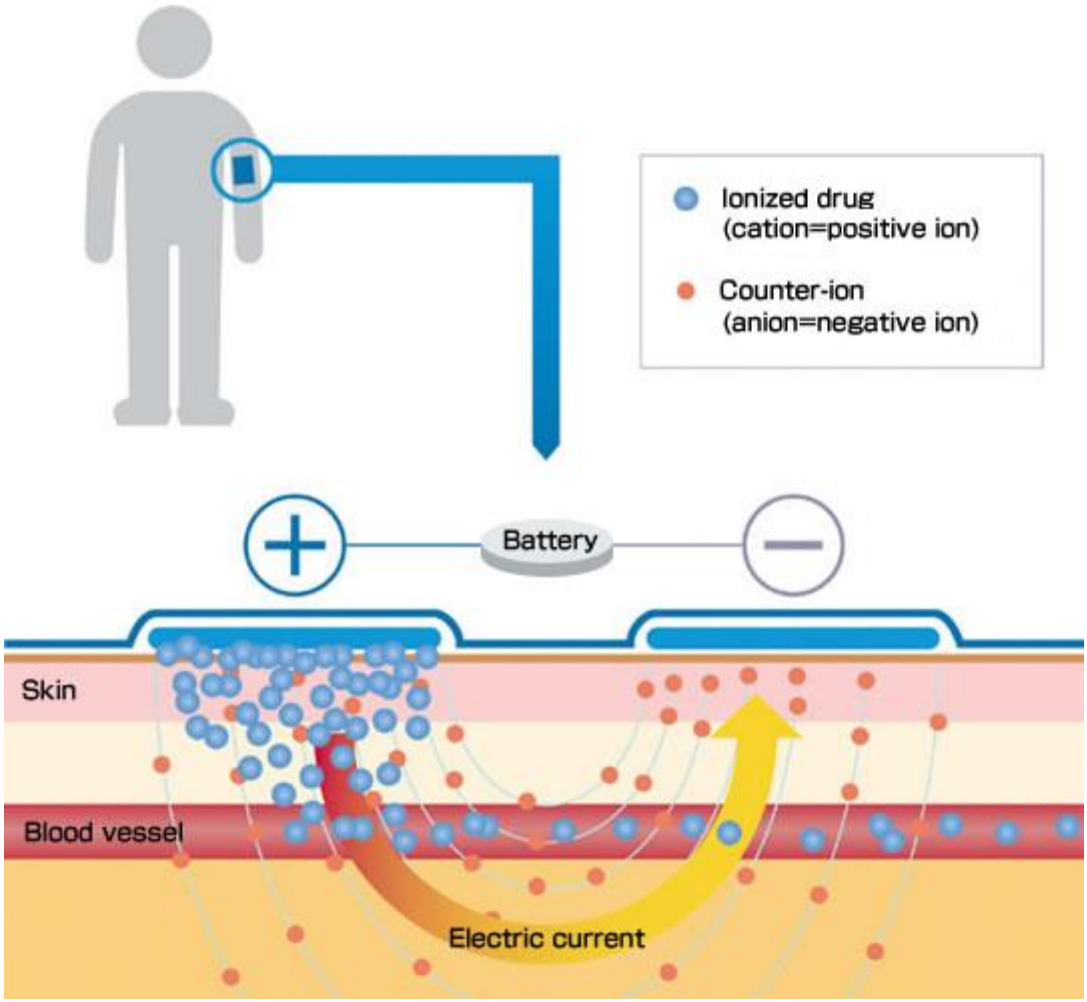

Figure 3.17 *The mechanism of iontophoresis (TTI ellebeau Inc. 2011).*

Another popular method is the use of microneedles to penetrate the outermost layer of the skin. The needles do not penetrate deeply enough to stimulate the nerves; therefore the process is virtually painless (Figure 3.18). This technology is often combined with an electronically controlled micropump that delivers the drug at a specific time or when needed. This method has a wide variety of possible applications for example in delivery of vaccines or pain medication. These devices have also potential to place drugs into a very specific location in the body where the special immune cells reside, making it possible to modulate the immune system of the body. (Hewlett Packard Company 2007; Simola 2010)

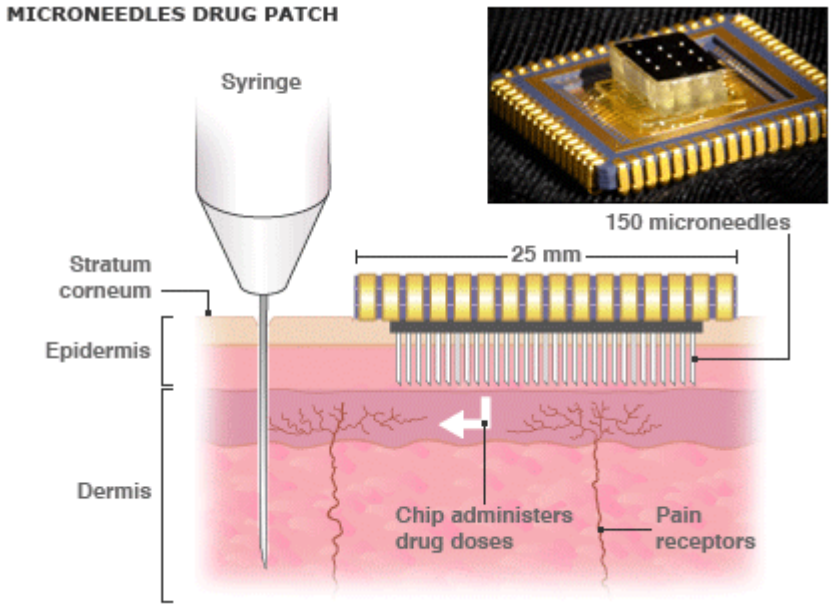

Figure 3.18 *Microneedles patch developed by Hewlett Packard. A microchip controls the dose and the time of the day the drug is released. The patch would be especially useful for example people suffering from diabetes (Hewlett Packard Company 2007, according to BBC News 19. September 2007).*

Measurement of skin impedance to obtain optimal drug delivery is an important factor. In addition to this, in case of wound healing treatment a small bioimpedance device could be installed to a patch type of drug delivery system to monitor the effectiveness of the treatment.

4 Materials and Methods

4.1 Hardware design

This section contains the description of the electronics design process of the bioimpedance device. Firstly, the proposed bioimpedance device is presented in a block diagram level with descriptions of the main functional parts of the device. Secondy, the bioimpedance device is represented in a more detailed schematic design level with reasoning for the component selections. Then, the hardware simulation results are presented comprising the current feeding circuit and the voltage measurement circuit. Finally, at the end of this chapter the key principles of the layout design of the bioimpedance device are described.

4.1.1 Block diagram

The Figure 4.1 represents the block diagram the bioimpedance device. The block diagram contains only the main functional parts of the device. For example, the power supply, the user interface, the microcontroller and other auxiliary parts are not included.

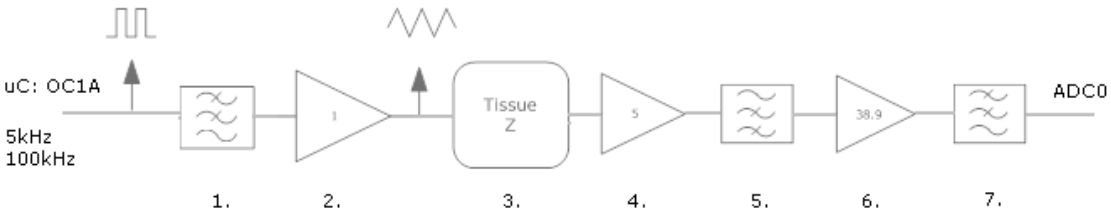

Figure 4.1 *A simplified block diagram of the bioimpedance device, current feeding and voltage measurement. 1. Low-pass filter. 2. Voltage to current converter. 3. Load. 4. Instrumentation amplifier. 5. High-pass filter 6. Operational amplifier (primary gain). 7. Moving average filter.*

Power supply

Unregulated supply voltage for the bioimpedance device is 6V. It is generated coupling two 3V lithium button battery cells in series. The battery holder is installed on a standalone PCB board and connected to the bioimpedance device via two leads, positive voltage and ground. The standalone PCB board for power supply makes it easier to deploy some other kind power source if necessary. A shunt regulator creates a stable

4.4V output from the unregulated 6V battery power supply. This 4.4V is used as supply voltage for the microcontroller, amplifiers and other components on the circuit. Reference voltages for the instrumentation amplifier and the microcontroller AD-converter can be chosen to be either 2.048V produced by a precision voltage reference or $V_{cc}/2$ from a buffered voltage divider. Also 2.56V internal reference voltage can be used for the AD-converter. Reasoning for the optional reference voltages is to make it possible to test the influence of fairly unstable voltage references like the voltage divider and the microcontroller internal reference to measurement accuracy. $V_{cc}/2$ is also used as a virtual ground for the voltage to current converter.

Push buttons

The bioimpedance device is controlled by the user with four pushbuttons. One button is used to output the 5kHz excitation current and another one to generate the 100kHz excitation current. Third button sends the measurement data to PC or erases the memory. One button is used for resetting the device in a fault situation.

Microcontroller

The microcontroller generates the square wave of desired frequency to one of its outputs to be transformed into triangular wave by the current feeding circuitry. It also executes the AD-conversion, averaging and storing of the measurement result. The microcontroller sets the digital potentiometer to the desired value, processes various interrupts and timer functions and also handles the data transfer to PC.

Current feeding

The current feeding circuit generates the triangular excitation current fed into tissue. The microcontroller produces the square wave of a desired frequency to one of its outputs. The square wave is then filtered by a passive low-pass filter and consequently transformed into the triangular waveform. The digital potentiometer is used for changing the cut-off frequency of the low pass filter according to frequency of the square wave. The triangular voltage is then converted to current by a simple transadmittance voltage to current converter. The resulting triangular current is then fed to the tissue via electrodes.

Voltage measurement

The current applied to tissue together with tissue impedance results in voltage difference which is measured differentially by using the instrumentation amplifier. Minimum gain of 5 is drawn from the instrumentation amplifier to maximize the usable frequency bandwidth and the main amplification is done by the second amplifier stage. Low-pass filters are introduced at the inputs of the instrumentation amplifier to provide artifact suppression and a path for DC bias current. After the first amplifier stage the DC level is removed by a high pass filter. After the second amplifier stage a moving

average filter is implemented to provide a stable but still sensitive enough DC voltage to be AD-converted by the microcontroller.

Analog to digital converter

The AD-converter converts the measured analog voltage signal into digital binary form. The measurement signal is effectively half wave rectified by the second amplifier stage cutting off the negative half wave of the signal. Therefore the maximum obtainable average value of the signal registered by the moving average filter is around 1V. For ATmega8A microcontroller the minimum AD-converter reference voltage is 2V. To achieve the best possible resolution the reference voltage of the AD-converter should be as close to 2V as possible. The reference voltage can be chosen to be precise external 2.048V, fairly unstable external $V_{CC}/2$ or internal 2.56V. Options are made available so that the effects of different reference voltages to resolution and accuracy can be estimated if wanted.

Data transfer

The measurement data is stored into the microcontroller EEPROM memory. The data from the memory is transferred to PC via external FTDI chip utilizing the USB protocol.

4.1.2 Schematic

The schematic as a whole is available in **the Appendix 1**. In this section, the design of the bioimpedance device is described block by block according to its functionality.

Power supply, regulation and reference voltages

The Figure 4.2 represents the schematic capture of the power supply circuit of the bioimpedance meter. The power supply is implemented by coupling two 3V CR2016 lithium button batteries in series producing 6V unregulated supply voltage. The battery holder is planted on a separate PCB board to save space from actual bioimpedance device board and to enable possibility to use different power supply easily. The batteries were chosen according their small size. A changeover SPDT slide switch acts as a power switch.

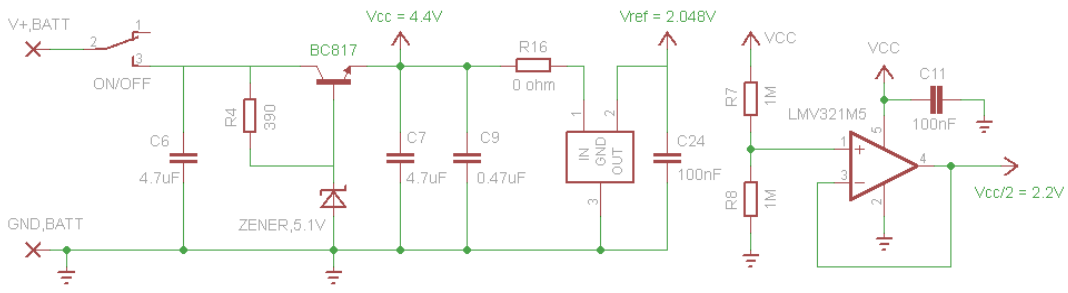

Figure 4.2 *The schematic capture of the power supply circuit.*

The power regulation is done by a simple linear regulator circuit consisted of a BJT transistor, a base current limiting resistor and a 5.1V zener diode. The value of the current limiting resistor R_4 is determined according to the equation 29. In the equation, I_B represents the transistor base current, I_{RL} is required load current, $h_{fe,min}$ is minimum DC current gain for transistor, R_4 is the current limiting resistor, V_{in} is unregulated input voltage, V_Z is the zener voltage, I_Z is the zener current and k is scaling factor ($k > 1$).

$$I_B = \frac{I_{RL}}{h_{fe,\min}} \tag{28}$$

$$R_4 = \frac{V_{in} - V_Z}{I_Z - kI_B} \tag{29}$$

The output voltage is 4.4V due to 0.7V voltage loss in the transistor base-emitter connection (V_{BE}). The use of IC components should be avoided when possible and therefore this type of solution was chosen although it under performs the IC regulators. However, the PCB layout is designed so that the transistor can be replaced by SMD IC regulator if necessary. A sole zener diode could have been used as a regulator but the regulation performance would have been much worse. This is because zener diode would have been directly exposed to the load variation, now the BJT transistor works as a kind of buffer for the zener diode, loading the zener diode only by its small base current. The current consumption is also greatly reduced by using the BJT transistor. Capacitors at the input and at the output of the regulator circuit further stabilize voltages and reduce effects of noise coupling.

Two different reference voltages are provided for test purposes on the board, these are connected to designated connections via jumpers. The first option is a 2.048V low dropout precision voltage reference IC, REF3020. This provides an extremely precise reference voltage for microcontroller AD-converter close to minimum recommended of 2V. It can be also used as a reference voltage for the instrumentation amplifier. The second option is a buffered voltage divider (virtual ground), which outputs $V_{CC}/2$ consequently 2.2V. The buffer amplifier is LMV321, a basic general purpose amplifier with s low current consumption. The disadvantage of this option is that the output of the reference is prone to drift along the V_{CC} and therefore may corrupt the measurement results. This is an evident problem especially when the AD-converter reference is in question. The reference for the instrumentation amplifier is not that sensitive in this case to the instability of the reference voltage, since the gain is kept low and the DC level is filtered out right after the instrumentation amplifier output and because of the discrete nature of the measurement itself.

Current feeding

The schematic capture of the current feeding circuit can be seen in the Figure 4.3. The microcontroller toggles the output pin OC1A creating a square wave of desired frequency determined in the software. The bioimpedance device is designed to create a 5kHz excitation current and a 100kHz excitation current which the user controls by using push buttons. The square wave is low pass filtered to suppress the harmonic frequencies of the square wave. After the passive low pass filter the waveform resembles triangle wave. The low pass filter has to be adjustable because the same channel should be able to provide two base frequencies. Therefore, a digital potentiometer whose resistance value can be determined in the software was chosen. The digital potentiometer, MCP4531-103E, has 10kΩ resistance with a wiper resistance of 75Ω. It has resistance resolution of 7-bits and therefore it provides 129 resistance steps. It is controlled over a two wire interface. To minimize the current consumption it can be set in a shutdown mode by the software. Capacitor of the low pass filter is 100nF. The cut-off frequency of the low pass filter is set to a reasonably low level to filter effectively the harmonic content of the square wave. The downside is that the amplitude of the output signal decreases. The decrease of amplitude itself is not a problem since requirement for the excitation current root-means-square value is low, around 115μA. However, power loss is evident although it is not a critical issue since each measurement takes only around three seconds to complete. The low-pass filter cut-off frequency can be determined according to the equations 30 and 31. In the equations, $f_{LF=5kHz}$ is the low-pass filter cut-off frequency for the 5kHz excitation, $R_{WA,5kHz}$ is the digital potentiometer resistance determined by the equation 39, $f_{LF=100kHz}$ is the low-pass filter cut-off frequency for the 100kHz excitation, $R_{WA,100kHz}$ is the digital potentiometer resistance determined by the equation 41, C_{13} is the value of the capacitor.

$$f_{LF=5kHz} = \frac{1}{2\pi R_{WA,5kHz} C_{13}} = \frac{1}{2\pi \times 9.6k\Omega \times 100nF} \approx 166Hz \tag{30}$$

$$f_{HF=100kHz} = \frac{1}{2\pi R_{WA,100kHz} C_{13}} = \frac{1}{2\pi \times 320\Omega \times 100nF} \approx 4.97kHz \tag{31}$$

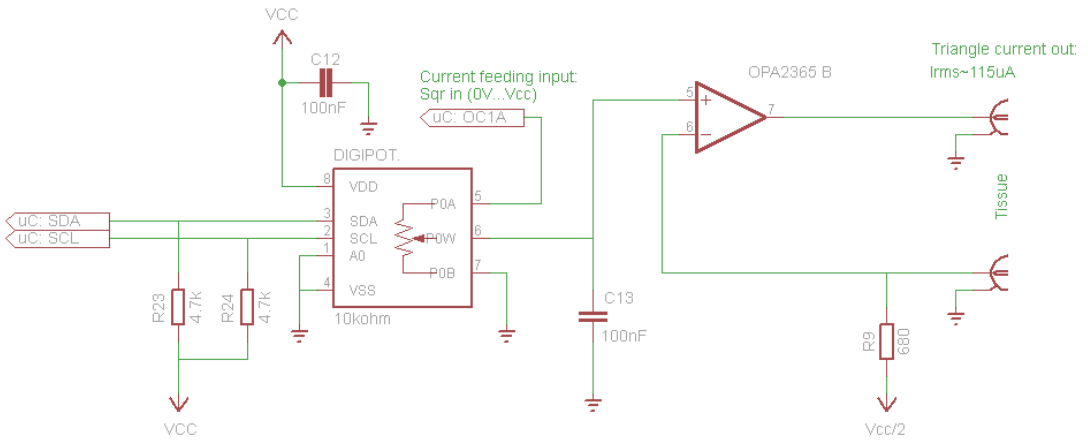

Figure 4.3 *The schematic capture of the current feeding circuit.*

After low pass filtering the signal is voltage to current converted by a simple non-inverting amplifier setup. The amplifier used in this case is OPA2365. The excitation current magnitude, which is kept at around 115µA, is determined by a resistor connected between an inverting input of OPA2365 and the virtual ground of $V_{CC}/2$. The resistor connected to the virtual ground effectively keeps the current value steady regardless of the situation in which V_{CC} drifts. This is important to ensure a safe operation of the device and to minimize data corruption. However, due to a voltage loss in the resistor R_9, a small offset current can be expected. Finally the excitation current is fed into tissue via disposable passive gel electrodes.

Voltage measurement

The voltage response is measured with the similar disposable passive gel electrodes as the current feeding is performed. The voltage is measured differentially by an instrumentation amplifier. The instrumentation amplifier amplifies the difference between the inputs and rejects the voltage common to both inputs. The AC coupling capacitors are connected to the both inputs of the instrumentation amplifier to block any DC voltage applied and the resistors are added to provide a discharge path for input bias currents. The resistors are connected to $V_{CC}/2$ to offer a maximum input dynamic range. Additionally, the high pass filter implementation with a cut-off frequency of 2.8Hz reduces the effects of movement artifacts. The Figure 4.4 represents the schematic capture of the voltage measurement circuit.

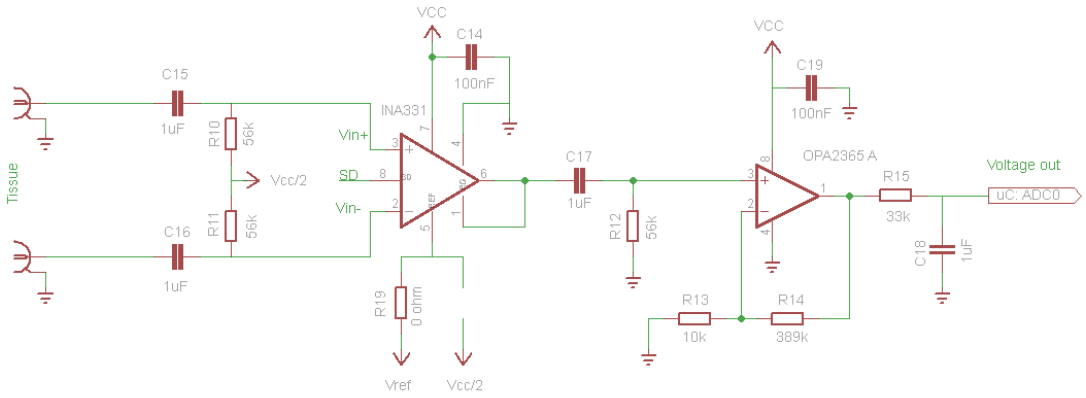

Figure 4.4 *The schematic capture of the voltage measurement circuit*

INA331 was chosen as the instrumentation amplifier. It offers good critical characteristics on the market for a single supply IA. It provides a gain bandwidth of 1MHz with a gain of 5, which is the minimum obtainable gain. In the design, the gain was chosen to be as low as possible to achieve the widest possible frequency range and to minimize the distortion caused by the high frequency harmonics of the triangular wave. Common mode rejection ratio, CMRR, is an important quality parameter of the instrumentation amplifier. It describes the differential amplifier's ability to reject a voltage appearing equally at both inputs. CMRR is defined as ratio of the differential signal gain and the common mode signal gain and it is often expressed in decibels. CMRR can be calculated according to the equation 56.

$$CMRR_{dB} = 20\log_{10}\left|\frac{A_{dm}}{A_{cm}}\right| \tag{32}$$

According to the datasheet of INA33, the CMRR is 90dB for 5kHz and 30dB for 100kHz. After 5kHz the decay of CMRR is very steep and at high frequencies it is barely satisfactory. The IA has to be able to respond to quite rapid but delicate voltage changes, therefore the slew rate has to be adequate. Insufficient slew rate is a common source of distortion at the output of an operational amplifier. The amplifier cannot follow the fast paced changes at the input signal and the output gets distorted. According to the datasheet the slew rate of INA 331 is 5V/µs. As mentioned earlier the gain is set to 5 for INA331. The maximum theoretical AC input and output voltages of INA331 are calculated below in the equation 53 and in the equation 54.

$$V_{i\max rms} = Z_{\max} \cdot I_{rms} = 120\Omega \cdot 115\mu A = 0.0138V \tag{33}$$

$$V_{o\max rms} = V_{i\max rms} \cdot G = 0.00138V \cdot 5 = 0.069V \tag{34}$$

The AC output signal lies on the 2.048V DC reference voltage, therefore the total maximum output rms voltage is 2.117V. To prevent distortion due to slew rate limitation the maximum frequency for output of 2.117V can be calculated according to the equation 55 (Franco 2002, p. 277).

$$f_C = \frac{SR}{2\pi \cdot 2.117V} = \frac{5 \cdot 10^6}{2\pi \cdot 2.117V} \approx 375kHz \tag{35}$$

INA331 provides a very low input bias current of 0.5pA, which can be neglected from the calculations. Most of the time the device is not operating, therefore low quiescent current of 490µA is preferable. When the shutdown mode is enabled, the current drawn by INA331 can be as low as 0.01µA. (Texas Instruments, Inc. 2005) The reference voltage, on which the amplified signal floats, can be chosen to be either 2.048V provided by precision voltage reference or $V_{CC}/2$ provided by the buffered voltage divider. The idea was to make it possible to assess whether the stable reference is really critical in this application. Initially, the 2.048V precision reference was connected. The supply voltage for INA331 is filtered by a 100nF capacitor.

The primary amplification is provided by OPA2365 after the DC voltage level is filtered out by a high pass filter. OPA2365 cuts off the negative half cycle of the signal. This was not considered as a serious drawback, since the signal is driven through a moving average filter before AD-conversion, although this has to be taken into account in the calculations. It was important to choose an amplifier which could reach both supply rails as well as possible. OPA2365 provides a rail-to-rail input and output with an output voltage swing of 10mV. Thus, 10mV is the lowest point the amplifier output can make and creates a base voltage level to amplifier output. The consequent error is systematic and therefore could be taken account in calculations. (Texas Instruments, Inc. 2009) OPA2365 is set to operate in a non-inverting mode with a gain of 38.9. The gain is set by the resistors R_{13} and R_{14} by using equation 32. OPA2365 has the gain bandwidth of 50MHz and therefore gain, even with high frequency input signal, will not introduce a bottleneck for measurements. The gain basically determines the measurement range and the impedance resolution for the bioimpedance device. The gain can be quite easily changed if necessary by replacing the resistor R_{14} with an appropriate one. The total gain of the measurement block is 194.5 (Eq. 33). Input bias current of OPA2365 is only 0.2pA and therefore can be ignored from calculations. Also the offset voltage is low enough to be ignored. Supply voltage for OPA2365 is filtered by 100nF capacitor. All in all, OPA2365 is a very good bargain for this application considering the fact that a single supply component is often compromised with the characteristics it offers.

$$G_{OPA2365A} = 1 + \frac{R_{14}}{R_{13}} = 1 + \frac{389k\Omega}{10k\Omega} = 38.9k\Omega \quad (36)$$

$$G_{total} = G_{INA331} G_{OPA2365A} = 5 * 38.9 = 194.5 \quad (37)$$

The measurement signal is averaged after amplification to reduce the bandwidth appropriate for AD-conversion to be conducted. AD-converted signal has to fulfill the Nyquist frequency manifested by the Nyquist sampling theorem. A simple moving average filter also known as anti-aliasing filter performs averaging of the measurement signal. In practice it is formed by a passive low-pass filter. The capacitor is charged to a mean value of the amplified measurement signal. The value of the capacitor determines the rise time and the fluctuation of the voltage over the capacitor. The value is chosen so that the rise time is few hundred milliseconds and the fluctuation is tolerable not hampering measurement accuracy. The voltage measurement circuitry is connected to ADC0 -pin of the ATmega8A

As the signal is being half wave rectified and then averaged, the input signal to AD-converter is limited to around 1V maximum. The minimum analog reference voltage to ATmega8A AD-converter is 2V. Consequently, there exists a loss in a measurement resolution although this is not considered to be significant.

USB-UART

USB to serial UART handles the transfer of the measurement data from the Atmega8A EEPROM memory to a PC. FT232R USB-UART was chosen to perform this task as it is widely available and affordable. USB-UART was assembled on a separate PCB board to save space. A standard USB-A receptable was chosen as a connector. The Figure 4.5 represents the schematic capture of the FTDI circuit.

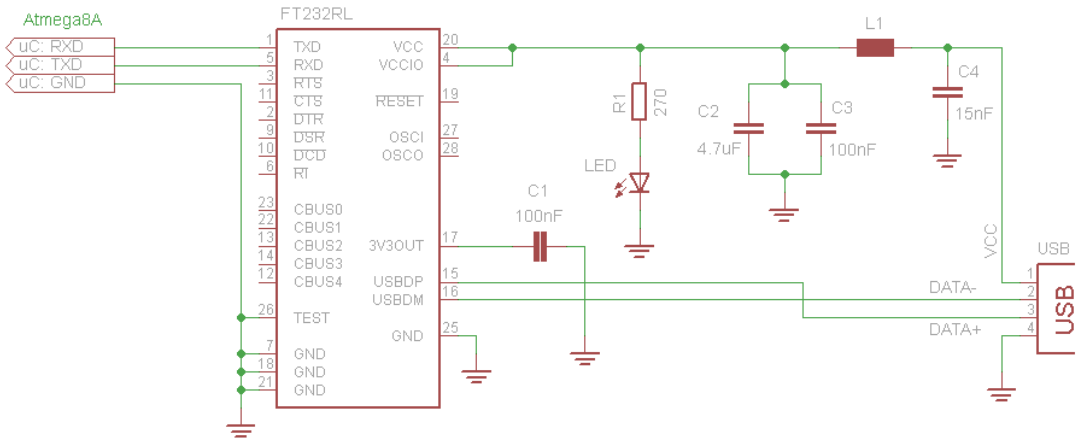

Figure 4.5 *The schematic capture of the FTDI circuit.*

The supply voltage of 5V for FT232R -chip is provided by the PC connected to the USB connector. A ferrite bead is connected to the supply voltage line to filter the high

frequency electromagnetic interference. In addition, capacitors are used to filter the low frequency interference. The power ON indicator LED with a current limiting resistor of 220Ω is also connected on the supply line. The USB connector data lines D+ and D- are connected to the USBDP and the USBDM -pins of FT232R. A coupling capacitor is connected to the 3V3OUT -pin as the datasheet of FT232R suggests. This ensures the proper function of the internal reference of FT232R. The datasheet also suggests the TEST -pin to be connected to ground. (FTDI, Ltd. 2010) The FT232R TXD -pin is connected to the ATmega8A RXD -pin and the FT232R RXD -pin to the ATmega8A TXD -pin. Also, a common ground is provided for both the bioimpedance board and the USB-UART board.

Push buttons

The bioimpedance device is operated by using three SPST -type push buttons. The Figure 4.6 shows the circuit diagram of the button S0 and its connections. The button S0 is used for launching the low frequency excitation current, S1 to launch the high frequency excitation current and S2 is used for starting the data transfer process to the PC. In addition to this, one miniature push button is used for resetting the device in a case of software crash. The buttons S0 and S1 are connected to the ATmega8A external interrupt pins INT0 and INT1. The button S2 is connected PC1 -pin of ATmega8A. All buttons are connected to RC low-pass filters to provide a debounce circuit for defending against a ripple signal that is often present in mechanical push buttons with electrical contacts. All buttons including the reset button are active low, meaning that when button is pushed the corresponding microcontroller pin is forced into a low state.

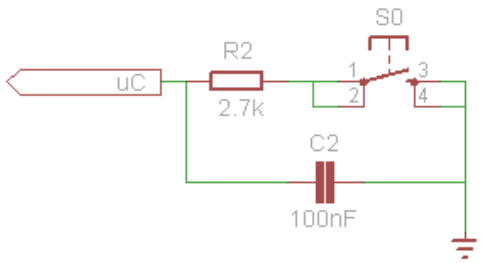

Figure 4.6 *The schematic capture of a button with debounce.*

Microcontroller

ATmega8A was chosen as the microcontroller for the bioimpedance device. It fulfilled or exceeded the requirements set for this type of device. It provides 512 bytes of EEPROM memory and 1k byte of SRAM. The amount of EEPROM is capable of storing around 250 measurement results. ATmega8A also provides plentiful peripheral features including three timer/counters with versatile operation modes, 10-bit internal

AD-converter, TWI interface, USART, SPI interface, an internal RC oscillator, external interrupt sources and various power saving modes. The Figure 4.7 represents the schematic capture of the ATmega8A connections.

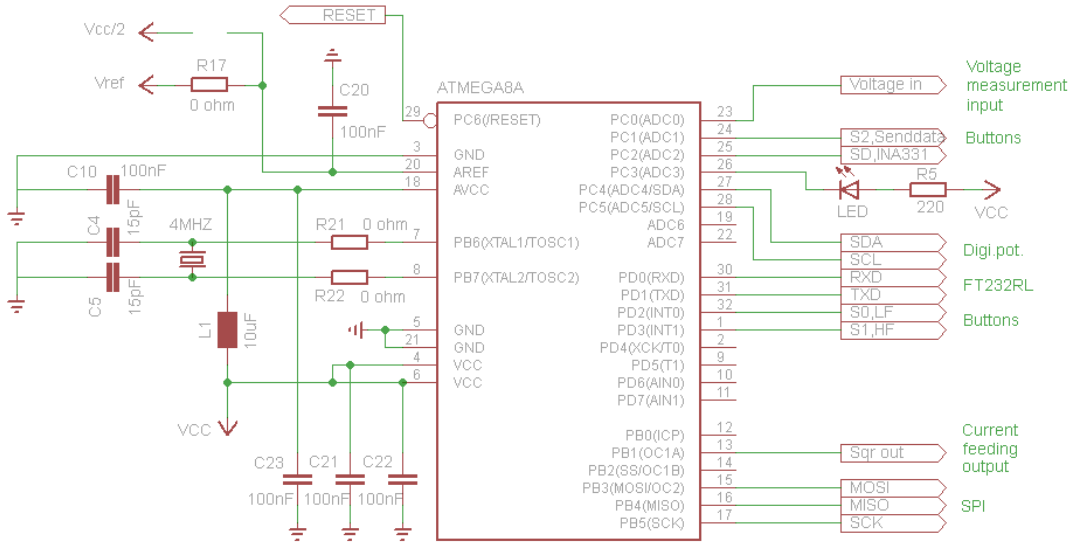

Figure 4.7 *The schematic capture of the ATmega8A microcontroller connections.*

Each of the supply voltage pins and AD-converter reference pin (AREF) of ATmega8A are connected to 100nF bypass capacitors to filter out a high frequency noise component. In addition, the supply voltage pin for AD-converter (AVCC) is connected to V_{CC} via LC low-pass filter as the datasheet of ATmega8A suggests (Atmel Corporation 2009, p. 204). As mentioned previously, the AD-converter reference voltage can be chosen to be either $V_{CC}/2$ or 2.048V supplied by precision voltage reference. The desired reference supply can be chosen by connecting AREF -pin via 0Ω resistor to the supply. Initially, the 2.048V precision reference was connected. 4MHz quartz crystal oscillator is connected to XTAL1 and XTAL2 -pins via 0Ω resistor to provide a possibility to use ATmega8A internal oscillator, if wanted. 15pF capacitors are added between the ground and the oscillator to suppress EMI. An indicator LED is connected to PC3 –pin via a 220Ω current limiting resistor. The LED turns on when the pin PC3 is set in a low state. ATmega8A is programmed via 6 pin SPI interface. The ATmega8A pin connections to the peripheral devices are listed on the Table 4.1.

4.1.3 Simulations

The simulations of the bioimpedance device circuit were performed with Texas Instruments TINA-TI 9.0 Spice based circuit simulation program. The simulation circuit comprised the current feeding circuitry, the voltage measurement circuitry and a load circuit. The simulation circuit can be seen in the Appendix 2**.** The load circuit included a 2R-1C series tissue model circuit (Figure 3.3). The bioimpedance circuit was simulated

for various load impedances. The excitation frequencies were 5kHz and 100kHz. The input signal was square wave. The objective was to confirm the overall functionality design, to evaluate the stability of the excitation current over changing load and to evaluate the impedance measurement accuracy of the device.

The simulations revealed that the low-pass filter did work as supposed in the current feeding block. High harmonic frequencies of the square wave were suppressed and the triangle waveform was generated for both 5kHz and 100kHz. The excitation current magnitude (I_{rms}) remained around 115µA for load impedances between 0.1Ω…15kΩ. The current magnitude started to decrease when load values higher than 15kΩ were applied. The accuracy of the voltage measurement circuit was proved to be reasonable for this application. The load was set to 50Ω for 5kHz, at the center of measurement range, and the voltage ($V_{Z,rms}$) over the load was calculated from equation 34. The measured impedance (Z_{Simu}) was then calculated according to equation 35.

$$V_{Z,rms} = \frac{4}{\sqrt{3}} \frac{V_{ADC\_IN}}{G_{total}} \tag{38}$$

$$Z_{Simu} = \frac{V_{Z,rms}}{I_{rms}} \tag{39}$$

The error between the actual impedance value and the measured impedance value was 3% for 5kHz and 10% for 100kHz. The measured impedances were lower than the actual impedances in both cases. The error sources include the small offset in the feeding current, the offset in the INA331 output and the inability to reach zero voltage level into OPA2365 output due to the output voltage swing. The increase in the error percentage over the frequency is probably due to limited bandwidth of the INA331, the limited bandwidth leads into distortion at higher frequencies and therefore reduce the measured voltage. Frequency of 100kHz is in the upper limits of the INA331 frequency characteristics and the triangular excitation waveform also endures higher harmonic frequencies. However, distortion was not visible in the output waveform of INA331 but this maybe due to the fact that the number of data points to be drawn was set to be fairly small to reduce the simulation time.

4.1.4 Layout design

Layout design is an important factor in minimizing noise coupling and improving the circuit performance. A decent circuit design can be easily ruined by careless layout design. This is especially true when dealing with high speed applications. (Ardizzoni 2005, p. 1) Even though the bioimpedance device does not involve high RF frequencies, it is important to put effort on an appropriate layout design due to the low signal levels

and the challenging nature of biological measurements. The layout design of the bioimpedance device and the FTDI cable was done by using CadSoft Eagle 5.11 schematic and PCB layout editor (CadSoft Computer 2011). The manufacturing work of the PCB board was ordered from Olimex Ltd. The layout design files were delivered to Olimex Ltd. with their DRC rules fulfilled (Olimex, Ltd. 2011).

Certain key points for a proper layout design can be listed. These steps were followed in the layout design process of the bioimpedance device as closely as possible. Bypass capacitors were used to level off voltage spikes associated with power supply. The bypass capacitors for the power supply pins should be placed in the close vicinity of pins in question. Any extra distance translates into additional series inductance, which decreases the self-resonant frequency, on the other words the useful bandwidth of the bypass capacitor (Schmitz & Wong 2007, pp. 1-2).

The ground plane should be kept unbroken to avoid undesired effect of a parasitic inductance to occur. The parasitic inductance and capacitance may cause instability and oscillations in the circuit operation (Ardizzoni 2005, p. 4). It is recommended to dedicate a whole layer for the ground plane, however this was not an option in the layout design of the bioimpedance device. Often, the analog and digital grounds are recommended to be kept separate from each other to avoid the fast rising edges from creating current spikes flowing in the ground plane. The noise created by these current spikes may deteriorate the analog performance of the circuit. The analog and digital grounds should be tied together at one common point; a convenient site would be ADC or DAC. (Ardizzoni 2005, p. 4; Texas Instruments, Inc. “PCB Layout Tips for High Resolution”) Separation of the analog and digital grounds may be reasonable when dealing with delicate high RF signals, but according to several hands-on engineers this practice might lead into even higher problems with the stability of the separate analog ground. For this reason, a decision was made to provide a one common ground for the analog and digital signals. The analog circuitry consisted of the current feeding and voltage measurement was planted over an unbroken ground plane to minimize any avoidable noise coupling.

Highest frequencies on the board are associated with the crystal oscillator. The oscillator was placed on the far end of the board away from signal traces. It was placed on the bottom side, where as the analog circuitry was planted on the top side. All in all, the components and traces incorporated with the high frequencies were placed as far away as possible from the analog circuit. The trace lengths were kept as short as possible. For testing purposes test points were added around the critical parts of the board. The layout pictures are presented in the Appendix 3.

4.2 Software design

The microcontroller ATmega8A runs the software that creates the square wave to one of its outputs. The square wave is then low pass filtered to suppress the high frequency

components. The resulting waveform resembles a triangular wave. Then a voltage to current conversion is executed and current of $115\mu A_{rms}$ is fed into the tissue. The frequency of the current is determined by the square wave and can be chosen by user to be either 5kHz or 100kHz. According to the desired frequency, the microcontroller sets the digital potentiometer of the low pass filter controlled via I2C bus into an appropriate value. The electrodes detect the voltage difference across the sample tissue induced by the excitation current. The amplified and filtered measurement voltage is then sampled by the AD-converter of the ATmega8A. The result is stored as millivolts into the ATmega8A internal non-volatile EEPROM memory. After the measurements are performed the voltage data can be transferred into a terminal program on PC via USB – UART.

4.2.1 Hardware interface

The pin descriptions of ATmega8A and the connections to the peripherals are listed on the Table 4.1.

Table 4.1 *Atmega8A pin connections to the peripheral devices.*

Atmega8A pin	***Peripheral device***	***Peripheral device pin***
PB0	Current feeding circuit: MCP4531 input	P0A
PB3 – PB5	SPI	MOSI, MISO, SCK
PC0	Voltage measurement circuit: OPA2365A output	
PC1	Button S2, Senddata	
PC2	INA331 shutdown	
PC3	LED	
PC4 – PC5	MCP4531	SDA, SCL
PD0 – PD1	USB – UART, FT232RL	TXD, RXD
PD2 – PD3	Buttons S0 and S1, LF and HF	

4.2.2 Functions and interrupt routines

This section provides a description of the key software methods used in the software of the bioimpedance device. Interrupts were utilized as effectively as possible in the software. The flowcharts describing the functions of the ISRs can be found in the Appendix 4 and 5. The flowchart of the main-function is represented in the Appendix 6.

After the power switch is put on, the first thing the code to do before entering the main loop is to load the initializations, allow the global interrupts and examine whether the EEPROM memory has been erased prior to the last time the device was shut down.

Main function

The primary task for the main function is to start AD-conversion process when time is correct and the conditions are met. The AD-conversion is started after two seconds has elapsed from the start of the excitation current feeding triggered by a push button, tagged either LF or HF. When the conversion result is ready, the main function stores the result into EEPROM memory. The results for the low and high frequency excitation are stored into own memory blocks in EEPROM. 20 individual results can be stored into EEPROM for each low and high frequency measurements. The main function also keeps record of the number of the measurements taken. The processes in the main function are mostly controlled by utilizing flags, announcing that a certain condition has been met by setting their value either “true” or “false”.

The main function processes also the data transfer into the terminal program on a PC. The request for this comes from the active low push button, tagged as SEND. The SEND button is two functional. In addition to indicating the senddata –request, it also signals the main function of the request for erasing the measurement results from the memory. The multifunctionality is implemented by a timer, counting the time the button is pressed. A short push indicates the senddata –request and one second push the erase EEPROM –request. The erasing is performed by updating the memory location by a zero value unless it is already zero. In this way unnecessary writes to EEPROM are avoided. In case of power on reset, the measurements can be continued from the same memory location as prior to the POR. Also, the measurements performed –counters continue from the same spot as before the POR. Therefore, the device can be shut down in between the measurements and continue afterwards when desired. Before entering the main loop, the number of the measurements taken is checked. If the value deviates from zero indicating that the memory erase has not been performed prior to shut down, the next memory location for storing the measurement data is calculated from the value of the counter keeping track of the number of measurements performed. This feature was added to the code to overcome the problem of excess current consumption due to lack of a shutdown mode in OPA2365.

External interrupts

The push buttons are connected to the external interrupt -pins, INT0 and INT1. The corresponding interrupt service routine is set to trigger on the falling edge of the pulse. The first thing to do in the ISR is to set the digital potentiometer in an appropriate value. After the digital potentiometer is set, timer1 is initialized to proper settings depending on which button is pushed. A flag is set to indicate which button is pressed. After this the timer0, timer1 and timer2 are launched. The timer1 is responsible for generating the low or high excitation frequency square wave to the OC1A output pin according to the

button pushed. The timer0 and timer2 are responsible for measuring the time elapsed from the moment the ISR was entered.

Timer/counters

Timer/counters are utilized widely over the program. The timer1 creates the square wave into the output OC1A -pin from which the excitation current fed into tissue is constructed. The timer1 is used in clear timer on compare match (CTC) –mode. The counter is cleared after the counter value in the TCNT1 –register reaches the value in the OCR1A -register set by the programmer. The OC1A –pin is set to toggle its output level when the compare match of TCNT1 and OCR1A -registers is noticed. The frequency of the square wave is therefore determined by the value set into OCR1A register. (Atmel Corporation 2009, pp. 90-91) The entire pin toggle process is automatic and contains no additional efforts in the software. The appropriate value for OCR1A –register is set in the initialization function of the timer1. The timer1 initialization is performed inside the external interrupt ISR every time the corresponding button is pushed. The settings for generating the output frequencies HF and LF are presented in the equation 36 and equation 37 accordingly (Atmel Corporation 2009, p. 90). In the equation, f_{OC1A} is the frequency at the ATmega8A OC1A output pin, f_{OC1A} is the system clock frequency, N is the prescaler value and OCR1A the value set into the output compare register.

$$f_{OC1A,LF} = \frac{f_{clk\_IO}}{2 \times N \times (1 + OCR1A)} = \frac{4MHz}{2 \times 8 \times (1 + 49)} = \frac{4MHz}{800} = 5kHz \quad (40)$$

$$f_{OC1A,HF} = \frac{f_{clk\_IO}}{2 \times N \times (1 + OCR1A)} = \frac{4MHz}{2 \times 1 \times (1 + 19)} = \frac{4MHz}{40} = 100kHz \quad (41)$$

As mentioned earlier, the timer1 is also used for time measurement when the SEND -button is pushed to examine which of the buttons dual function is to be activated, the senddata or erase memory.

The timer2 measures the time elapsed from entering into the external interrupt routine. The timer2 is set to raise a “start_ADC” flag after two seconds has passed. Timer1 is set to give overflow interrupt after the TCNT2 -register has reached the value of 255. A variable, time_cntr2_2SEC, keeps track of the number of the interrupts occurred. As the variable reaches the value of 30, two seconds has passed and the program sets a flag “start_ADC” and reloads the timer2 ready for the next external interrupt. The flag “start_ADC” announces that AD -conversion can be initiated.

The timer0 measures the time elapsed from entering the external interrupt ISR as well. The purpose of timer0 is to stop the timer1 from outputting the square wave after three seconds has passed. The timer0 works in a similar manner as the timer2. The timer0 gives an overflow interrupt after the counter TCNT0 -register reaches the value of 255. Every time when the overflow interrupt is launched, a variable

"time_cntr0_3SEC" is incremented. As the variable reaches a value of 47, three seconds has passed since entering the external interrupt ISR and timer1 is stopped. This means that a single measurement has been performed.

AD -conversion

The analog voltage induced by the excitation current is brought into ADC0 -pin of the ATmega8A and converted in to a digital form. The ATmega8A internal AD -converter is used in a 10-bit mode.

The AD -conversion process is launched in the main function after the conditions are met. The conditions are such that the flags "start_ADC" and either "LF" or "HF" is "true" and that under 21 results are stored into the EEPROM in either case. During a single measurement the AD -conversion is performed 50 times, each conversion result is added up in a variable. The value in the variable is then divided by 50 and the resulting averaged value is transformed into millivolts. Now, the AD -conversion process is ready and the flag "start_ADC" is set to "false" for next measurement. The averaged result is then returned into the calling function and stored into EEPROM.

EEPROM

ATmega8A -microcontroller provides 512 bytes of non-volatile EEPROM memory. The measurement data and the number of measurements performed -data are stored into the EEPROM memory. The number of measurements -data occupies a one single byte memory location and the actual measurement data two bytes of memory. The list of the employed memory locations are presented on the Table 4.2.

Table 4.2 *Employed EEPROM memory locations.*

Address	***Datatype***
0	Number of LF measurements
1	Number of HF measurements
2…41	LF measurement data
42…81	HF measurement data
82…511	Empty

Transfer of the measurement data

The data stored into EEPROM memory is transferred into TeraTerm -terminal program via USB-UART interface (Ayera Technologies, Inc. 2011). The data gathered by the device is printed on the terminal program screen and can be saved into the .csv -format to be further edited by using for example Microsoft Excel -software.

The main -function constantly checks if the SEND -button is pressed. If the button is pressed SENDDATA -bit is cleared and the condition in the IF -statement is fulfilled. If the button still is pressed after one second, then the erase memory sequence starts. If the button is released before one second has elapsed, the data transfer routine is started. The send_values() -function is called and will handle the entire data transfer routine. Basically, programmer's duty is to get the content of the memory location into the UART peripherals transfer buffer register, the rest is operated automatically by the UART. The content of a one memory location is transferred as follows. Firstly, the content of the memory location the pointer designates is read and the value is stored into a variable. Then the unsigned integer -type value is converted into an ASCII string of digits with a base number of 10 (decimal). The resulting string of decimal numbers is then stored one by one in a character array of the output buffer, when process is over a terminating nul (0) -character is added at the end of the output buffer. Thus, one character type variable in the output buffer contains one decimal number. After this the content of the output buffer is sent and stored one by one into the UART transfer buffer register (UDR). The aforementioned transfer process is done for all of the memory locations allocated to the use of the measurement data.

Digital potentiometer, I^2C

The 10kΩ digital potentiometer, MCP4531-103EE, is controlled via the I^2C bus. The I^2C is a two wire serial interface with SCL -pin for the serial clock from master device and SDA -pin for the serial data signal. ATmega8A acts as a master device and generates a 100kHz SCL frequency for controlling the digital potentiometer. MCP4131-103E has a 7-bit resistor network, so that the resistance between the wiper and the terminal B can be determined by the equation 38 for 5kHz excitation and by the equation 40 for the 100kHz excitation (Microchip Technology, Inc. 2008, p. 42). The actual resistance contributing to the low-pass filter is the resistance between the wiper terminal and the terminal A. In the equations, R_{WB} refers to the resistance between the wiper terminal and the terminal A. R_{WA} is the resistance between the wiper terminal and the terminal A. R_{AB} is the total resistance between the terminal A and the terminal B. N is the wiper setting value and R_W is the wiper resistance.

$$R_{WB,5kHz} = \frac{R_{AB}N}{128} + R_W = \frac{10k\Omega \times 4}{128} + 75\Omega \approx 388\Omega \tag{42}$$

$$R_{WA,5kHz} = R_{AB} - R_{WB,5kHz} = 10k\Omega - 388\Omega \approx 9.6k\Omega \tag{43}$$

$$R_{WB,100kHz} = \frac{R_{AB}N}{128} + R_W = \frac{10k\Omega \times 123}{128} + 75\Omega \approx 9.68k\Omega \tag{44}$$

$$R_{WA,100kHz} = R_{AB} - R_{WB,100kHz} = 10k\Omega - 9.68k\Omega \approx 320\Omega \tag{45}$$

The bioimpedance device employs only one slave device on the I^2C bus. Therefore, the general call addressing is utilized. The Microchip extension of the general call format can be seen on the Figure 4.8b. In the general call format the device addressing is overridden by sending a byte of nulls on the line after the start bit. Then the acknowledge response from the slave device is waited for. After that a 7-bit command is sent on the line, which tells the device to write the incoming data bits on the volatile memory of the digital potentiometer. The acknowledge bit then confirms that the master device has been heard. Finally, 8-bits of data determining the resistance value is sent on the live and an acceptance is confirmed by the slave device by the acknowledge bit. The stop -bit is sent to the slave to signal the end of the transmission sequence. (Microchip Technology, Inc. 2008, pp. 46-47)

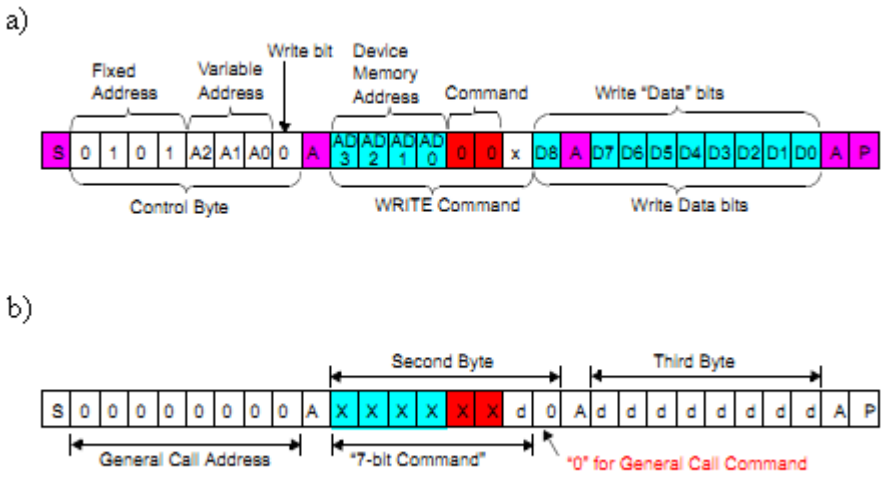

Figure 4.8 *a) The standard I^2C write sequence. b) The Microchip extension of the General call format (Microchip Technology Inc. 2008, p. 50, 57).*

Sleep modes and power saving

By using different sleep modes the current consumption can be substantially reduced. For the proposed bioimpedance device the power saving modes can make a big difference since the actual measurements take only around three seconds each. The rest of the time the device is basically idle. To take this into account, the software for the bioimpedance device is designed so that it is possible to shut down the power entirely from the power switch between the measurements without losing the data stored into the memory. When the power is turned on again, the next measurement result will be stored into the next available memory location following the measurement before turning the power off.

4.3 Measurement configurations

The initial base impedance measurements were performed to obtain information about the scale of the impedance to be measured with the bioimpedance device. This information was used in the design process of the device.

The purpose of the test measurements was to confirm the appropriate functionality and to evaluate the performance of the developed bioimpedance device in a controlled environment. The test measurements consisted of a performance testing of the current feeding circuit, a performance testing for standalone voltage measurement circuit with a function generator input signal, a system test with purely resistive load and a system test with a 2R-1C test circuit. All the test circuits were assembled on a solderless breadboard (Wisher Enterprice, Ltd. 2011). The components used in the test circuits were measured with a Fluke 115 True RMS multimeter (Fluke Corporation 2011). The test measurements were performed in a computer class due to practical reasons, although EMI situation in such a test environment is not very good. Finally, the bioimpedance device was tested in vivo and the obtained results were compared to the results obtained by using a reference measurement system.

4.3.1 Initial base impedance measurements

The Initial baseline impedance measurements were performed in the early phase of bioimpedance meter design process. The objective was to obtain generic information about the magnitude scale of bioimpedance modulus from various electrode locations. The consecutive results were used for supporting the design process itself. The measurements also gave some information about the effect of close proximity of different tissue types to bioimpedance data. In addition the effect of swelling to the bioimpedance data was investigated using a tourniquet. The baseline impedance measurements were performed using Solartron 1260A Frequency Response Analyzer and Solartron 1294A Impedance Interface.

Solartron 1260A and Solartron 1294A

Solartron 1260A is a frequency response analyzer providing a wide frequency range with high frequency resolution for impedance analysis (Solartron Analytical, Solartron Group, Ltd. 2005a). The wide frequency range ensures detailed information about the electrical properties of subject material. In our setup the Solartron 1260A is used in conjunction with Solartron 1294A Impedance Interface. The Solartron 1260A provides the AC stimulus current and takes care of the correlation analysis of the output from the Solartron 1294A. The correlation analysis is a key part in reducing the adverse effects of the non-linearities arising from the sample under investigation (Hinton & Sayers 1998). The Solartron 1294A provides a one 4-terminal connection satisfying the IEC 601-1 safety standards. The connection is current limited and is designed specifically for medical applications. (Solartron Analytical, Solartron Group, Ltd. 2005b) The

combination of these instruments has an impedance measurement range up to 100MΩ and frequency range from 10μHz to over 1MHz (limited by IEC 601-1 from 100Hz to over 1MHz). In the design of the Solartron 1294A has been paid special attention to further improvement of the signal-to-noise ratio for better adaptation to bioelectrical measurements. The device is operated through a PC interface. (Hinton & Sayers 1998)

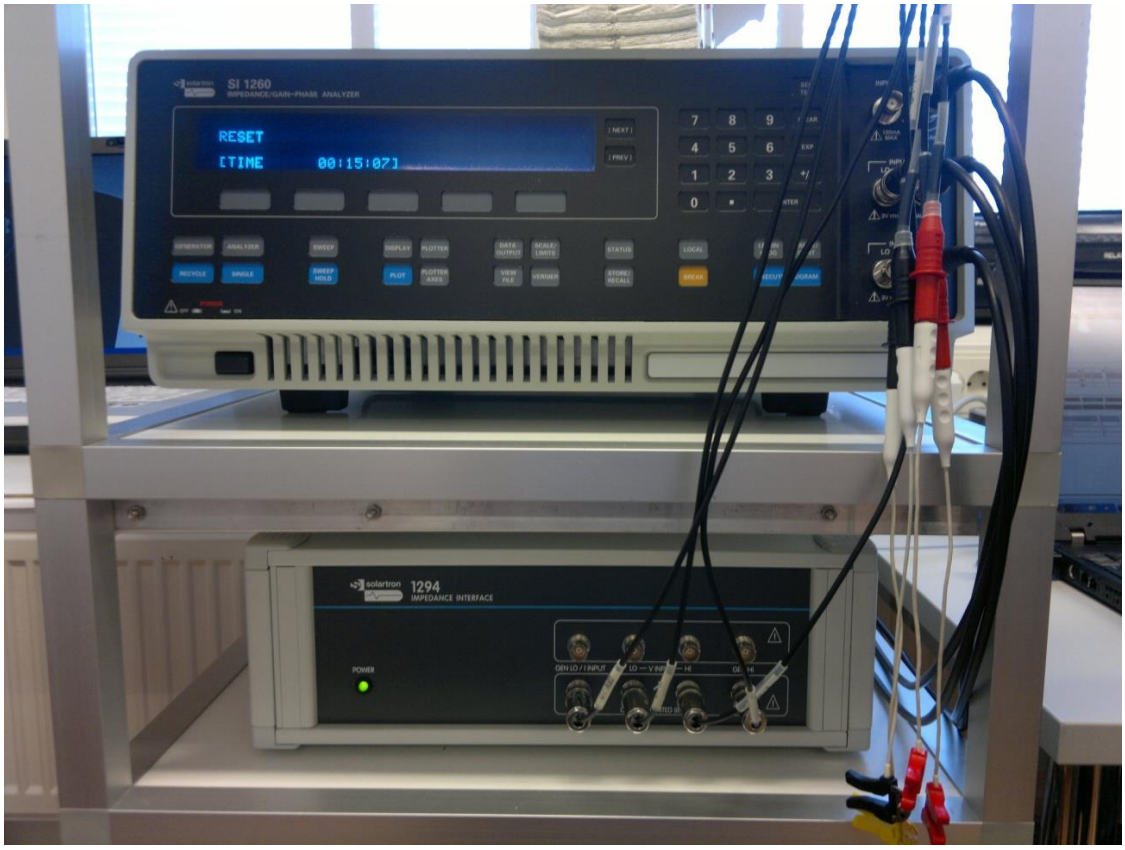

Figure 4.9 *Solartron 1260A Impedance/Gain-Phase Analyzer (above) and Solartron 1294A Impedance Interface (below).*

Electrode placement

The applied electrodes were disposable Ambu Blue Sensor P Ag/AgCl surface electrodes. The electrodes were placed in a sequential configuration as the Figure 4.10 suggests. As one of the major objectives in the base impedance measurements was to obtain information of the effect of different tissue types to the bioimpedance signal the electrode locations were chosen as seen in the Figure 4.10.

The measurement procedure

As the measurements were merely used to demonstrate the scale of impedance magnitude, strict clinical guidelines for the measurement protocol were not followed. The subject was male; height was around 190cm and weight 88kg. The subject had no underlying medical conditions. During the measurements the subject was in a sitting

position, the subject was relaxed and breathing normally. Any kind of skin preparation was not performed.

The measurements were performed using four different electrode locations (Figure 4.10). The distance between the electrodes was minimized since the proposed bioimpedance device would eventually be integrated to a plaster to measure relatively small volumes. The impedance was also measured after pressure was added to shin and forearm by using tourniquet causing a mild temporary ischemia and fluid accumulation into tissue. This was done just to verify that the change in the impedance was measurable, this measurement also gave a coarse estimate of the scale of change to be expected in the case interfered vascular activity.

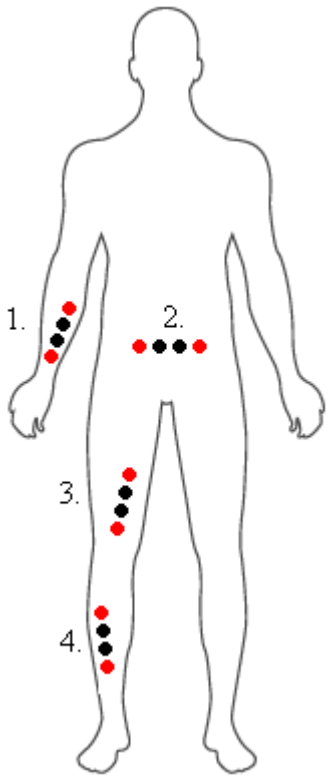

Measurement No.	*Site*	*IES*	*Tourniquet*
1a.	Forearm	3.5cm	No
1b.	Forearm	3.5cm	Yes
2.	Abdomen	3.5cm	No
3.	Thigh	3.5cm	No
4a.	Shin	3.5cm	No
4b.	Shin	3.5cm	Yes

Figure 4.10 *Electrode placements in the measurements. Red color indicates current feeding electrode and black color voltage measurement electrode.*

4.3.2 Excitation current measurements

The purpose of the excitation current measurements was to assess the performance of the current feeding circuit. In an ideal case the excitation current would be totally independent of the applied load and would remain at around 115µA_{rms}. However, in reality the output impedance of the operational amplifier is not infinite and the current can be expected to be affected by the load variation. The simulations results propose the

current should remain fairly constant over the load up to 10kΩ with a very small current offset level.

The excitation current measurements were performed by connecting the bioimpedance device's current feeding leads without electrodes on the breadboard. The measurements were taken with several load resistor values between 5Ω and 2kΩ. Between 5Ω and 100Ω load values the measurements were taken more densely. The excitation current measurements were performed for both 5kHz and 100kHz excitation. Unfortunately, the current cannot be measured by using multimeter since neither the frequency bandwidth nor the resolution meet the demands of the test. Therefore, the current had to be measured indirectly by measuring the voltage over the resistor with oscilloscope. The rms value of the excitation current (I_{rms}) was calculated according to the equation 42. The measurement setup can be seen on the Figure 4.11.

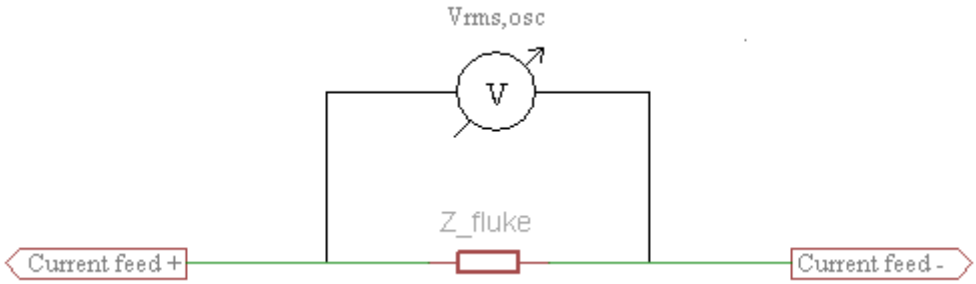

Figure 4.11 *Excitation current measurement setup.*

$$I_{rms} = \frac{V_{rmsOSC}}{Z_{FLUKE}} \tag{46}$$

The oscilloscope used in the measurements was LeCroy Wavejet 322 digital oscilloscope (LeCroy Corporation 2011). The oscilloscope was set into a differential measurement mode. The channel 1 of the oscilloscope measured the front end voltage of the resistor while the channel 2 measured the other end voltage, the oscilloscope then generated the difference signal automatically. The frequency, the rms voltage ($V_{rms,OSC}$) and the offset voltage (V_{MEAN}) was measured by the oscilloscope from the difference signal. $V_{rms,CALC}$ represents the nominal rms voltage over the load resistor induced by an rms current magnitude of 115µA.

4.3.3 Measurements with function generator input

Function generator input was used for assessing the performance of the voltage measurement circuit of the bioimpedance device. The possibility of using the obtained data from these measurements for determination of a correction factor to overcome the problems with current feeding circuit was also considered. The function generator used

in the measurements was Kenwood FGE1202. The excitation current which is desired is 115µA (I_{rms}). The load resistance values were between 4.8Ω and 111Ω. The current magnitude and the measurement range were so small that the function generator could be used without a complex external circuit.

The function generator was set to generate a triangular signal with an rms voltage of approximately 5.5V with zero offset voltage. The function generator output was adjusted and confirmed with oscilloscope by measuring the rms voltage over the test circuit. Some voltage drift was observed with increasing frequency. The voltage drift was corrected, although exactly the same rms voltage for each frequency could not be generated, the input voltage varied between 5.48V_{rms} and 5.51V_{rms} over the load circuit. This results in a small difference of approximately 1µA in the current fed into the test load. The measurements were performed for triangle wave frequencies 5kHz, 100kHz and 200kHz. The measurements were performed also for sinusoidal voltage input to assess the effect of the harmonic high frequencies of the triangular wave into the measurement results. The measurements for sinusoidal signal were performed for frequencies 5kHz, 100kHz, 200kHz with sparser load resistance steps.

The current limiting series resistor (R_S) was applied to the breadboard with a high resistance value. The value of the R_S was determined according to equation 43, the resistor chosen had a resistance value of 47.62kΩ. In the calculations the current fed into the test circuit was approximated as 115µA. The Figure 4.12 represents the measurement setup of the function generator input measurements.

$$R_S = \frac{V_{rms,GEN}}{I_{rms}} = \frac{5.5V}{115\mu A} = 47.83k\Omega$$
$$\rightarrow \qquad (47)$$
$$R_S = 47.62k\Omega$$

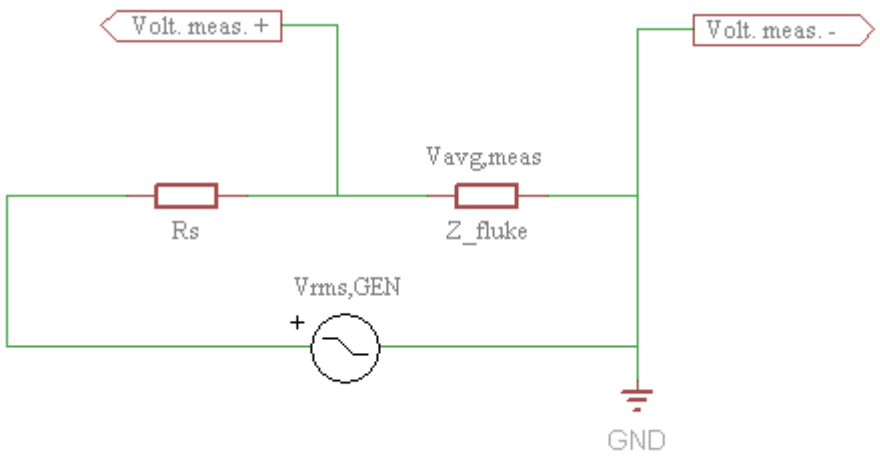

Figure 4.12 *The setup of the function generator input measurements.*

The load resistor (Z_{FLUKE}) is connected in series with the series resistor (R_S). Consequently, relatively small load impedance values will not affect the rms current (I_{rms}) fed into the test circuit effectively at all. The voltage over the load resistor is measured with the bioimpedance device ($V_{avg,MEAS}$), from which the rms voltage ($V_{rms,MEAS}$) can be calculated using the equations 45 and with the equation 46 the resistance can be determined (Z_{MEAS}). For the sinusoidal input the equation 44 was used to calculate the rms voltage over the load resistor and the resistance was determined by using the equation 46.

$$V_{rms,MEAS} = \frac{\pi}{\sqrt{2}} \frac{V_{avg,MEAS}}{G_{total}} \tag{48}$$

4.3.4 System test with purely resistive load

The first system test for the bioimpedance device was performed with a purely resistive load. The purpose was to assess the capability of the bioimpedance device to correctly indicate the direction of the change in the load value, to obtain information about the accuracy of the device and to evaluate whether the error in the measurement was systematic.

The current feeding leads of the bioimpedance device were connected into the breadboard without electrodes, then the voltage measuring leads were connected and finally the resistor load was connected in between the positive and the negative lead of the voltage measurement input. The measurement set-up can be seen on the Figure 4.13.

Figure 4.13 *The setup of the system test with purely resistive load.*

The gain of the voltage measurement circuit is set so that the voltage measurement is reliable up to around 120Ω. Above the 120Ω load resistance the voltage at the output of OPA2365 starts to get clipped. Several voltage measurement sets were taken for each load value between 4.8Ω and 111Ω to see whether there was variation between the measurement sets. Each measurement set consisted of both 5kHz and 100kHz excitation frequencies. After each measurement set, the voltage measurement data stored into memory of the bioimpedance device was uploaded into the TeraTerm software on a PC. The voltage measurement data is the average value of the amplified (G_{total}) and half

wave rectified triangle voltage over the load resistor. From the voltage measurement data ($V_{avg,MEAS}$) the rms voltage value ($V_{rms,MEAS}$) is calculated according to equation 45.

$$V_{rms,MEAS} = \frac{4}{\sqrt{3}} \frac{V_{avg,MEAS}}{G_{total}} \tag{49}$$

The excitation current was assumed to remain fairly constant during the measurement. With the known value of the excitation current (I_{rms} = 115µA), we are able to calculate the value of the resistor (Z_{MEAS}) according to equation 46.

$$Z_{MEAS} = \frac{V_{rms,MEAS}}{I_{rms}} \tag{50}$$

The measured resistance value (Z_{MEAS}) is then compared to the actual resistance value (Z_{FLUKE}) determined by using the multimeter.

4.3.5 System test with 2R-1C load circuit

The second system test was performed with a 2R-1C test circuit (Figure 4.14). The measurement arrangement was basically the same as in the purely resistive load measurement. The 2R-1C circuit was assembled on the breadboard.

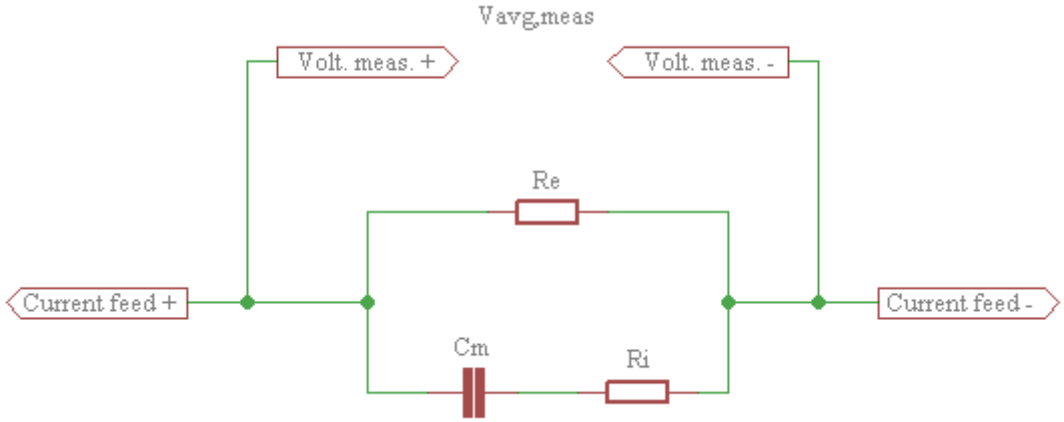

Figure 4.14 *The setup of the system test with 2R-1C load circuit.*

The capacitor value (C_m) in the test circuit is constant 19.5nF along with the 22Ω resistor R_I in every measurement and the total impedance was set on the measurement range by changing the value of the resistor R_E. The value of the capacitor was chosen quasi-randomly knowing that the tissue capacitance would be in the nanofarad range. The capacitor value was measured with a Mastech MS8217 multimeter (Mastech Instruments, LLC. 2011). The aim was to use pretty much the same total impedance values as was used in the measurements with the purely resistive load so that the results

would be comparable. The fact of the matter is that the addition of the capacitor should not affect on the measurement results as the total impedance is kept same as in the purely resistive measurements. The actual total impedance of the 2R-1C load circuit was calculated according to the equation 47. The equation 47 is derived in the section 3.1.2. The measured impedance from the voltage measurement data can be determined according to the equation 48 and the equation 49.

$$|\bar{Z}| = \sqrt{\left(\frac{R_E{}^2 R_I + R_E R_I{}^2 + R_E \bar{X}_C{}^2}{R_E{}^2 + 2R_E R_I + R_I{}^2 + \bar{X}_C{}^2}\right)^2 + \left(\frac{R_E{}^2 \bar{X}_C}{R_E{}^2 + 2R_E R_I + R_I{}^2 + \bar{X}_C{}^2}\right)^2} \quad (51)$$

$$V_{rms,MEAS} = \frac{4}{\sqrt{3}} \frac{V_{avg,MEAS}}{G_{total}} \quad (52)$$

$$Z_{MEAS} = \frac{V_{rms,MEAS}}{I_{rms}} \quad (53)$$

4.3.6 In vivo measurements

The purpose of the in vivo measurements was basically to verify the proper operation of the bioimpedance device. Secondary target was to evaluate the accuracy of the device and to find out whether there was a systematic error present in the results. The measurements were very limited and performed only on one test subject. The results obtained with the developed bioimpedance device were compared to the results obtained with a reference device with the same electrode placements. The reference device used in the measurements was the Solartron bioimpedance spectroscopy instrumentation.

The subject was a 27 year-old male, his height was 178cm and weight 76kg. The subject was in normal health. The subject was in a sitting position during the measurements. The measurements were taken from two locations on the body surface, the forearm and the calf. The measurement locations were chosen as such because the most of the chronic ulcers appear at the body extremities. Also, the skin on those sites is not very thick and therefore skin impedance is minimal. The amount of underlying soft tissue is also fairly high.

Eight electrodes were placed in sequence on the posterior side of the forearm and three measurements were taken with different interelectrode spaces; 17.5cm, 10.5cm and 3.5cm. On the forearm measurements disposable Ambu Blue Sensor P with skin contact size of 34mm was used (Ambu, A/S. 2011a). Six electrodes were attached in sequence arrangement on the skin of the calf and two measurements with different IES were taken; 15cm and 5cm. The electrodes used in this case were disposable Ambu Blue Sensor R electrodes with a larger 48mm skin contact area (Ambu, A/S. 2011b).

The figure 4.15 shows a sketch of the electrode placements in the measurements and the Table 4.3 the electrodes used in each measurement.

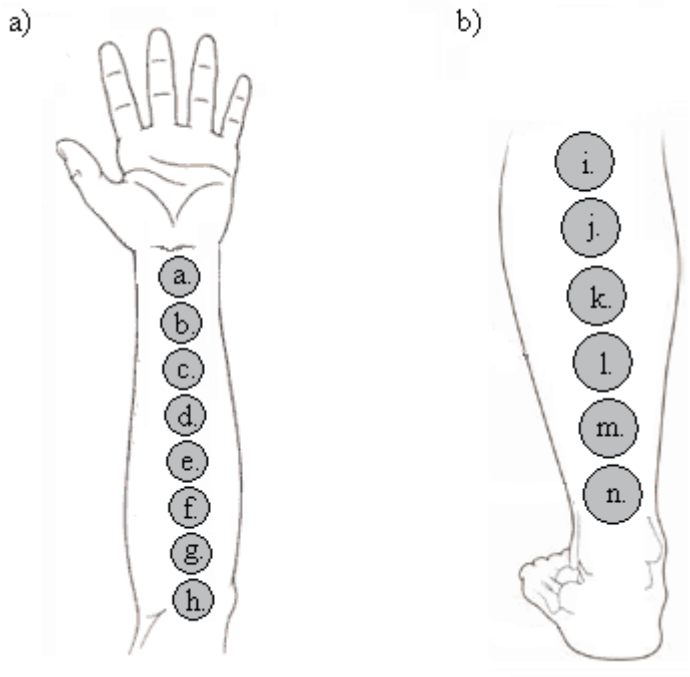

Figure 4.15 *Electrode placements. Forearm 8 electrodes and calf 6 electrodes.*

Table 4.3 *The electrodes used in the measurements.*

Measurement No.	***Site***	***Electrodes***	***IES***
1.	Forearm	Current: a. and h. Voltage: b. and g.	17.5cm
2.	Forearm	Current: b. and g. Voltage: c. and f.	10.5cm
3.	Forearm	Current: c. and f. Voltage: d. and e.	3.5cm
4.	Calf	Current: i. and n. Voltage: j. and m.	15cm
5.	Calf	Current: j. and m. Voltage: k. and l.	5cm

Several measurements were taken from each measurement location with 5kHz and 100kHz excitation frequencies by using the bioimpedance device. The approximate average was taken from these values and the impedance was calculated according to the equation 49. The impedance was then compared to the results obtained with the reference device.

5 Measurement Results

This section represents the results of the measurements described in the section 4.3. Firstly, the initial baseline impedance measurement results obtained by the Solartron BIS device are presented briefly. Secondly, the outlook and operational characteristics of the developed bioimpedance device are introduced. Then, the test measurement results obtained by the bioimpedance device are presented. The error sources, issues with the device and other undesired phenomena which may have contributed into the measurements are also discussed. Finally, the results of the in vivo measurements are presented.

5.1 Base impedance measurements

The Table 5.1 shows the results of the base impedance measurements. The interelectrode space was equal in all measurements and the smallest possible to be obtained with the electrodes applied. The largest impedance was measured from the abdomen for both 5kHz and 100kHz excitation current. Abdomen contains large portions of fat tissue which has lower conductivity than muscle tissue and the results are in line with this fact. Nevertheless, the impedance values are fairly close to each other especially with 5kHz excitation. Larger difference in the impedance between the measurement sites are detected with 100kHz excitation. The introduction of a tourniquet seems to have a decreasing effect on the impedance measured. The similar effect was measured from the both measurement sites in which the tourniquet was applied. The impedance decreased by 5.0Ω for 5kHz excitation and 4.6Ω for 100kHz when the tourniquet was applied to the forearm. When the tourniquet was applied to the shin, the impedance decreased by 1.6Ω for 5kHz and 2.1Ω for 100kHz. The decrease in impedance was expected as highly conductive fluid starts to accumulate into the tissue under ischemia.

Table 5.1 *The results of the base impedance measurements.*

Measurement No.	Site	Tourniquet	IES (cm)	Frequency (kHz)	Z (Ω)
1a.	Forearm	No	3.5	5	65.4
				100	44.8
1b.	Forearm	Yes	3.5	5	60.4
				100	40.2
2.	Abdomen	No	3.5	5	69.7
				100	55.3
3.	Thigh	No	3.5	5	63.0
				100	41.5
4a.	Shin	No	3.5	5	62.3
				100	53.2
4b.	Shin	Yes	3.5	5	60.7
				100	51.1

5.2 The Appearance and the characteristics of the device

The developed bioimpedance device is presented in the Figure 5.1. The uppermost device is the FTDI chip with USB connector for the data transfer into the PC terminal program. The FTDI chip is connected into the bioimpedance device, seen in the middle of the photo, with three pin connector.

The bioimpedance device is assembled on a two sided PCB board. The bottom layer accommodates the high frequency components for example the microcontroller and the crystal oscillator. The high frequency signal routes were placed on the bottom side when feasible. The top layer visible on the Figure 5.1 accommodates the user interface, the analog components and the connectors.

The bioimpedance device is controlled by the user with a column of three push buttons on the left side of the device; SEND/ERASE, LF, HF accordingly. The current feeding leads are placed on the lower right hand corner of the device. The voltage measuring leads are placed above the current feeding leads. The red cable color indicates the positive lead and the black cable color the negative lead. The electrodes not visible on the Figure 5.1 are disposable Ag/AgCl surface electrodes. On the bottom of the Figure 5.1 is a regular matchbox to give a perspective of the size of the bioimpedance device.

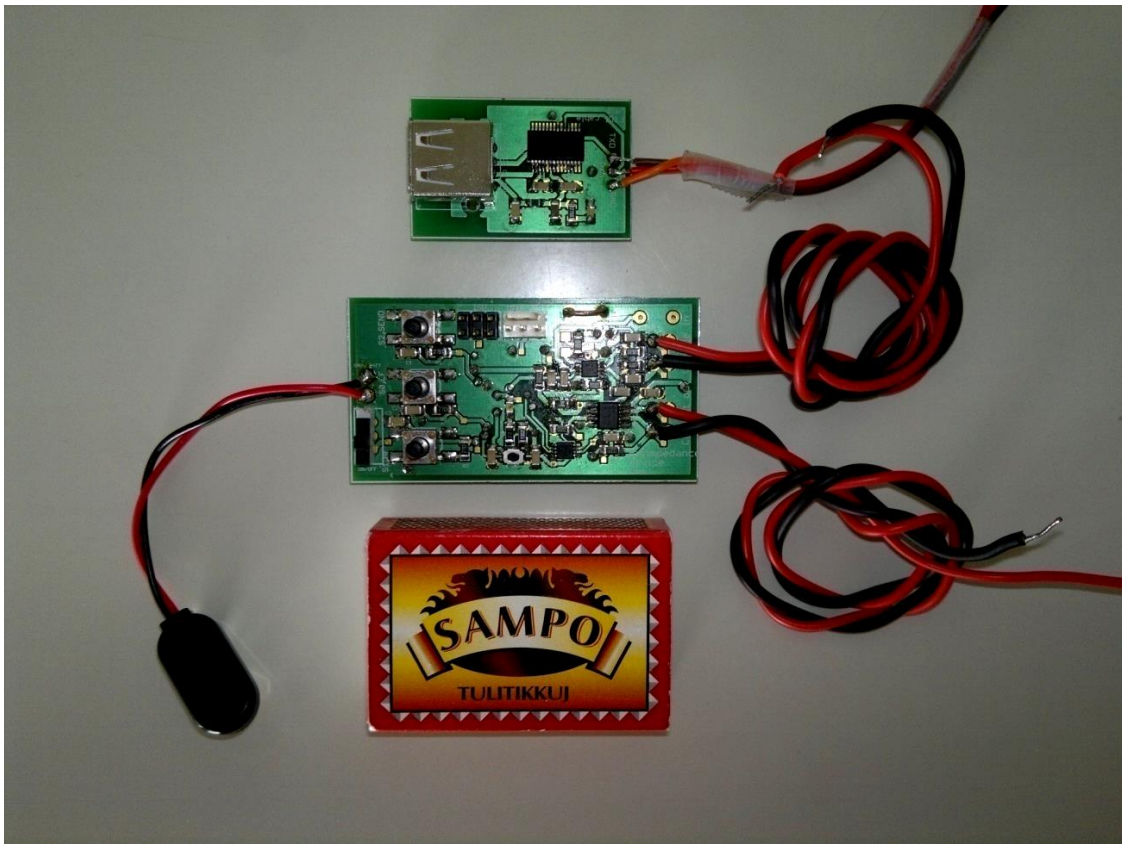

Figure 5.1 *The FTDI chip (above) and the bioimpedance device (below).*

The Table 5.3 lists the fundamental parameters referring to the performance of the bioimpedance device. Term “idle” in the current consumption section points to the case in which no current feeding or voltage measurement is under work but the device is in ON -position. It has to be mentioned that the power saving modes were not utilized in the bioimpedance device. The operational amplifier OPA2365 does not include any kind of power saving mode and therefore it takes 5mA even when idling. In addition, the power supply circuit is not optimized for 9V battery, which was used in the measurements. Taking these factors in consideration the current consumption in the idle mode could be easily reduced to around 4mA.

Table 5.2 *Characteristics of the bioimpedance device. Subscript [1] refers to datasheet of INA331 (Texas Instruments Inc. 2005).*

Dimensions:	64 x 34 x 17 mm
Measurement range:	~ 120Ω max
Impedance resolution:	0.1Ω (I_{rms} = 115μA)
Current consumption	
Idle:	9.5 mA
Active:	22.0mA
Output impedance	
5kHz:	11.4kΩ
100kHz	10.7kΩ
Input impedance[1]:	1*10^13Ω
CMRR[1]	
5kHz:	90dB
100kHz:	23dB
Frequency range:	~ 40kHz

The output impedance of the current feeding circuit was measured as follows. The current feeding leads were measured differentially first without a load using an oscilloscope and the rms voltage (V_{rms}) induced by the current was recorded. Then a load resistor (R_L) of 50Ω was placed on the breadboard and the current induced rms voltage ($V_{rms,L}$) measured differentially. The output impedance (Z_{out}) was calculated according to the equation 50 for 5kHz and 100kHz.

$$Z_{out} = \frac{R_L\left(V_{rms} - V_{rms,L}\right)}{V_{rms,L}} \tag{54}$$

The output impedance should be as high as possible so that the load would have minimal effect on the current magnitude. The measured output impedance was not as high as desired, but considering the fact that the voltage to current converter is extremely simple in design and that the impedance measurement range of the bioimpedance device is relatively small the output impedance of around 11kΩ at the middle of the measurement range should be fairly reasonable.

The frequency range for the bioimpedance device was measured using similar measurement arrangement as in the section 4.3.3 is presented. The function generator used was Kenwood FGE1202. The frequency range was measured by using 50Ω load

resistor. The frequency performance was measured for triangle wave input. The excitation frequency was increased gradually from 5kHz and the output of OPA2365 was measured simultaneously with the oscilloscope. The excitation frequency at which the output of OPA2365 started to show signs of distortion was concluded to be the maximum frequency of the bandwidth. For triangle input the frequency maximum was at around 40kHz.

5.3 Test measurements

This section represents the test measurement results obtained by the developed bioimpedance device. Firstly, the measurement results of the excitation current feeding measurement are introduced. Secondly, the measurement results with the function generator input for both triangle and sine wave provided. Thirdly, the system measurement test results for the purely resistive load are presented followed by the system measurement test results for the 2R-1C load. Finally, the in vivo measurement results are introduced.

5.3.1 Excitation current measurements

The results of the excitation current measurements for both 5kHz and 100kHz excitation frequency can be seen on the Table 5.3. From the results can be seen that the excitation current I_{rms} remains fairly constant between 2.012kΩ and 38.4Ω load resistance values with approximately 10.1mA variation. From this point on, the current namely increases in quite a rapid manner. The results with the 10.2Ω and 5.0Ω load should be discarded.

Table 5.3 *The results of the excitation current measurements.*

Z_{FLUKE} (Ω)	Frequency (kHz)	$V_{rms,CALC}$ (mV)	$V_{rms,OSC}$ (mV)	V_{MEAN} (mV)	I_{rms} (μA)
2012.0	5	231.4	232.0	-71.2	115.3
	100		231.0	-79.4	114.8
1020.0	5	117.3	114.0	-35.0	111.8
	100		116.0	-39.6	113.7
520.0	5	59.8	59.5	-17.7	114.4
	100		60.1	-19.2	115.6
201.0	5	23.1	22.7	-6.27	112.9
	100		22.7	-7.04	112.9
151.0	5	17.4	17.0	-4.94	112.6
	100		17.1	-5.57	113.2
101.0	5	11.6	11.4	-3.39	112.9
	100		11.4	-3.79	112.9
81.8	5	9.41	9.31	-2.69	113.8
	100		9.35	-3.08	114.3
68.0	5	7.82	7.84	-2.18	115.3
	100		7.83	-2.39	115.1
56.5	5	6.50	6.64	-1.99	117.5
	100		6.65	-1.93	117.7
50.0	5	5.75	5.93	-1.51	118.6
	100		5.97	-1.79	119.4
47.3	5	5.44	5.58	-1.56	118.0
	100		5.59	-1.67	118.2
38.4	5	4.42	4.70	-1.17	122.4
	100		4.71	-1.30	122.7
33.0	5	3.80	4.56	-1.10	138.2
	100		4.59	-1.23	139.1
22.0	5	2.53	3.33	-0.80	151.4
	100		3.28	-0.84	149.1
15.1	5	1.74	2.99	-0.50	198.0
	100		2.92	-0.54	193.4
10.2	5	1.17	4.83	-0.02	480.0
	100		4.15	-0.35	411.0
5.0	5	0.58	7.95	-0.13	1590.0
	100		7.99	-0.02	1598.0

The increase of the measured excitation current between 38.4Ω and 15.1Ω load resistance values can partly be explained by the fact that the signal to noise ratio

declines significantly with the decreasing load resistance or in other words with the decreasing voltage measured over the resistor. Decreasing SNR is clearly distinctive on the Figure 5.2, which represents the waveform of the voltage over the load resistor ($V_{rms,OSC}$) measured by the oscilloscope. From top down the load resistance values of the Figure 5.2 are 101.0Ω, 68.0Ω, 50Ω and 33Ω accordingly. The vertical and the horizontal scales are same in every curve.

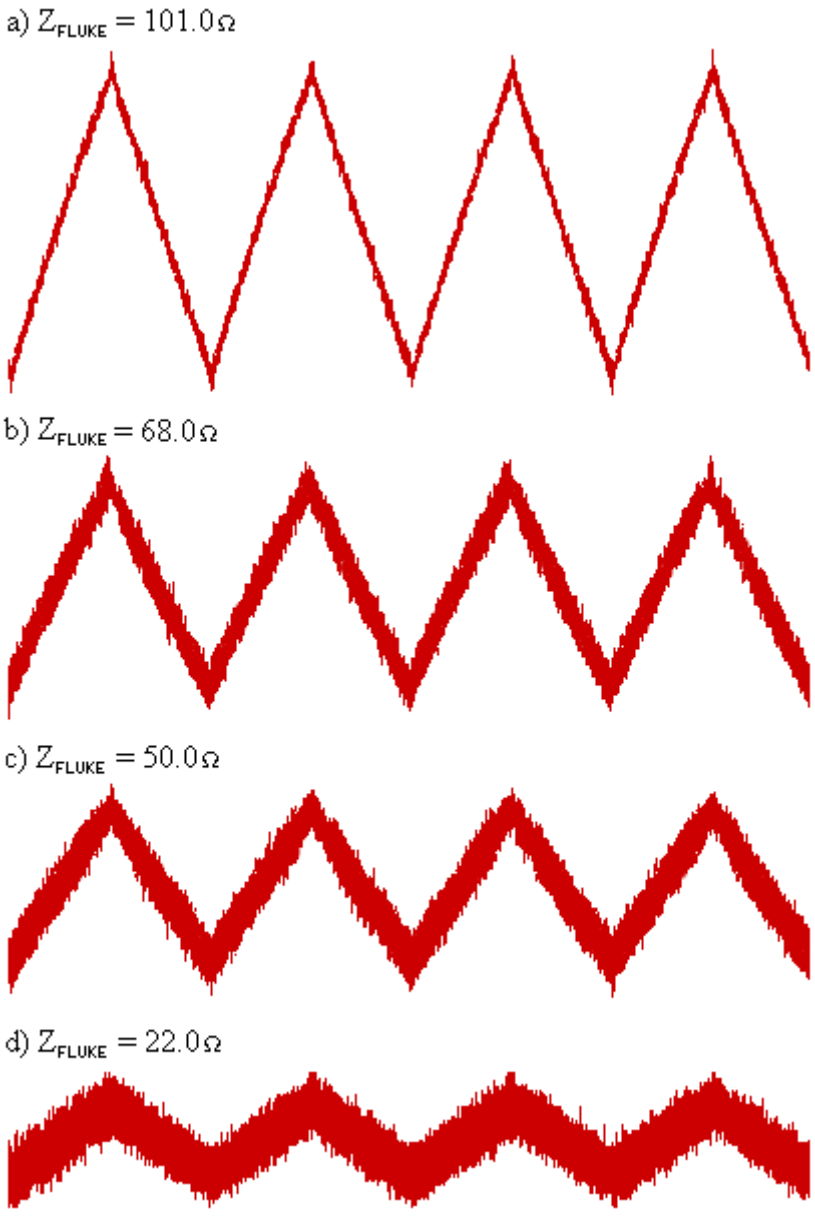

Figure 5.2 *5kHz excitation current waveform with decreasing resistive load: 101.0Ω, 68.0Ω, 50Ω and 22Ω.*

The high frequency base level noise clearly starts to kick in with the decreasing resistance and affects to the rms voltage measured by the oscilloscope. The base level

noise was measured with the oscilloscope when no input or load is connected, the leads were basically floating. The base level rms voltage did vary randomly in time between 0.3mV and 1.6mV. Introducing a load between the oscilloscope leads did not have any noticeable effect to the rms voltage. The fairly high base level voltage creates obvious uncertainty into the excitation current measurements at low load resistance levels. Therefore, the excitation current measurement results at the low load resistance levels should be interpreted with caution. One contributing factor for the base level noise is the fact that due to practical reasons the all measurements, not just the excitation current measurements, had to be performed indoors and in the presence of high frequency noise sources like personal computers. The base level noise has had some effect on all the following results presented.

Another possible noise source affecting all of the measurements is the breadboard on which all of the test circuits were assembled. A breadboard is notoriously prone to noise coupling due to the fact that the intermittent connections and the long wires present an antenna like formation. Breadboards are prone to capacitive coupling.

5.3.2 Measurements with function generator input

The section 5.3.2 represents the test measurement results of the voltage measurement block of the bioimpedance device. The input waveform was generated by a function generator. The Tables 5.4, 5.5 and 5.6 introduce the results of the triangle waveform excitation for frequencies of 5kHz, 100kHz and 200kHz accordingly. The Tables 5.7, 5.8 and 5.9 introduce the results of the sine wave excitation for frequencies of 5kHz, 100kHz and 200kHz accordingly.

The equation 51 and the equation 52 were used for calculating the mean error and the standard deviation of the error of the results obtained. These equations are used throughout the results section.

$$\bar{x} = \frac{1}{n} \cdot \sum_{i=1}^{n} x_i = \frac{\left(x_1 + \ldots + x_n\right)}{n} \tag{55}$$

$$\sigma = \sqrt{\frac{\sum_{i=1}^{n} \left(x_i - \bar{x}\right)^2}{n-1}} \tag{56}$$

The Table 5.4 shows the results of the 5kHz triangle input. The results reveal that the mean error $\bar{x}$ of the measured impedance in percentage ($\Delta Z\%$) between the calculated value (Z_{FLUKE}) and the value measured by the bioimpedance device (Z_{MEAS}) remains at 1.51% between 111.0Ω and 22.0Ω with a standard deviation σ of 0.42%. Below the load resistance of 22.0Ω the error percentage increases substantially and the device can be considered to be insensitive for such load values.

The mean error of 1.51% with a low standard deviation of 0.42% indicates that the error systematically follows the decreasing load resistance. The error is likely due to external noise coupling into the test circuit and to the measurement circuit itself. The noise is manifested by a high frequency noise level on the signal and by a relatively high magnitude voltage spikes with a lower frequency. Both noise components are seemingly constant in magnitude regardless of the load resistance used. The tests were performed in a PC lab and therefore under significant noise exposure from the surrounding electronics. In addition, the breadboard used in the measurements might have contributed into the noise coupling. The noise coupling starts to affect into the measurement accuracy at the lower load resistance values as the signal to noise ratio decreases. This can be seen as an increase in relative error ΔZ% at the lowest load values. However, the direction of the change in the measured resistance follows the change in the actual load values in all cases, even when the smallest change in the actual load resistance is 2.8Ω. There was no indication of distortion at the output of the OPA2365 at the excitation frequency of 5kHz as can be noticed from the Figure 5.3a.

Table 5.4 *Measurement results of the 5kHz triangle wave excitation. Function generator input.*

Z_{FLUKE} (Ω)	$V_{avg,MEAS}$ (mV) - baselevel	$V_{rms,MEAS}$ (mV)	Z_{MEAS} (Ω), I_{rms}=115μA	Error ΔZ (Ω)	Error ΔZ (%)
111.0	1096	13.01	113.1	+2.1	+1.9
101.0	996	11.82	102.8	+1.8	+1.8
81.4	804	9.54	83.0	+1.6	+2.0
72.0	710	8.42	73.3	+1.3	+1.8
65.0	638	7.57	65.8	+0.8	+1.2
60.2	590	7.00	60.9	+0.7	+1.2
56.4	556	6.60	57.4	+1.0	+1.8
50.0	490	5.82	50.6	+0.6	+1.2
47.2	464	5.51	47.9	+0.7	+1.5
43.2	424	5.03	43.8	+0.6	+1.4
38.4	376	4.46	38.8	+0.4	+1.0
33.0	324	3.85	33.5	+0.5	+1.5
26.8	262	3.11	27.0	+0.2	+0.7
22.0	218	2.59	22.5	+0.5	+2.2
15.0	152	1.80	15.7	+0.7	+4.6
10.2	106	1.26	10.9	+0.7	+6.9
4.8	60	0.71	6.2	+1.4	+29.2

The Table 5.5 shows the measurement results for 100kHz triangular excitation. The mean error $\bar{x}$ of the measured impedance in percentage (ΔZ%) compared to the actual

impedance value (Z_{FLUKE}) is -1.54 % between the load resistances of 111.0Ω and 26.8Ω with a standard deviation σ of 0.37%. The low standard deviation of ΔZ% suggests that the error percentage in measured impedance follows systematically decreasing load resistance. As the measurement arrangement was equal with the 5kHz excitation frequency measurement above, the same noise sources can be suggested. However, a trend of decreasing value of the mean error in percentage as the excitation frequency increases can be observed, that is confirmed by the results with a 200kHz excitation frequency visible on the Table 5.6. The main contribution to this is clearly visible on the Figure 5.3b. The output of the OPA2365 is distorted. The signal gets distorted due to the frequency limitations of the instrumentation amplifier (INA331). There was also a seemingly constant voltage spike observed in the output signal of OPA2365. The voltage spike is not clearly visible at the load values above 43.2Ω. However, below 43.2Ω load resistances it starts to get uncovered gradually and stays fairly constant in magnitude with decreasing load. This is a significant contributor to the increased average voltage measured by the bioimpedance device ($V_{avg,\ MEAS}$) at the lowest load resistance values and a reason for decreasing error in ohms (ΔZ) at the load resistances below 50Ω as it starts to compensate the distortion effect. The origins of the voltage spike are not known. The direction of change in the measured resistance is correct for all load resistance values.

Table 5.5 *Measurement results of the 100kHz triangle wave excitation. Function generator input.*

Z_{FLUKE} (Ω)	$V_{avg,MEAS}$ (mV) - baselevel	$V_{rms,MEAS}$ (mV)	Z_{MEAS} (Ω), I_{rms}=115μA	Error ΔZ (Ω)	Error ΔZ (%)
111.0	1064	12.63	109.8	-1.2	-1.1
101.0	966	11.47	99.7	-1.3	-1.3
81.4	780	9.26	80.5	-0.9	-1.1
72.0	686	8.14	70.8	-1.2	-1.7
65.0	618	7.34	63.8	-1.2	-1.8
60.2	572	6.79	59.0	-1.2	-2.0
56.4	538	6.39	55.6	-0.8	-1.4
50.0	474	5.63	49.0	-1.0	-2.0
47.2	450	5.34	46.4	-0.8	-1.7
43.2	410	4.87	42.3	-0.9	-2.1
38.4	368	4.37	38.0	-0.4	-1.0
33.0	316	3.75	32.6	-0.4	-1.4
26.8	256	3.04	26.4	-0.4	-1.5
22.0	212	2.52	21.9	-0.1	-0.5
15.0	148	1.76	15.3	+0.3	+2.0
10.2	104	1.23	10.7	+0.5	+4.9
4.8	62	0.74	6.4	+1.6	+33.0

The Table 5.6 introduces the measurement results of the 200kHz triangular excitation waveform. The mean error $\bar{x}$ of the measured impedance in percentage (ΔZ%) is -2.27% between the load resistance values of 111.0Ω and 43.2Ω with a standard deviation σ of 0.84%. The results with 101.0Ω and 81.4Ω may be corrupted. The mean error in percentage seems to follow systematically the decreasing resistance like it does for 5kHz and 100kHz excitation frequencies as well. The mean error of -2.27% confirms the decreasing trend of error percentage with increasing frequency, for 5kHz and 100kHz the mean error in percentage was 1.51% and -1.54% accordingly. From the Figure 5.3c we may notice that the distortion is present at 200kHz triangle excitation and gets worse with increasing frequency. Voltage spike with a somewhat constant magnitude was observed at 50Ω and below load resistance values with 200kHz excitation frequency and starts to affect increasingly to the measurements results. That is the main contributor to the increasing average voltage measured by the bioimpedance device ($V_{avg,\ MEAS}$). The direction of change in the measured resistance correlates with the actual change in the load resistance as it did in the previous cases.

Table 5.6 *Measurement results of the 200kHz triangle wave excitation. Function generator input.*

Z_{FLUKE} (Ω)	$V_{avg,MEAS}$ (mV) - baselevel	$V_{rms,MEAS}$ (mV)	Z_{MEAS} (Ω), I_{rms}=115μA	Error ΔZ (Ω)	Error ΔZ (%)
111.0	1046	12.42	108.0	-3.0	-2.7
101.0	970	11.51	100.1	-0.9	-0.9
81.4	772	9.16	79.7	-0.7	-0.9
72.0	676	8.02	69.7	-2.3	-3.2
65.0	610	7.24	63.0	-2.0	-3.1
60.2	566	6.72	58.4	-1.8	-3.0
56.4	534	6.34	55.1	-1.3	-2.3
50.0	472	5.60	48.7	-1.3	-2.6
47.2	448	5.32	46.3	-0.9	-1.9
43.2	410	4.87	42.3	-0.9	-2.1
38.4	368	4.37	38.0	-0.4	-1.0
33.0	318	3.77	32.8	-0.2	-0.6
26.8	260	3.09	26.9	+0.1	+0.4
22.0	218	2.59	22.5	+0.5	+2.2
15.0	154	1.83	15.9	+0.9	+6.0
10.2	114	1.35	11.8	+1.6	+15.7
4.8	74	0.88	7.7	+2.9	+60.4

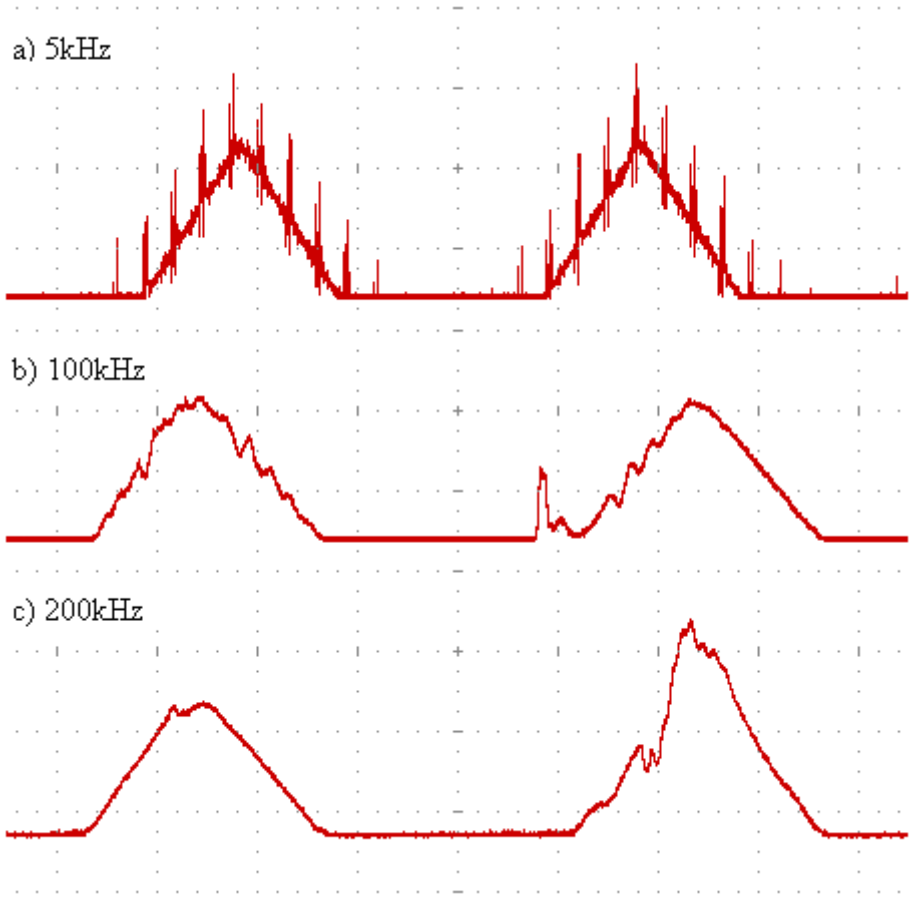

Figure 5.3 *The Oscilloscope screen capture of the OPA2365 output with a triangle input and 50Ω resistive load. The vertical axis is equal in all cases. a) 5kHz b) 100kHz c) 200kHz excitation frequency. The distortion is clearly visible in the figures b) and c). The voltage spice is visible in the figure c).*

The Table 5.7 presents the measurement results of the 5kHz sine wave excitation. Sine wave excitation measurements were performed in addition to triangular to investigate whether the excitation waveform had effect on the measurement accuracy of the bioimpedance device's voltage measurement block. The Table 5.7 show that the mean error $\bar{x}$ of the measured impedance in percentage ($\Delta Z\%$) compared to the actual impedance (Z_{FLUKE}) is 1.77% between 111.0Ω and 22.0Ω load resistance values with a standard deviation σ of 0.42%. There is no significant difference in accuracy when compared to the 5kHz triangular excitation, the mean error for the 5kHz triangular excitation was 1.51% with a standard deviation of 0.42%. Similar load resistance dependent systematic error can be found from the 5kHz sine excitation as well. A low amplitude high frequency noise level on the signal and fairly high magnitude voltage spikes with a lower frequency were observed from the output of the OPA2365. Both noise components are seemingly constant in magnitude regardless of the load resistance used. Direction of change in the measured impedance correlates with the direction of change of the actual load resistance (Z_{FLUKE}) in all cases. There was no distortion observed in the output of the OPA2365 as can be seen from the Figure 5.4a.

Table 5.7 *Measurement results of the 5kHz sine wave excitation. Function generator input.*

Z_{FLUKE} (Ω)	$V_{avg,MEAS}$ (mV) - baselevel	$V_{rms,MEAS}$ (mV)	Z_{MEAS} (Ω), I_{rms}=115μA	Error ΔZ (Ω)	Error ΔZ (%)
111.0	1144	13.06	113.6	+2.6	+2.3
101.0	1040	11.88	103.3	+2.3	+2.1
81.4	838	9.57	83.2	+1.8	+2.2
72.0	738	8.43	73.3	+1.3	+1.8
60.2	614	7.01	61.0	+0.8	+1.3
56.4	578	6.60	57.4	+1.0	+1.8
50.0	512	5.85	50.9	+0.9	+1.8
47.2	484	5.53	48.1	+0.9	+1.9
43.2	440	5.03	43.7	+0.5	+1.2
38.4	392	4.48	38.9	+0.5	+1.3
33.0	336	3.84	33.4	+0.4	+1.2
22.0	226	2.58	22.5	+0.5	+2.3
10.2	106	1.21	10.5	+0.3	+2.9
4.8	56	0.64	5.6	+0.8	+16.7

The Table 5.8 presents the measurement results of the 100kHz sine wave excitation. The mean error $\bar{x}$ of the measured impedance in percentage (ΔZ%) is -0.15% between 111.0Ω and 33.0Ω load resistance values with a standard deviation σ of 0.48%. The results of the 100kHz sine excitation show that the mean error in percentage follows quite systematically the decreasing load resistance and that direction of change in the measured impedance is correct in all cases. In comparison to 100kHz triangular excitation there is a rather clear difference observed in the mean error percentage, the 100kHz triangular excitation shows a mean error of -1.54% with a standard deviation of 0.37%. This is probably due to the more significant distortion of the triangle excitation because of the high harmonic frequencies. The output waveform of OPA2365 with 100kHz sine excitation can be seen in the Figure 5.4b. The output of OPA2365 is rather distinctively distorted and a constant magnitude voltage spike similar to 100kHz triangle excitation can be seen at the sine excitation output. The voltage spike starts to get uncovered at around 50Ω load resistance and remains constant in magnitude as the load resistance decreases. The voltage spike increases the value of the average voltage ($V_{avg,MEAS}$) measured by the bioimpedance device. The increase in the relative error (ΔZ%) at low load resistance values is mostly due to this voltage spike as the signal to noise ratio deteriorates.

Table 5.8 *Measurement results of the 100kHz sine wave excitation. Function generator input.*

Z_{FLUKE} (Ω)	$V_{avg,MEAS}$ (mV) - baselevel	$V_{rms,MEAS}$ (mV)	Z_{MEAS} (Ω), I_{rms}=115μA	Error ΔZ (Ω)	Error ΔZ (%)
111.0	1124	12.84	111.7	+0.7	+0.6
101.0	1020	11.65	101.3	+0.3	+0.3
81.4	824	9.41	81.9	+0.5	+0.6
72.0	724	8.27	71.9	-0.1	-0.1
60.2	602	6.88	59.8	-0.4	-0.7
56.4	566	6.47	56.2	-0.2	-0.4
50.0	500	5.71	49.7	-0.3	-0.6
47.2	474	5.41	47.0	-0.2	-0.4
43.2	432	4.94	42.9	-0.3	-0.7
38.4	386	4.41	38.3	-0.1	-0.3
33.0	332	3.79	33.0	0	0
22.0	224	2.56	22.3	+0.3	+1.4
10.2	112	1.28	11.1	+0.9	+8.8
4.8	64	0.73	6.4	+1.6	+33.3

The Table 5.9 shows the measurement results of the 200kHz sine wave excitation. The mean error $\bar{x}$ of the impedance measurement in percentage (ΔZ%) between 111.0Ω and 43.2Ω load resistance values is -2.89% with a standard deviation σ of 0.34%. In comparison to triangular excitation at 200kHz the mean error in percentage seems to be at around same level. This indicates that the sine wave starts to get seriously distorted at the frequencies over 100kHz whereas the triangle excitation is badly distorted already at the frequencies below 100kHz. The voltage measurement block has higher frequency range with the sine excitation. The output of the OPA2365 with the 200kHz sine excitation can be seen at the Figure 5.4c. The output is clearly distorted. The measurements results of 200kHz sine excitation show a continuum to the previous measurement results, so that the mean error in percentage seems to systematically follow the decreasing load resistance values. Direction of change in the measured impedance is correct for all actual load resistance values. The error in percentage (ΔZ%) starts to spin out of the systematic range at 43.2Ω load resistance value. The output of the OPA2365 with 200kHz excitation shows also a similar constant voltage spike as it did at 200kHz triangular excitation. The effect of the voltage spike on the measurement accuracy increases as the load resistance decreases and the signal to noise ratio declines. The voltage spike compensates the distortion effect and at the smallest load resistance values it is the dominating factor of the error.

Table 5.9 *Measurement results of the 200kHz sine wave excitation. Function generator input.*

Z_{FLUKE} (Ω)	$V_{avg,MEAS}$ (mV) - baselevel	$V_{rms,MEAS}$ (mV)	Z_{MEAS} (Ω), I_{rms}=115μA	Error ΔZ (Ω)	Error ΔZ (%)
111.0	1084	12.38	107.7	-3.3	-3.0
101.0	986	11.26	97.9	-3.1	-3.1
81.4	798	9.12	79.3	-2.1	-2.6
72.0	702	8.02	69.7	-2.3	-3.2
60.2	586	6.69	58.2	-2.0	-3.3
56.4	554	6.33	55.0	-1.4	-2.5
50.0	488	5.57	48.5	-1.5	-3.0
47.2	464	5.30	46.1	-1.1	-2.3
43.2	422	4.82	41.9	-1.3	-3.0
38.4	380	4.34	37.7	-0.7	-1.8
33.0	328	3.75	32.6	-0.4	-1.2
22.0	226	2.58	22.5	+0.5	+2.2
10.2	114	1.30	11.3	+1.1	+10.8
4.8	72	0.82	7.2	+2.4	+50.0

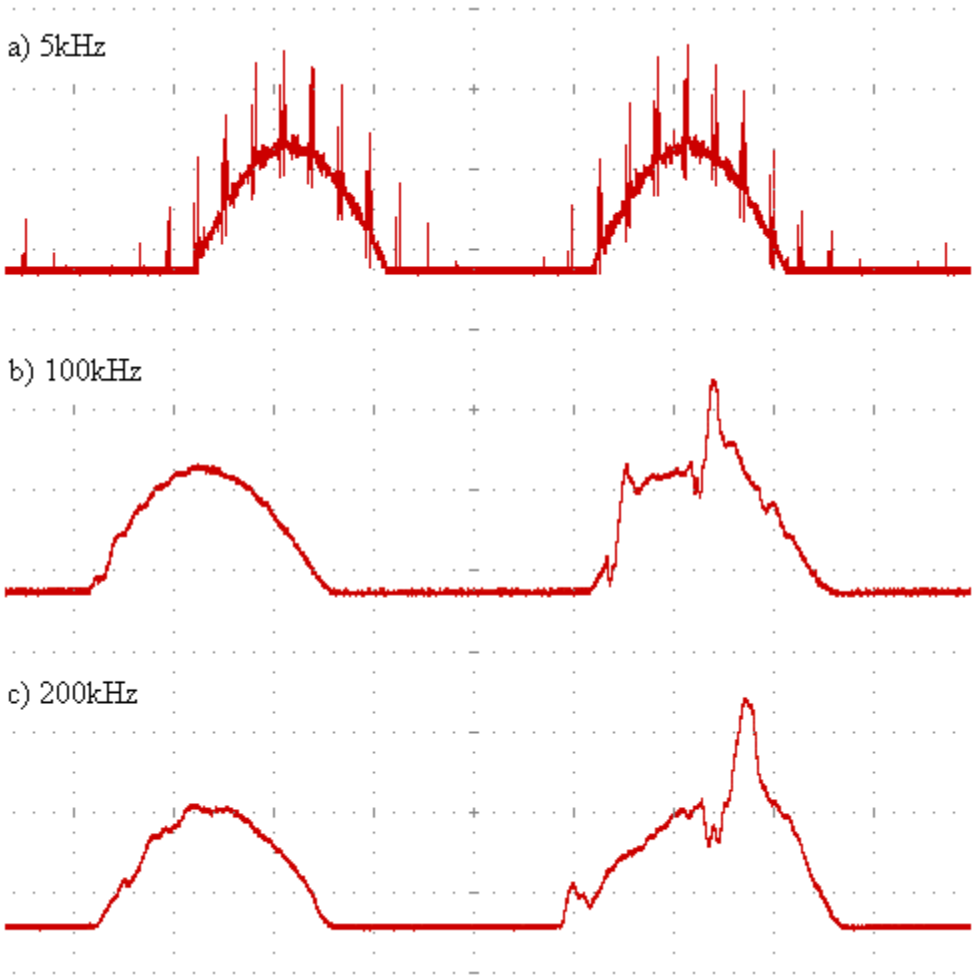

Figure 5.4 *The Oscilloscope screen capture of the OPA2365 output with a sine input and 50Ω resistive load. The vertical axis is equal in all cases. a) 5kHz b) 100kHz c) 200kHz excitation frequency. The distortion and the voltage spike are clearly visible in the figures b) and c).*

5.3.3 System test with a purely resistive load

The section 5.3.3 represents the results of the system test with a purely resistive load. The test load values (Z_{FLUKE}) used in the measurements were between 4.8Ω and 111.0Ω. For calculating the impedance measured (Z_{MEAS}) by the bioimpedance device from the obtained voltage data ($V_{rms,MEAS}$) the excitation current magnitude (I_{rms}) was assumed to be 115µA_{rms}. This assumption was made on the basis of the fact that the excitation current measurement results of the section 5.3.1 could not be absolutely trusted, on the other hand the current measurements did show that the excitation current magnitude remains fairly constant at least down to 38.4Ω.

The Table 5.10 represents the results impedance measurement results of the 5kHz excitation current. The results show that the error (ΔZ) of the measured impedance compared to the actual impedance value (Z_{FLUKE}) is fairly small. The mean error $\bar{x}$ of

the impedance measurement in ohms (ΔZ) between the load resistances (Z_{FLUKE}) of 101.0Ω and 15Ω is +0.18Ω with a standard deviation of 0.75Ω. The output of OPA2365 was not distorted as the Figure 5.7a suggests. The constant background noise starts to affect on the signal to noise ratio at the low load resistance values. The noise coupling increases the average voltage measured by the bioimpedance device and therefore the error in ohms increases at the positive direction at the smallest load resistance values. Direction of change in the measured impedance follows the change in the actual load values in all cases.

Table 5.10 *System test results with purely resistive load. 5kHz excitation frequency.*

Z_{FLUKE} (Ω)	$V_{avg,MEAS}$ (mV) - baselevel	$V_{rms,MEAS}$ (mV)	Z_{MEAS} (Ω), I_{rms}=115µA	Error ΔZ (Ω)	Error ΔZ (%)
111.0	1060	12.58	109.4	-1.6	-1.4
101.0	986	11.70	101.8	+0.8	+0.8
81.4	798	9.47	82.4	+1.0	+1.2
72.0	704	8.36	72.7	+0.7	+1.0
65.0	640	7.60	66.1	+1.1	+1.7
60.2	588	6.98	60.7	+0.5	+0.8
56.4	554	6.58	57.2	+0.8	+1.4
50.0	488	5.79	50.3	+0.3	+0.6
47.2	460	5.46	47.5	+0.3	+0.6
43.2	420	4.99	43.3	+0.1	+0.2
38.4	376	4.46	38.8	+0.4	+1.0
33.0	314	3.73	32.4	-0.6	-1.8
26.8	252	2.99	26.0	-0.8	-2.9
22.0	204	2.42	21.1	-0.9	-4.1
15.0	134	1.59	13.8	-1.2	-7.8
10.2	106	1.26	10.9	+0.7	+6.9
4.8	60	0.71	6.2	+1.4	+29.2

The Table 5.11 shows the impedance measurement results of the 100kHz excitation current. The mean error $\bar{x}$ of the measured impedance in ohms between load resistance values of 101.0Ω and 15.0Ω is -4.07Ω with a standard deviation of 0.36Ω. The main contribution to the negative mean error is clearly visible on the Figure 5.7b. The output of the OPA2365 is clearly distorted. The signal gets distorted due to the frequency limitations of the instrumentation amplifier (INA331). The relatively small standard deviation points at a constant error in the measurement. Occasionally the bioimpedance device gives corrupted results; the corrupted results are presented in brackets. These corrupted results seem to show up when the load resistance is small. Some sort of

voltage spikes at the input of the AD -converter may be the reason behind the faulty results. However, when the input of the AD -converter was measured with an oscilloscope no significant spikes were observed. Simultaneously with the oscilloscope, measurements were performed also with the bioimpedance device; the obtained voltage results ($V_{rms,MEAS}$) were uncorrupted and correlated with the rms voltage measured by the oscilloscope. Another reason for the corrupted results could be that the ripple voltage induced by the moving average filter is large enough to contribute to the measurement values. Decreasing the corner frequency of the filter would result into a higher rise time but lower ripple voltage. Increasing the averaging in the software did not remove the source of the data corruption. As was the case in 5kHz excitation results, the background noise coupling affects the measurement results at low load resistance values as the signal to noise ratio declines.

Table 5.11 *System test results with purely resistive load. 100kHz excitation frequency.*

Z_{FLUKE} (Ω)	$V_{avg,MEAS}$ (mV) - baselevel	$V_{rms,MEAS}$ (mV)	Z_{MEAS} (Ω), I_{rms}=115µA	Error ΔZ (Ω)	Error ΔZ (%)
111.0	1006	11.94	103.8	-7.4	-6.5
101.0	938	11.13	96.8	-4.2	-4.1
81.4	752	8.93	77.6	-3.8	-4.6
72.0	660	7.83	68.1	-3.9	-5.4
65.0	594	7.05	61.3	-3.7	-5.7
60.2	546	6.48	56.4	-3.8	-6.3
56.4	512	6.08	52.8	-3.6	-6.4
50.0	448	5.32	46.2	-3.8	-7.5
47.2	418	4.96	43.1	-4.1	-8.7
43.2	374	4.44	38.6	-4.6	-10.1
38.4	334	3.96	34.5	-3.9	-10.2
33.0	282 (256)	3.35	29.1	-3.9	-11.8
26.8	216 (180)	2.56	22.3	-4.5	-16.8
22.0	170 (252)	2.02	17.5	-4.5	-20.2
15.0	100 (360)	1.19	10.3	-4.7	-31.3
10.2	62 (444)	0.74	6.4	-3.8	-37.3
4.8	46 (508)	0.55	4.8	0	0

The Figure 5.5 visualizes the measurement results with a purely resistive load. The green line refers to measured impedance values with 5kHz excitation current. 100kHz results are marked with a blue line. The red line refers to the actual resistance values with no error. As the graph implies both 5kHz and 100kHz measurements results seem to follow linearly the decreasing load. It also visualizes the fact that error in ohms of the

100kHz measurement results remains fairly constant over the actual load resistance range of 101.0Ω and 15.0Ω.

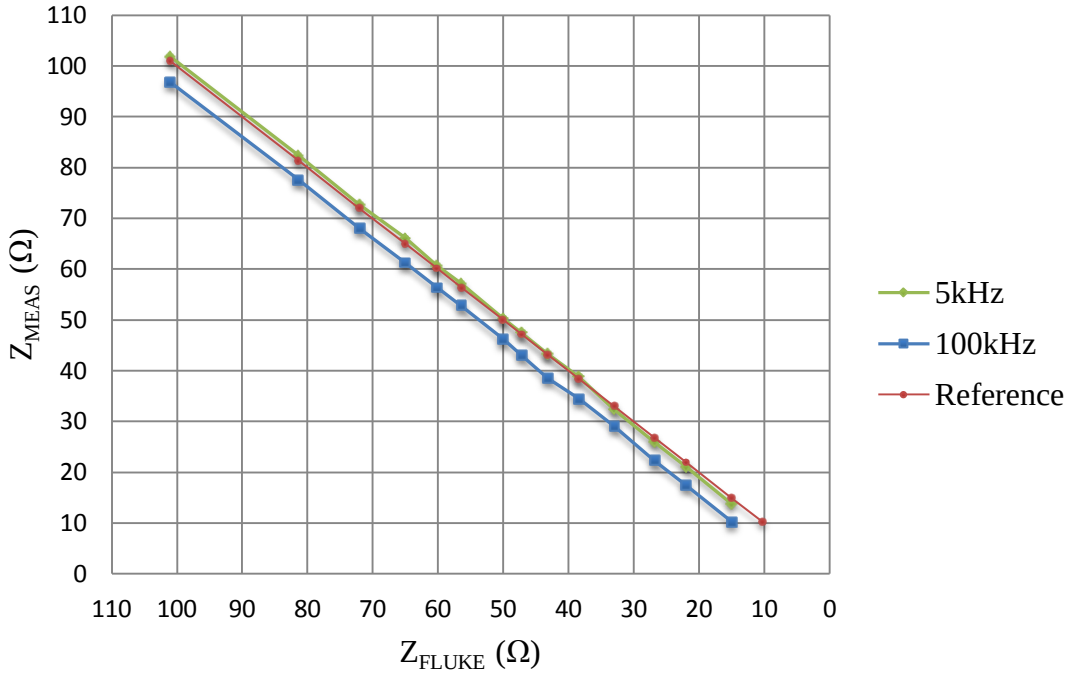

Figure 5.5 *The measurement results with a purely resistive load. The green line refers to measured impedance values with 5kHz excitation current. 100kHz is marked with a blue line. The red line refers to the actual values with no error.*

The Figure 5.6 shows the error ΔZ for 5kHz and 100kHz excitation in ohms over load resistance values of 101.0Ω and 15.0Ω. The trend line or the regression line is marked in a black color. The R^2 is the correlation factor of the regression line and tells how well the regression formula describes the measurement results. The R^2 is a ratio value of how well the suggested model fits the data. In empirical models value of 0.7 to 0.9 is considered good. (Haario 2004, p. 10; Laine 2007, p. 31, 41) The linear regression model describes quite poorly the formation of the error ΔZ. Logarithmic regression model would give better results. However, the standard deviation in the error is small enough to be covered by the random error sources like measurement site, slight difference in electrode placement and movement artifact in practice. Therefore applying any correlation factor in this case is not meaningful.

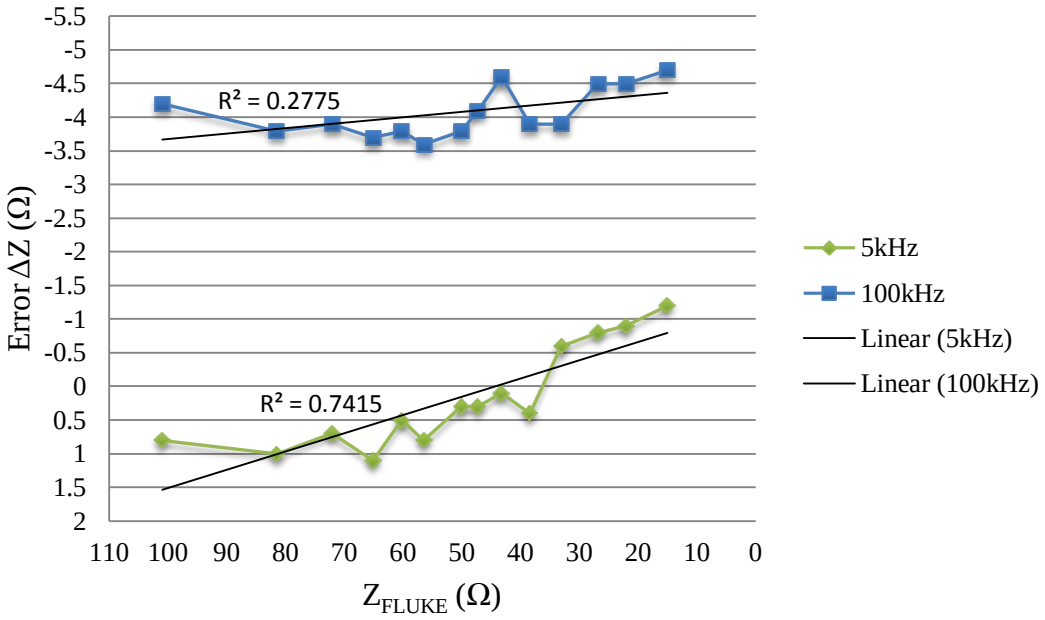

Figure 5.6 *Error ΔZ for 5kHz and 100kHz excitation in ohms over the load resistance values of 101.0Ω and 15.0Ω. Black line is the trendline.*

The Figure 5.7 shows the output of the OPA2365 for 5kHz and 100kHz excitation. The load resistance is 50Ω. The distortion at 100kHz is clearly visible on the Figure 5.7b and that is the main contributor to the error. In comparison, the 5kHz signal is not distorted. The constant voltage spike which was present at the function generator input measurements in the section 5.3.1 is not detected. The distortion at 100kHz triangular excitation is mainly due to the INA331 bandwidth limitations. The Figure 3.8c represents the triangular waveform Fourier series from which we can observe that in addition to the base frequency high frequency harmonics exist. These harmonic frequencies exceed the frequency characteristics of the INA331 so that at the high end of the frequencies the gain will fall. This results into the signal deformation.

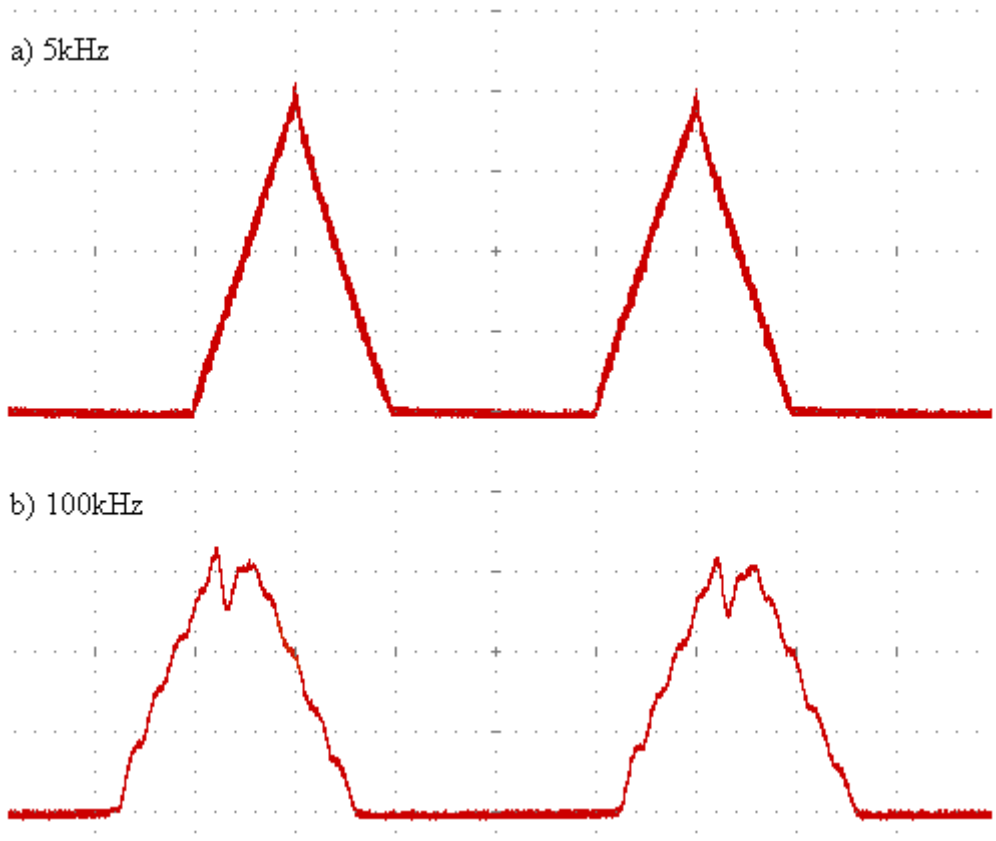

Figure 5.7 *The Oscilloscope screen capture of the OPA2365 output with 50Ω purely resistive load. The vertical axis is equal in both cases. a) 5kHz b) 100kHz excitation frequency. The signal is clearly distorted at the 100kHz excitation frequency.*

5.3.4 System test with 2R-1C load circuit

The section 5.3.4 represents the results obtained by using the 2R-1C test circuit as a load. For calculating the measured impedance (Z_{MEAS}) by the bioimpedance device from the obtained voltage data ($V_{rms,MEAS}$) the excitation current magnitude (I_{rms}) was assumed to be 115µA_{rms}. The total impedance (Z_{CALC}) was kept in the measurement range by changing the R_E, the other components were constant (C_m = 19.5nF, R_I = 22Ω).

The Table 5.12 introduces the measurement results of the 5kHz excitation. The mean error $\bar{x}$ of the impedance measurement in ohms (ΔZ) between the load resistances (Z_{CALC}) of 100.7Ω and 22.3Ω is +0.10Ω with a standard deviation of 0.71Ω. There was no indication of distortion at the output of OPA2365 as the Figure 5.10a suggests. The results below the load impedance of 22.3Ω were discarded as the output waveform of the OPA2365 was such heavily infiltrated by the noise. The noise coupled into the circuit seems to be somewhat constant in magnitude and starts to affect on the signal to noise ratio at low load impedance values. The noise increases the average

voltage measured by the bioimpedance device and therefore the error in ohms (ΔZ) increases into positive direction at the low load impedance values.

Table 5.12 *System test results with 2R-1C load circuit. 5kHz excitation frequency.*

Z_{CALC} (Ω)	R_E (Ω)	$V_{avg,MEAS}$ (mV) - baselevel	$V_{rms,MEAS}$ (mV)	Z_{MEAS} (Ω), I_{rms}=115uA	Error ΔZ (Ω)	Error Z (%)
100.7	101.0	964	11.44	99.5	-1.2	-1.2
81.2	81.4	790	9.38	81.6	+0.4	+0.5
67.9	68.0	662	7.86	68.3	+0.4	+0.6
56.3	56.4	546	6.48	56.4	+0.1	+0.2
49.9	50.0	480	5.70	49.5	-0.4	-0.8
47.1	47.2	454	5.39	46.9	-0.2	-0.4
38.4	38.4	368	4.37	38.0	-0.4	-1.0
33.0	33.0	322	3.82	33.2	+0.2	+0.6
27.1	27.1	270	3.20	27.8	+0.7	+2.6
22.3	22.3	230	2.73	23.7	+1.4	+6.3
15.0	15.0	160	1.90	16.5	+1.5	+10.0
10.2	10.2	114	1.35	11.8	+1.6	+15.7

The Table 5.13 presents the measurement results of the 2R-1C test circuit with a 100kHz excitation. The mean error $\bar{x}$ of the impedance measurement in ohms (ΔZ) between the load resistances (Z_{CALC}) of 57.8Ω and 20.3Ω is -7.85Ω with a standard deviation of 0.75Ω. The output of the OPA2365 was clearly distorted as can be seen from the Figure 5.10b. The results below the load impedance of 20.3Ω were discarded as the output waveform of the OPA2365 was distorted basically beyond recognition and infiltrated by the noise decreasing the signal to noise ratio into an unacceptable level. Occasionally the bioimpedance device indicated falsified data. Therefore oscilloscope was used to confirm the validity of the data obtained by the bioimpedance device by measuring the input of the AD -converter ($V_{rms,OSC,ADCinput}$). The corrupted measurement results are presented in the brackets. Data corruption was not observed when the ADC input was measured by the oscilloscope simultaneously with the bioimpedance device measurements. This was also the case during the purely resistive load measurements in the section 5.3.3.

Table 5.13 *System test results with 2R-1C load circuit. 100kHz excitation frequency.*

Z_{CALC} (Ω)	R_E (Ω)	$V_{avg,MEAS}$ (mV) - baselevel	$V_{rms,MEAS}$ (mV)	Z_{MEAS} (Ω), I_{rms}=115uA	Error ΔZ (Ω)	Error Z (%)	$V_{rms,OSC.ADCinput}$ (mV)
57.8	101.0	484(376)	5.74	50.0	-7.8	-13.5	494
52.2	81.4	444(356)	5.27	45.8	-6.4	-12.3	416
47.3	68.0	384(366)	4.56	39.6	-7.7	-16.3	397
42.1	56.4	328(366)	3.89	33.9	-8.2	-19.5	338
38.8	50.0	304(370)	3.61	31.4	-7.4	-19.1	310
37.3	47.2	274(354)	3.25	28.3	-9.0	-24.1	283
32.0	38.4	226(390)	2.68	23.3	-8.7	-27.2	235
28.4	33.0	196(416)	2.33	20.2	-8.2	-28.9	203
24.1	27.1	164(434)	1.95	16.9	-7.2	-29.9	173
20.3	22.3	120(430)	1.42	12.4	-7.9	-38.9	129
14.1	15.0	76(470)	0.90	7.8	-6.3	-44.7	86
9.8	10.2	50(382)	0.59	5.2	-4.6	-46.9	60

The figure 5.8 visualizes the results listed on the Table 5.12 and the Table 5.13. The 5kHz measurement results follow the reference line of the actual impedance values with no visible error. The relatively low deviation around the mean value over the load range in 100kHz excitation indicate that a systematic error is present. This view is strengthened by the Figure 5.8 showing that the 100kHz measurement results seem follow quite linearly the reference line of the actual load impedance values.

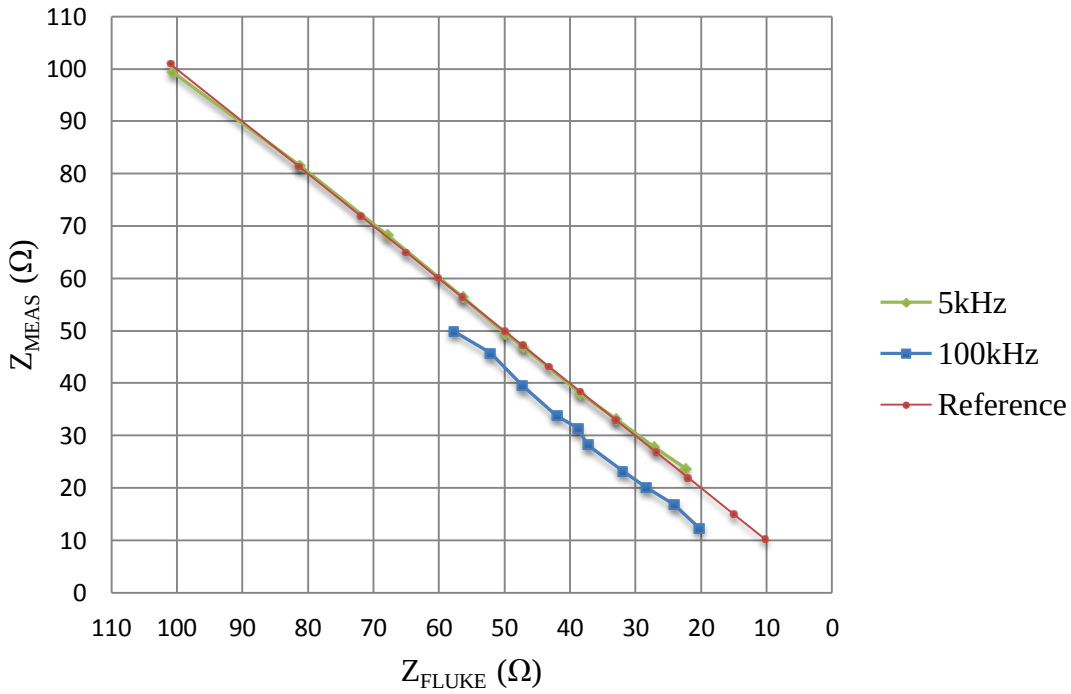

Figure 5.8 *The measurement results with a 2R-1C test circuit. The green line refers to measured impedance values with 5kHz excitation current. 100kHz is marked with a blue line. The red line refers to the actual values.*

The Figure 5.9 shows the error ΔZ for 5kHz and 100kHz excitation in ohms plotted over the load resistance values of 101.0Ω and 15.0Ω. The regression line is marked in a black color. The trend line or the regression line is marked as a black color. The linear regression model describes very poorly the error ΔZ formation. Logarithmic regression model would give better results in case of 5kHz excitation. However, as it was the case with the purely resistive load results the standard deviation in the error is small enough to be covered by the random error sources in practice. Therefore applying correction factor in this case is not appropriate.

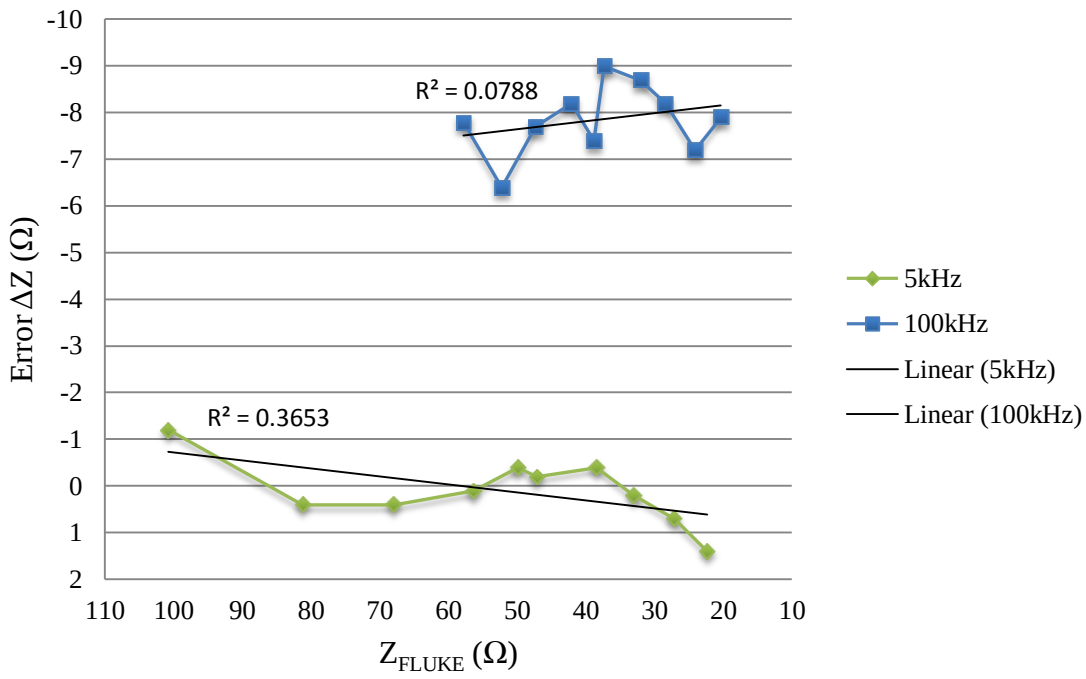

Figure 5.9 *Error ΔZ for 5kHz and 100kHz excitation in ohms over the load resistance values of 101.0Ω and 15.0Ω. The trendline is marked with a black color.*

The results of the 5kHz excitation with purely resistive load revealed fairly small error and deviation from the actual values, similarly the error in the 5kHz excitation measurement results with 2R-1C test circuit is such small as is the standard deviation that it can be consider to be statistical variation. The figure 5.10 shows the output of the OPA2365 for 5kHz and 100kHz excitation with a load impedance of 47.1Ω and 47.3Ω accordingly. The 100kHz output is clearly distorted as it was at the same frequency with a purely resistive load visible the Figure 5.7b. The 5kHz output instead seems to be unaffected by the distortion. The error in the 100kHz excitation results is mainly due to the distortion as a result of the INA331 bandwidth limitations.

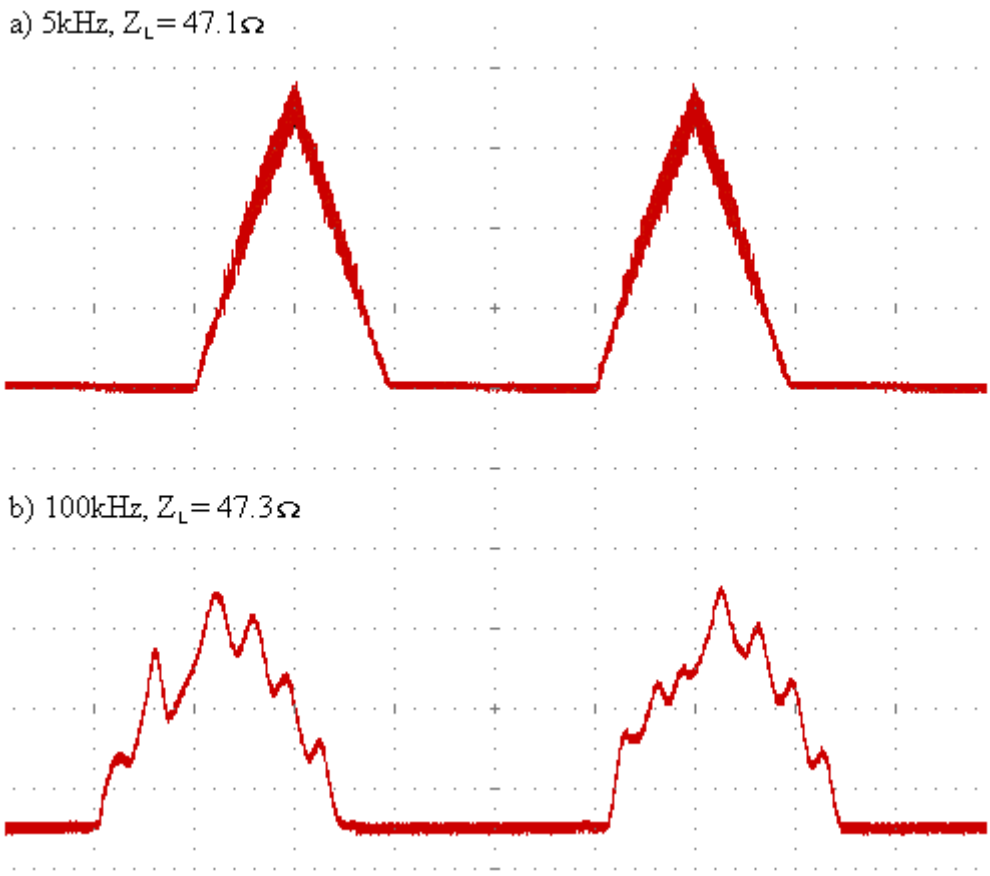

Figure 5.10 *The Oscilloscope screen capture of the OPA2365 output The vertical axis is equal in both cases. a) 5kHz excitation frequency and 47.1Ω load b) 100kHz excitation frequency and 47.3Ω load. The signal is clearly distorted at the 100kHz excitation frequency.*

5.4 In vivo measurements

The table 5.14 represents the results obtained from the forearm by developed bioimpedance device. The table 5.15 shows he results of the measurement taken from the shin.

The measurements from forearm were taken with three different interelectrode spaces (IES). The impedance values (Z_{MEAS}) obtained by the bioimpedance were compared to the values obtained by the Solartron instrumentation (Z_{REF}). The output of the OPA2365 was measured with an oscilloscope which confirmed that the waveform was correct. With the 5kHz excitation the output waveform was fairly clean half wave rectified triangular wave with no distortion. With the 100kHz excitation the output was clearly distorted triangular wave as was anticipated. All in all the both waveforms did resemble very much the output waveforms obtained with the purely resistive test load in the section 5.3.3 and the 2R-1C test circuit in the section 5.3.4 presented in the figure 5.7 and in the figure 5.10. The results reveal a significant difference between the values

obtained with the bioimpedance device and the reference device. The measurements number 1 and number 2 with IES 17.5cm and 10.5cm accordingly show that there might be a constant difference to reference measurement of around -20Ω, however the measurement number 3 with IES of 3.5cm is not in line with this view. The reason behind such high difference is not known; after all the output waveforms were exactly as expected. All three measurements show that with 100kHz excitation the difference is larger (more negative) which is in line with the results of the section 5.3.3 and 5.3.4. This is presumably due to the distortion.

Table 5.14 *The results of the forearm measurements with three different IES. Electrodes used in the measurement were Ambu Blue Sensor P with 34mm skin contact area.*

Meas. No.	IES (cm)	Freq. (kHz)	Z_{REF} (Ω)	$V_{avg,MEAS}$ (mV)	$V_{rms,MEAS}$ (mV)	Z_{MEAS} (Ω), I_{rms}=115µA	Diff. ΔZ (Ω)	Diff. Z (%)
1.	17.5	5	**101.0**	772	9.16	**79.7**	-21.3	-21.1
		100	**80.0**	500	5.93	**51.6**	-28.4	-35.5
2.	10.5	5	**76.0**	540	6.41	**55.7**	-20.3	-26.7
		100	**53.2**	290	3.44	**29.9**	-23.3	-43.8
3.	3.5	5	**35.0**	285	3.38	**29.4**	-5.6	-16.0
		100	**22.8**	140	1.67	**14.4**	-8.4	-36.8

The Table 5.15 shows the measurements results taken from shin. The measurements were performed by using larger electrodes with larger skin contact area. Consequently, the impedance results presented here are not comparable with the results previously in the Table 5.14. Different electrodes had to be used because of the availability problems. The measurement number 4 and 5 suggest that some form of constant difference to reference measurement is present. Both measurements at 5kHz excitation frequency indicate -6.3Ω difference and at the 100kHz frequency the difference is very close to each other in both cases. The output of the OPA2365 was measured with an oscilloscope during the measurements and output waveforms were as expected. The difference is higher at 100kHz than in 5kHz due to the distortion in the waveform at the output of INA331.

Table 5.15 *The results of the shin measurements with two different IES. Electrodes used in the measurement were Ambu Blue Sensor R with 48mm skin contact area.*

Meas. No.	EIS (cm)	Freq. (kHz)	Z_{REF} (Ω)	$V_{avg,MEAS}$ (mV)	$V_{rms,MEAS}$ (mV)	Z_{MEAS} (Ω), I_{rms}=115µA	Diff. ΔZ (Ω)	Diff. Z (%)
4.	15.0	5	**60.0**	520	6.17	**53.7**	-6.3	-10.5
		100	**40.5**	310	3.68	**32.0**	-8.5	-21.0
5.	5.0	5	**29.0**	220	2.61	**22.7**	-6.3	-21.7
		100	**18.7**	110	1.31	**11.4**	-7.3	-39.0

It has to be mentioned that the number of the measurements is not by far high enough to tell anything conclusive. Additionally, the results of the Table 5.14 and the Table 5.15 are not comparable due to the different electrodes.

6 Discussion

The purpose of this thesis was to develop a first prototype of a bioimpedance meter for monitoring a chronic wound healing. The idea was to find a way to implement the device with a simple and cost effective design while measuring the change in the impedance reliably. The device should be miniaturizable by modern manufacturing technologies and therefore a simple core design with no complex internal structure components was an important standpoint.

In this chapter the most important measurement results and the issues concerning the device and the design are discussed. Suggestions for the future development considering the device and the measurement settings are presented at the end of each subsection.

6.1 The Bioimpedance device

The overall operation of the developed bioimpedance device was proven to be as intended. However, certain faults were detected and some improvements can be done.

6.1.1 Observed problems with the device

The results obtained with the bioimpedance device revealed a distortion at the output of the INA331 when operated at 100kHz excitation frequency. When the voltage measurement block was tested with the function generator input, it was noticed that triangular input started to get distorted at around 40kHz frequency while with the sine input the frequency was at around 100kHz. The reason behind the lower frequency bandwidth for triangular wave lies on the frequency content of the wave. As sine wave ideally contains only the fundamental frequency, the triangular wave comprises in addition to the fundamental frequency harmonic multiples of the fundamental frequency, although the amplitude of the harmonic frequencies rolls off rapidly with increasing harmonic order.

Even though the slew rate of INA331 was initially considered reasonable it still might be the largest contributor to the distortion at the output of the INA331 which

eventually results in error at the impedance measurement at the 100kHz frequency. This is due to high frequency harmonics of triangular wave as listed in the table 3.3.

An electronic amplifier at very low frequencies without feedback amplifies the input signal by the value of the openloop gain, the highest possible gain to be achieved. As the operating frequency increases, stray capacitances start to kick in and form a low pass filter with small internal resistances, consequently the gain diminishes with the frequency. With no feedback the frequency bandwidth of an amplifier is very low. Electronic amplifier suffers, like all electronic devices, from some form of non-linear behavior. The electronic amplifier is normally used in a negative feedback mode. The negative feedback reduces the non-linearity effects, improves gain stability and frequency response. By reducing the gain factor of the negative feedback a larger bandwidth can be obtained. The gain bandwidth product describes this trade between the bandwidth and the gain. The instrumentation amplifier INA331 is operated at the minimum gain of 5 to maximize the bandwidth and the primary gain of 38.9 is drawn from the OPA2365. According to the datasheet of INA331 the gain starts to fall from 5 at the frequency of around 1MHz and -3dB point is at 3MHz (Texas Instruments, Inc. 2005, p. 4). According to the Table 3.3, the harmonics above order of 9 of 100kHz excitation exceed the 1MHz limit and start to lose the gain. Although, the amplitude contribution of such high order harmonics to the signal is small this may have some effect on the deformation to the output signal.

The resistance mismatch at the input of the instrumentation amplifier in the primary contributor to non-infinite CMRR. The CMRR is also frequency dependent. As the frequency of the signal increases from DC the parasitic frequency dependent components such as capacitance and inductance start to bring in. This causes phase shift between the common mode signals at the inputs of the instrumentation amplifier. Therefore, the common mode signal is effectively turned into a differential error signal and is amplified. As a result the CMRR degrades as the signal frequency increases. (Franco 2002, pp. 86-87) According to the datasheet INA331 provides 94dB CMRR at frequencies below 3kHz, as the frequency increases CMRR deteriorates and at the 100kHz frequency CMRR is barely 25dB (Texas Instruments, Inc. 2005, p. 4). The low CMRR should appear as an increased high frequency noise component in the output signal, at an extreme case it should saturate the whole output. Nevertheless, the output signal of INA331 did not reveal any extreme noise coupling in any of the measurements. With decreasing load impedance the signal in fact was experiencing deteriorating signal to noise ratio, but that was anticipated and due to decreasing measurement signal magnitude more than excessive noise coupling.

The results of the excitation current measurement in the section 5.3.1 are not entirely reliable especially at the lower load resistance values because of the external noise coupling into the measurement circuit, to the test load circuit and particularly to the leads of the oscilloscope as mentioned previously. However, it is probable that the excitation current increases somewhat with the decreasing load resistance.

Occasionally, during the system test with purely resistive load and with 2R-1C test circuit the bioimpedance device at 100kHz excitation gave obviously corrupted results as mentioned in the section 5.3.3 and in the section 5.3.4. The fundamental reason for this behavior is not clear. The output signals of both INA331 and OPA2365 did appear to be exactly as assumed. Therefore, the problem lies most likely in the moving average filter or in the AD converter itself. Increasing averaging in the software did not solve the problem. The corrupted results show such high error that it is not probable that the ripple voltage at the output of the moving average filter would be the actual cause. However, by decreasing the cut-off frequency by increasing the resistor value of the moving average filter would increase the rise time of the output voltage but the ripple voltage would decrease.

During the test measurements a problem was observed in the software of the bioimpedance device. The bioimpedance device was intended to be able to resume from the last memory location before the power on reset (POR). In practice this would have worked so that between the measurement sets the operator would have been able to turn off and on again the device and continue performing measurements without extracting the data and erasing the memory. This piece of software did not work well. It does not affect the measurement results, but it adds inconvenience and should be repaired. The bug in the software is likely to be quite easily solved.

6.1.2 Future development of the device

There exists a need for certain rather obvious improvements to be done on the developed bioimpedance device. First of all the instrumentation amplifier should be changed into a more suitable one with the emphasis on the better frequency characteristics and better CMRR at high frequencies. This would reduce the effects of the distortion at 100kHz excitation. Although the repertory of such components of the major manufacturers was quite extensively studied to find the best instrumentation amplifier for this application, more effort should be put on it. It was noticed that the components with better aforementioned parameters exist, but unfortunately those did require a dual supply. The instrumentation amplifier could also be designed from discrete components, however that may not be reasonable without highly sophisticated design and manufacturing capabilities.

There is some uncertainty with the excitation current magnitude and as mentioned previously it is highly probable that the current magnitude does increase with the decreasing load at least in some degree. All the measurement results presented in the section 5.3 and in the section 5.4 are calculated with an assumption that the rms value of the excitation current is constant 115µA. Even fairly small +10µA deviation from the assumed constant 115µA current magnitude would result in an approximately +8.6Ω error with 100Ω load impedance, this is a significant error. Therefore, it would be preferable to install a current sensing resistor at the output of the voltage to current converter or some more sophisticated current measurement block. The current sensing

resistor would be very easy to implement and it would require only two additional pins from the microcontroller. It might be a good idea to replace the present current to voltage converter with the Howland topology, this would not add much complexity to the overall circuit since only four additional resistors would be required. The Howland voltage to current converter would increase the output impedance of the current feeding circuitry, thus improving the stability of the current magnitude.

The current consumption could be reduced significantly by changing the operational amplifier OPA2365. OPA2365 does not provide shut down mode and therefore even in the idle mode the current consumption is unnecessarily increased by around 5mA. The current consumption in the idle mode could be further reduced to around 4mA or even less by utilizing sleep modes of other components and optimizing the current limiting resistor of the power supply regulation circuitry.

The physical size of the device could be greatly reduced by using multilayer instead of the current two layer PCB. Certain unnecessary components, which were placed on the board for testing purposes, exist in the current design and should be removed. In addition, passive SMD components such as resistors and capacitors are in 1206 package and could be changed to smaller ones. The microcontroller ATmega8A might be a bit too hefty for this application and could be changed to a more modest one.

6.2 The Measurement Results

6.2.1 System test with purely resistive load and 2R-1C test circuit

The results of the purely resistive load measurements in the section 5.3.3 with 5kHz excitation show a very small mean error $\bar{x}$ of +0.18Ω with a standard deviation of 0.75Ω between the load range of 101Ω and 15.0Ω. As a comparison the results of the 2R-1C test circuit in the section 5.3.4 with 5kHz excitation show similarly a very small mean error $\bar{x}$ of +0.10Ω with a standard deviation of 0.71Ω between the load range of 100.7Ω and 22.3Ω. The results in both cases are very good and essentially equal. The error can be considered as a statistical variation. Also the behavior of the error is similar in both cases at the smallest load values, the error in ohms tends to increase into the positive direction due to decreasing signal to noise ratio. In both cases there was no distortion observed at the output of the INA331 as anticipated. Considering the nature of the device as an indicator of the change in the impedance rather than measurement device for absolute impedance values, it is very important to notice that the direction of the change was correct in all cases, even though the smallest difference between the actual impedance values was fairly small 2.8Ω. These results show that at low frequencies the triangular wave excitation might be reliable and accurate for measuring the impedance.

The results of the purely resistive load and 2R-1C test circuit with 100kHz excitation frequency are more controversial. Basically, adding a capacitor into the test

circuit should not affect the measurement accuracy. Nevertheless, there exists quite significant difference in accuracy between the results obtained. The measurement results of the purely resistive load with 100kHz excitation frequency reveal a mean error $\bar{x}$ of -4.07Ω with a standard deviation of 0.36Ω between the load range of 101.0Ω and 15.0Ω. The 2R-1C test circuit shows a mean error $\bar{x}$ is -7.85Ω with a standard deviation of 0.75Ω between the load impedance range of 57.8Ω and 20.3Ω. The error in both cases seems somewhat constant in the measurement range and it is mainly due to distortion at the output of INA331 as it decreases the moving average of the signal from which the impedance value is calculated. The difference in mean error between the purely resistive load and 2R-1C test circuit might be due to the addition of the capacitor into the circuit, although that should not affect to the total impedance measured. More testing with various capacitor values should be performed to confirm that this is really the case. To emphasis the indicator function of the device, it is important to mention that in all cases the measured impedance did follow the change in the actual impedance values. If we take a look at the equation 24, which represent the ratio of Z_{5kHz} and Z_{100kHz}, it shows that under certain preconditions the change in the measured bioimpedance is a function of the extracellular resistance R_E only. Therefore the error in the absolute value of the Z_{100kHz} does not hamper the indicator function of the bioimpedance device if the error remains constant, in other words it is systematic. It is necessary that the total membrane capacitance of the tissue volume of the interest remains somewhat constant between the measurement sets and over time.

The results obtained with the purely resistive load and 2R-1C test circuit at 5kHz excitation show a very small error compared to the actual load value. According to these test results there is no need for a correction factor to be implemented. The results with 100kHz instead show a significant, seemingly systematic error in the measured impedance. Unfortunately, the magnitude of the error seems also to be dependent on the capacitance value of the test circuit or perhaps some other unknown factor. If this is the case, it is practically impossible to derive a generalized correction factor or algorithm. Obviously, it might be possible to perform extensive measurements with various capacitor values and deduce from the obtained data whether there exists some form pattern of correlation between the capacitor value and the magnitude of the mean error in the measured impedance values. Even if a correlation was found and the dependency could be traced, the correction factor most certainly would not be applicable to clinical use of the device since the total capacitance of the tissue is heavily dependent for example on the subject's physical and anatomical characteristics and of course on the volume the measured tissue.

6.2.2 In vivo measurements

The results of the in vivo measurements are somewhat controversial and not in line with the test measurements discussed in the section 6.2.1. The test measurements and in vivo

measurements both show a negative difference to reference measurement and the difference is larger with the 100kHz excitation, but the magnitude is absolutely in a different range. As the test measurements with the purely resistive load and 2R-1C test circuit at 5kHz excitation did not show notable error compared to the actual values, the in vivo measurements introduce a very different case. The difference is very significant particularly in the measurements number 1 and 2 taken from the forearm. The reason behind this behavior is not known, the OPA2365 output waveform was as expected in both 5kHz and 100kHz excitation.

6.2.3 Future development of the measurement settings

The test measurements of the developed bioimpedance device were fairly extensive. However, certain additional measurements should be performed. The difference in the mean error of the measured impedance with 100kHz excitation between the purely resistive load and the 2R-1C remains mostly unanswered. At 100kHz frequency the output of INA331 and consequently the output of the OPA2365 were distinctively distorted in both cases. Distorted output may lead to unpredictable results, in this case however fairly small standard deviation in the error (ΔZ) indicates that the error is somewhat constant. Therefore more test measurements with 100kHz excitation by using different capacitor values in the 2R-1C circuit should be performed to see whether the mean error still remains constant and whether the capacitor values have some effect on the mean error and look for a possible pattern.

The test measurements were taken in an environment which was most likely highly contaminated by EMI. The additional measurements should be performed preferably in a RF anechoic chamber to indicate the effect of the noise coupling. The test circuit should be assembled, not on the breadboard prone the noise coupling, but on a standalone PCB board.

Much more extensive in vivo measurements should be also performed by using both larger and smaller surface area electrodes. The reason behind the large difference to reference measurement in the impedance value when using the Ambu Blue Sensor P electrodes should be investigated. In the measurements taken from the forearm the output of OPA2365 was confirmed to be as expected, 5kHz excitation did show clean triangular output and at 100kHz excitation the output was distorted. In the in vivo measurements the electrodes were placed in a sequential arrangement. A parallel arrangement should also be tested, that would probably be much more suitable for a patch integrated device.

In addition to aforementioned, some measurements should be done by using the optional components, for example the reference voltage sources and the internal oscillator, to perceive their effect on the measurements.

7 Conclusions

The object of this Master of Science thesis was to develop a prototype of a bioimpedance device for monitoring of chronic wound healing. The device measures the impedance at 5kHz and 100kHz excitation frequencies. A chronic wound is trapped into an ongoing inflammation. As a result of this the site of the wound is swollen. The swelling is due to the vasodilatation and the increased permeability of capillaries. The highly conductive fluid accumulates into the extracellular space and can be detected as decreasing impedance when the low frequency excitation is applied. The measured tissue volumes are small and therefore also the impedance range and the changes are fairly small.

Eventually, the device was intended to be integrated on a patch type drug delivery system. The design priority was to provide a possibility for down scaling the device, the cost and power consumption. Therefore, the excitation waveform was chosen to be triangular which is simply derived from the microcontroller square wave output. ICs and other components with a complex internal structure were avoided when possible. The device does not measure the phase shift thus distinction between the extracellular and intracellular contribution to the impedance cannot be made. However, the 5kHz excitation frequency correlates mainly with the extracellular fluid, this was considered to be adequate for this type of a fluid changes indicating device.

The device did mainly operate as intended. However, certain issues were noticed. For some unknown reason the device did occasionally output corrupted data, the cause behind this this should be identified and corrected. A software bug related to power saving was noticed. The device was supposed to resume from the last memory location before a power on reset, but this did not work. Most probably the bug is easily corrected. Also, certain components should be replaced to reduce the power consumption even further.

The measurement results with a purely resistive load and 2R-1C test circuit were fairly good. The results at 5kHz excitation were very close to the actual values in both cases. The results at 100kHz did reveal quite significant error particularly when using the 2R-1C circuit. This may result from degrading CMRR of the INA331 at high frequencies. However, the results did also indicate that in both cases the error may be systematic by nature. A systematic error could be easily nulled. The problem is that the mean error between the purely resistive and the 2R-1C circuits was not equal, it seems that adding a capacitor to the circuit may have had an effect on the magnitude of the error. If this is the case, it is difficult to find a factor or algorithm for nulling since in

practice the contribution of the membrane capacitances is not known. The direction of the change in the actual impedance was correctly indicated in all measurements.

The in vivo measurements were taken from the shin and the forearm. The measurements were very limited and the results obtained from the shin and the forearm is not comparable to each other. The results were controversial and did show a very significant error. The output waveforms after the amplification stages were investigated and were as expected.

The triangular excitation waveform in addition to the fundamental frequency contains high harmonic frequencies. The instrumentation amplifier INA331 provides relatively poor frequency characteristics. These factors are the primary reason for the error observed at 100kHz excitation frequency. The output of the INA331 and consequently the output of OPA2365 were clearly distorted at 100kHz, at 5kHz there was no distortion noticed. The bottleneck of the design is therefore the INA331 and should be replaced with an instrumentation amplifier with better frequency characteristics. The good test measurement results at 5kHz did show that the triangular waveform excitation is fundamentally as good as the conventional sine wave excitation and that accurate results are possible to obtain with a much more simple and cost effective design with a low power consumption. Some unanswered questions and problems remain, and to solve them more measurements should be performed. The additional measurements should focus on clarifying the effect of the capacitance at high frequency excitation, on finding out the possible pattern and on the in-vivo measurements.

References

Abboud, M., Guardo, R., et al. 1995. "Monitoring of peripheral edema using electrical bioimpedance measurements". *Engineering in Medicine and Biology Society:* IEEE 17th Annual Conference, vol. 1, pp. 641-642.

Ambu, A/S. 2011a. *Datasheet:* Ambu Blue Sensor P. 2 p. Available: http://www.ambu.com/Admin/Public/Download.aspx?File=/Files/Billeder/MediaDB/Originals/IE_P_493101201_V01_0910.pdf

Ambu, A/S. 2011b. *Datasheet:* Ambu Blue Sensor R. 2 p. Available: http://www.ambu.com/Admin/Public/Download.aspx?File=/Files/Billeder/MediaDB/Originals/IE_R_493101501_V01_0910.pdf

Analog Devices, Inc. 1999. A Technical Tutorial on Digital Synthesis. 121 p. Available: http://www.analog.com/static/imported-files/tutorials/450968421DDS_Tutorial_rev12-2-99.pdf

Ardizzoni, J. 2005. "A Practical Guide to High-Speed Printed-Circuit-Board Layout". *Analog Dialogue*, vol. 39, no. 9. Analog Devices, Inc. 6 p. Available: http://www.analog.com/library/analogDialogue/archives/39-09/layout.pdf

Atmel Corporation 2009. *Datasheet:* ATmega8A. 301 p. Available: http://www.atmel.com/dyn/resources/prod_documents/doc8159.pdf

Ayera Technologies, Inc. 2011. TeraTerm –software, version 3.1.3. Available: http://www.ayera.com/teraterm/

BI Technologies. *R-2R Resistor Ladder Networks*. 6 p. Available: http://www.bitechnologies.com/pdfs/resistorladder.pdf

Brown, B.H., Wilson, A.J. & Bertemes-Filho, P. dec. 2000. "Bipolar and Tetrapolar Transfer Impedance Measurements from Volume Conductor". *Electronics Letters*, vol. 36, no. 25, pp. 2060-2062.

Bourne, J.R. 1996. Critical Reviews in Biomedical Engineering. Begel House, Inc. Vol. 25, issues 4-6, pp. 223-681.

Burns, J.L., Mancoll, J.S. & Phillips, L.G. 2003. *Clinics in Plastic Surgery. Wound Healing*, vol. 30, no. 1, pp. 47-56.

CadSoft Computer 2011. Eagle Layout Editor. Homepage. Available: http://www.cadsoftusa.com/

Cho, S. & Atwood, J.E. 2002. "Peripheral Edema". The American Journal of Medicine, vol. 113, no. 7, pp. 580-586.

Day, J. & Stein, R. 1997. *Application Note AN655:* A Conversion Using PWM and R-2R Ladders to Generate Sine and DTMF Waveforms. Microchip Technology, Inc. 17 p. Available: http://ww1.microchip.com/downloads/en/AppNotes/00655a.pdf

De Lorenzo, A., Andreoli, A., Matthie, J., Witthers, P. 1996. "Predicting body cell mass with bioimpedance by using theoretical methods: a technological review". *Journal of Applied Physiology*, vol. 82, no. 5, pp.1542-1558.

Finland's National Institute for Health and Welfare (THL). 2011.Methicillin-resistant Staphylococcus aureus (MRSA). Available: http://www.ktl.fi/portal/suomi/osastot/bato/yksikot/sairaalabakteerilaboratorio_saba/mrsa__metisilliiniresistentti_staphylococcus_aureus_/

Fluke Corporation 2011. *Datasheet:* Fluke 115 Multimeter. 24 p. Available: http://assets.fluke.com/manuals/114_____umeng0100.pdf

Franco, S. 2002. *Design with Operational Amplifiers and Analog Integrated Circuits*, 3rd edition. McGraw-Hill. 658 p.

Frounchi, J., Karimian, G. & Keshtkar, A. 2009. "An Artificial Neural Network Hardware for Bladder Cancer". *European Journal of Scientific Research*, vol. 27, no. 1, pp. 46-55.

FTDI, Ltd. 2010. *Datasheet:* FT232RL USB UART IC. 43 p. Available: http://www.ftdichip.com/Support/Documents/DataSheets/ICs/DS_FT232R.pdf

Greenhalgh, D.G. 2003. "Wound healing and diabetes mellitus". *Clinics in Plastic Surgery. Wound Healing*, vol. 30, no. 1, pp. 37-45.

Grimnes, S. & Martinsen, O.G. 2005. "Cole Electrical Impedance Model – A Critique and an Alternative". *IEEE Transactions on Biomedical Engineering*, vol. 52, no. 1, pp. 132-135.

Grimnes, S. & Martinsen, O.G. 2006. *Wiley Encyclopedia of Biomedical Engineering: Bioimpedance*, 1st edition. Wiley Interscience. 4152 p.

Grimnes, S. & Martinsen, O.G. 2007. “Sources of Errors in Tetrapolar Impedance Measurements on Biomaterials and Other Ionic Conductors”. *Journal of Physics D: Applied Physics*, vol. 40, no. 1, pp. 9-14.

Grimnes, S & Martinsen, O.G. 2008. *Bioimpedance and Bioelectricity Basics*, 2nd edition. Academic Press. 471 p.

Grimnes, S & Martinsen, O.G. 2010. “Alpha dispersion in human tissue”. *Journal of Physics: Conference Series*, vol. 224, no. 1, pp. 1-4.

Haario, H. 2004. Statistical analysis of models (Mallien tilastollinen analyysi). Lecture notes. Lappeenranta University of Technology. 33 p. Available: http://www2.it.lut.fi/kurssit/04-05/010294100/statmode_lectures_fin.pdf

Haemmerich, D., Ozkan, O.R., et al. 2002. “Changes in electrical resistivity of swine liver after occlusion and postmortem”. *Medical & Biological Engineering & Computing*, vol. 40, no. 1, pp. 29-33.

Hambley A.R. 2000. *Electronics*, 2nd edition. Prentice Hall. 888 p.

Hewlett Packard Company 2007. “Patch promises painless injection”. BBC News. Available: http://news.bbc.co.uk/2/hi/health/7002482.stm

Hietanen, H., Iivanainen, A., Seppänen, S. & Juutilainen, V. 2003. *Haava*, 1-2.painos. WSOY. 268 p.

Hinton, A.J. & Sayers, B. 1998. “Advanced Instrumentation for Bioimpedance Measurements”. Solartron Analytical, Solartron Group, Ltd. 7 p. Available: http://www.korozja.pl/html/eis/ap04.pdf

Holder, D.S. 2004. *Electrical Impedance Tomography: Methods, History and Applications*, 1st edition. Appendix A: Brief introduction to bioimpedance. Taylor & Francis. 456 p.

Hospital District of Helsinki and Uusimaa (HUS). 2007. MRSA sairaalabakteeri. Available: http://www.hus.fi/default.asp?path=1,32,818,1733,1996,2586

Hunter, J.C., Savin, J. & Dahl, M. 2002. *Clinical Dermatology*, 3rd edition. Wiley-Blackwell. 365 p.

Ivorra, A. 2003. *Bioimpedance Monitoring for Physicians: An Overview*. Biomedical Applications Group, Centre National de Microelectronica, Spain. 35 p.

Jensen, B.M., McCreath, H.E., Kono, A., et al. 2007. "Subepidermal Moisture Predicts Erythema and Stage 1 Pressure Ulcers in Nursing Home Residents: A Pilot Study". *Journal of American Geriatrics Society*, vol. 55, no. 8, pp. 1199 – 1205

Johnson, G.L. 2001. *Solid State Tesla Coil. Chapter 3: Lossy Capacitors*. Available: http://www.tfcbooks.com/special/sstc_glj.htm

Jungueira, L.C & Carneiro, J. 1997. *Biologia Celular e Molecular*, 6th edition. Guabara – Koogan. 299 p.

Koch K.P., Schuettler M. & Stieglitz T. 2002. "Considerations on Noise of Amplifiers and Electrodes for Bioelectrical Signal Recording". *Biomed. Technology*, vol. 47, no. 1, part 2, pp. 514-516.

Kyle, U.G., Bosaeus, I. & De Lorenzo, A.D. 2004a. "Bioelectrical impedance analysis – Part 1: Review of principles and methods". *Clinical Nutrition*, vol. 23, no. 5, pp. 1226-1243.

Kyle, U.G., Bosaeus, I., De Lorenzo, A.D., et al., 2004b. "Bioelectrical Impedance analysis-part II: utilization in clinical practice". *Clinical nutrition*, vol. 23, no. 6, pp. 1430-1453.

Laine, M. 2007. Modelling course (Mallinnuskurssi). Lecture notes. Palmenia, University of Helsinki. 144 p. Available: http://www.helsinki.fi/~mjlaine/Palmenia/mallinnus/mallinnus4a4.pdf

Lauronen, J. 2009. "Development of Bioimpedance Meter". Master of Science thesis. Tampere University of Technology. 50 p.

Lawrence, W.T. 1998. "Physiology of the Acute Wound". *Clinics in Plastic Surgery. Wound Healing: State of Art*, vol. 25, no. 3, pp. 321-340.

LeCroy Corporation 2011. *Getting Started –guide:* LeCroy WaveJet 322 Digital Oscilloscope. 65 p. Available: http://www.lecroy.com/Support/TechLib/registerPDF.aspx?documentID=1800

Mancini, R. & Palmer, R. 2001. *Application Report SLOA060:* Sine-Wave Oscillator. Texas Instruments, Inc. 20 p. Available: http://www.ece.ucsb.edu/courses/ECE137/137B_S11Theo/oscillators.pdf

Martinsen, O.G., Grimnes, S. & Haug E. 1999. "Measuring depth depends on frequency in electrical skin impedance measurements". *Skin Research and Technology*, vol. 5, no. 3, pp- 179-181.

Mastech Instruments, LLC. 2011. *Mastech product page:* Mastech MS8217 Multimeter. Available: http://www.mastech-hy.com/products_detail/&productId=0bc993fc-7b13-416e-8009-9e282f7551cf&comp_stats=comp-FrontProducts_list01-004.html

Matthie, J.R. 2008. "Bioimpedance Measurements of Human Body Composition: Critical Analysis and Outlook". *Expert Review of Medical Devices,* vol. 5, issue 2, pp. 239-261.

Medscape. 2011. Effects of Living Skin Equivalent: Case Reports. Available: http://www.medscape.com/viewarticle/407585_2

Memorial Hospital of South Bend. 2011. Skin Cancer Screening. Available: http://www.qualityoflife.org

Microchip Technology, Inc. 2008. *Datasheet:* MCP4531-103E/MC. 88 p. Available: http://ww1.microchip.com/downloads/en/DeviceDoc/DS-22096a.pdf

Monaco, J.L. & Lawrence, W.T. 2003. "Acute wound healing: An Overview". *Clinics in Plastic Surgery. Wound Healing*, vol. 30, no. 1, pp. 1-12.

Morin, E. 2009. Lecture notes *ELEC-408:* Electrodes and Electrode theory. Queen's University. 5 p. Available: http://www.ece.queensu.ca/Current-Students/Undergraduate/Course-Homepages/ELEC-408/files/ELEC408_ElectrodeTheoryNotes_Nov09.pdf

Morrow, T. 2004. "Transdermal Patches Are More Than Skin Deep". *Managed Care Magazine.* Available: http://www.managedcaremag.com/archives/0404/0404.biotech.html

Myers, W.T., Leong, M. & Phillips, L.G. 2007. "Optimizing the Patient for Surgical Treatment of the Wound". *Clinics in Plastic Surgery. Wound Surgery*, vol. 34, no. 4, pp. 607-620.

National Semiconductor, Inc. 2009. *Application Note 263:* Sine Wave Generation Techniques. 15p. Available: http://www.national.com/an/AN/AN-263.pdf

Nilsson, J.W. & Riedel, S.A. 2001. *Electric Circuits,* 6th edition. Prentice Hall. 1018 p.

Nordbotten, B.J., Martinsen, O.G & Grimnes, S. 2010. "Methods for calculating phase angle from measured whole body impedance modulus". *Journal of Physics: Conference Series,* vol. 224, no.1, pp. 1-4.

Nwomeh, B.C., Yager, D.R. & Cohen, I.K. 1998. "Physiology of the Chronic Wound". *Clinics in Plastic Surgery. Wound Healing: State of Art*, vol. 25, no. 3, pp. 341-356.

Olimex, Ltd. 2011. Homepage. Available: http://www.olimex.com/

Panuncialman, J. & Falanga, V. 2007. "The Science of Wound Bed Preparation". *Clinics in Plastic Surgery. Wound Surgery*, vol. 34, no. 4, pp. 621-632.

Pukki, T. 2006. "Ikääntymisen vaikutukset haavan paranemiseen". *Haava –lehti*, no. 1, pp. 10-15.

Ragheb, A.O., Geddes, L.A., Bourland, J.D. & Tacker, W.A. jan. 1992. "Tetrapolar electrode system for measuring physiological events by impedance". *Medical & Biological Engineering & Computing*, vol. 30, no. 1, pp. 115-117.

Ramasastry, S.S. 1998. "Chronic Problem Wounds". *Clinics in Plastic Surgery. Wound Healing: State of Art*, vol. 25, no. 3, pp. 367-396.

Riordan, L. "Skin Impedance Analysis Aids Active and Passive Transdermal Delivery". *Analog Dialogue –forum*. Analog Devices, Inc. 3 p. Available: http://www.analog.com/library/analogDialogue/archives/43-04/transdermal_delivery.html

Rubin, E. & Farber, J.L. 1999. *Pathology*, 3rd edition. Lippincott Williams & Wilkins. 1648 p.

Schmitz, T & Wong, M. 2007. Application note AN1325.0: Choosing and Using Bypass Capacitors. Interstil Corporation. 10 p. Available: http://www.intersil.com/data/an/an1325.pdf

Seppänen, S. & Hjerppe, A. 2008. "Haavanhoitotuotteiden saatavuus Suomessa". Suomen Haavanhoitoyhdistys ry. Julkaisusarja nro. 3. 54 p.

Shai, A & Maibach, H.I. 2005. *Wound Healing and Ulcers of Skin*. Springer. 279 p.

Sievers, B. 2006. The Amateur Gentleman's Introduction to the Principles of Music Synthesis. Available: www.beausievers.com/synth/synthbasics

Simola, K. 2010. ”Tutkimusryhmä kehitti kivuttoman rokotustavan”. *Tekniikka & Talous.* Available: http://www.tekniikkatalous.fi/tk/tutkimusryhma+kehitti+kivuttoman+rokotustavan/a475905

Solartron Analytical, Solartron Group, Ltd. 2005a. Operating manual: Solartron 1260A Impedance/Gain-Phase Analyzer. 215 p. Available: http://mm.ece.ubc.ca/mediawiki/images/8/8b/1260_manual.pdf

Solartron Analytical, Solartron Group, Ltd. 2005b. Datasheet: Solartron 1294 Impedance Interface. 4 p. Available: http://www.solartronanalytical.com/Pages/DataSheets/1294ImpedanceInterfaceBioimpedance.pdf

Stanford Research Systems, Inc. 2011. *Application Note 5:* Direct Digital Synthesis. 5 p. Available: http://www.thinksrs.com/downloads/PDFs/ApplicationNotes/DDS.pdf

Starling’s Hypothesis. 2011. *Fluid Physiology* -online book: Chapter 4.2. Anesthesia Education Website. Available: http://www.anaesthesiamcq.com/FluidBook/index.php

Suomen Diabetesliitto ry. 2010. Tampere, Diabeteskeskus. Available: http://www.diabetes.fi

TCT™ summary. TTI ellebrau Inc. 2011.

Terry, M., Halstead, L.S., O’Hare, P., et al. 2009. “Feasibility Study of Home Care Wound Management Using Telemedicine”. Advances in Skin & Wound Care, vol. 22, no. 8, pp. 358-364.

Texas Instruments, Inc. “PCB Layout Tips for High Resolution”. Precision Analog Applications Seminar, section 9. 22 p. Available: http://focus.ti.com/lit/ml/slyp167/slyp167.pdf

Texas Instruments, Inc. 2005. *Dataheet:* INA331. 13 p. Available: http://focus.ti.com/lit/ds/symlink/ina331.pdf

Texas Instruments, Inc. 2009. *Datasheet:* OPA2365. 15 p. Available: http://focus.ti.com/lit/ds/symlink/opa365.pdf

Tuuliranta, M. 2007. ”Milloin leikkaushaava on infektoitunut”. *Haava –lehti,* no. 3, pp. 24-25.

Työterveyskirjasto. 2011. Duodecim. Available: www.tyoterveyskirjasto.fi

University of Guelph, Department of Physics 2008. *Physics Tutorial: DC Circuits, Part A.* Ohm's law. Available: http://www.physics.uoguelph.ca/tutorials/ohm/Q.ohm.intro.html

Vilhunen, T. 2000. "Biologisen materian sähkönjohtavuus ominaisuuksien määritys". Master of Science thesis. Kuopio University. 90 p.

Wallace, G.F. 2007. "Debridement of Invasive Diabetic Foot Infections". *Clinics in Plastic Surgery. Wound Surgery,* vol. 34, no. 4, pp. 731-734.

Wisher Enterprice, Ltd. 2011. *Datasheet:* WBU-504. 1 p. Available: http://www.farnell.com/datasheets/96984.pdf

York, S.L., Ward, L.C. & Czerniec, S. 2009. "Single frequency versus bioimpedance spectroscopy for the assessment of lymphedema". *Breast Cancer Research and Treatment,* vol. 117, no. 1, pp. 177-182.

Webster, J.G. 2008. *Medical Instrumentation: Application and Design*, 3rd edition. John Wiley & Sons, Inc. 691 p.

Young, H.D. & Freedman, R.A. 2000. *University Physics*, 10th edition. Addison Wesley Longman, Inc. 1513 p.

Appendix 1: The schematic diagram

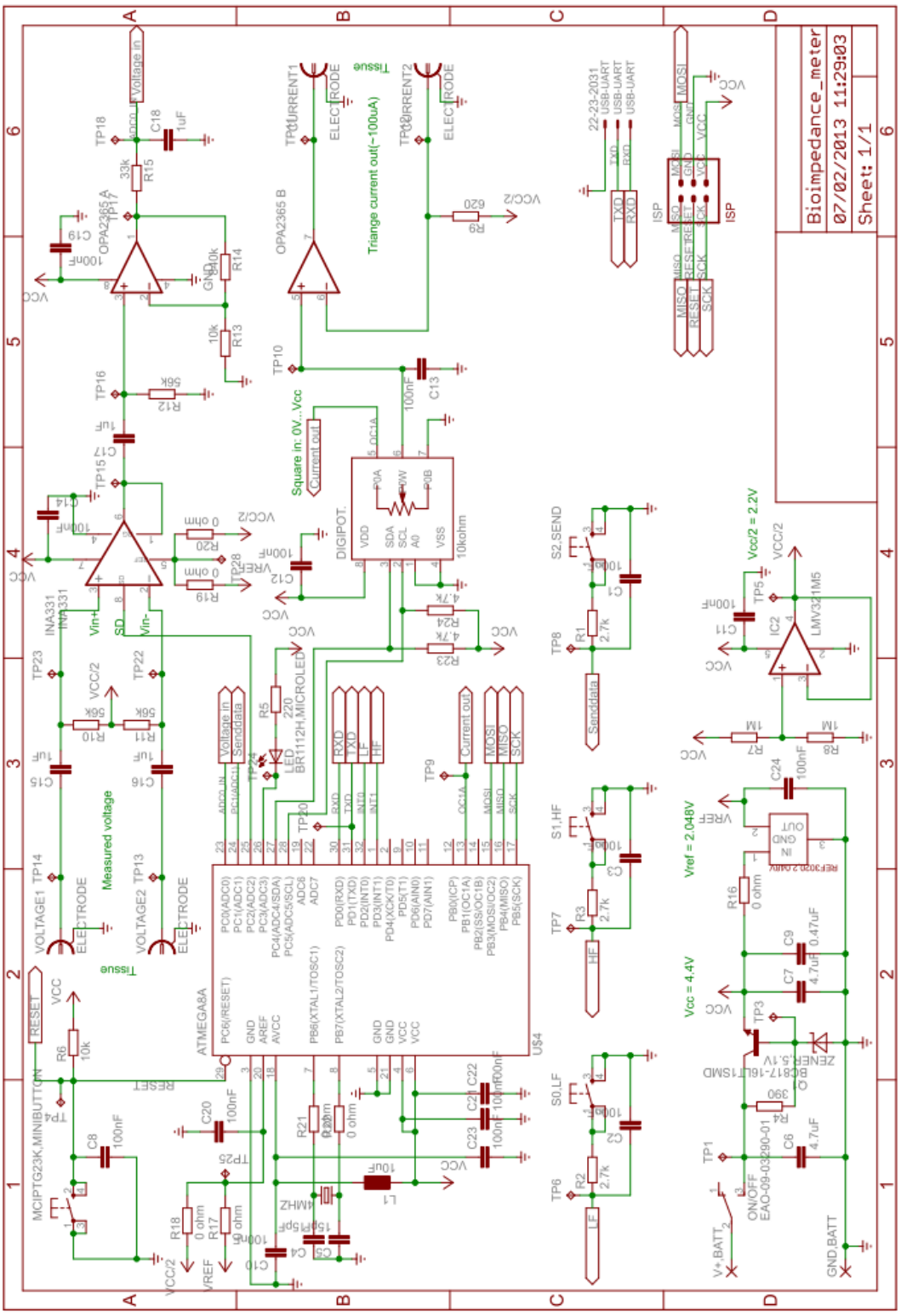

Appendix 2: The simulation circuit

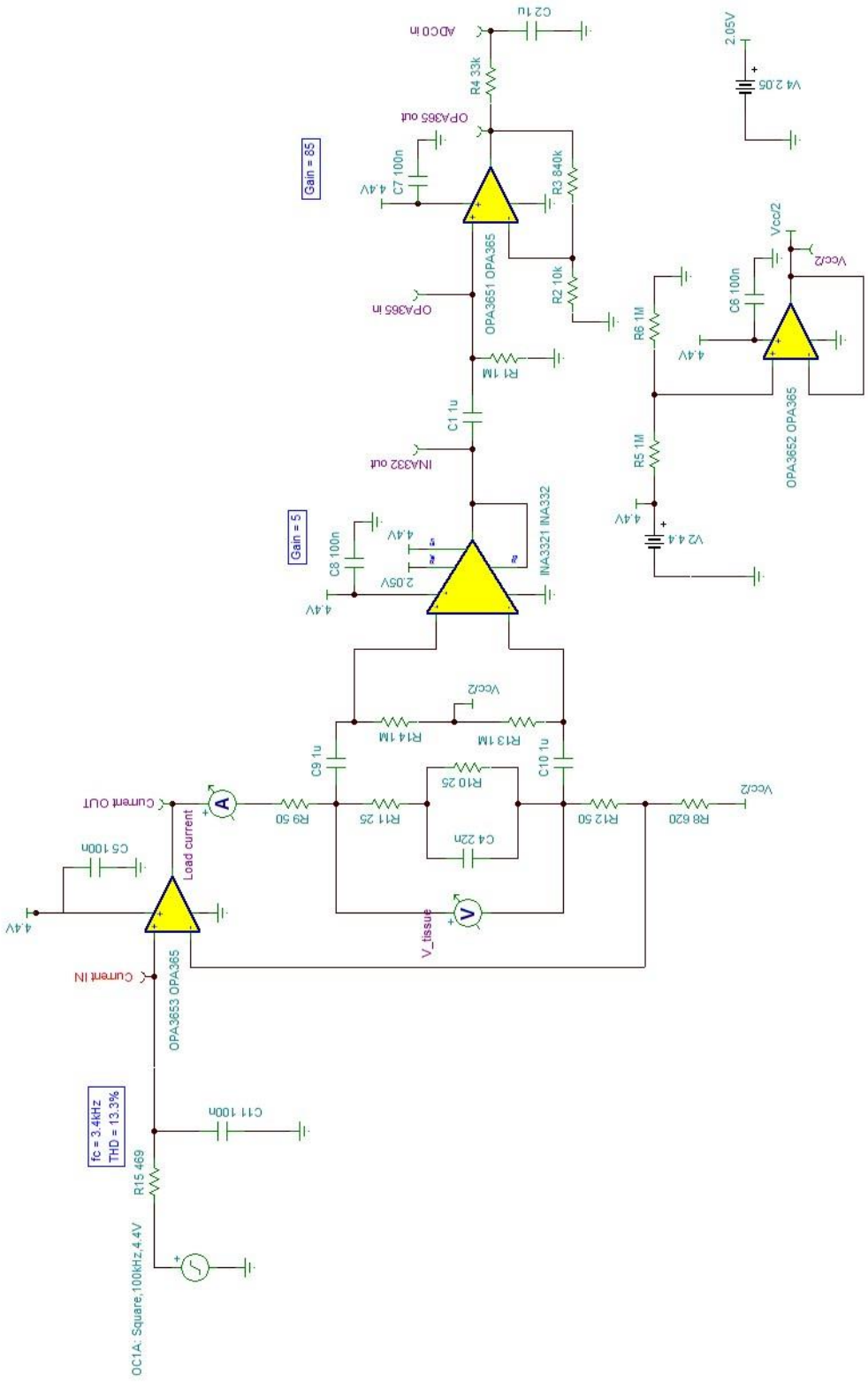

Appendix 3: Layout of the bioimpedance device and the FTDI cable

a) The top layer (red) and the bottom layer (blue) of the layout of the bioimpedance device. The figures are not in the actual size.

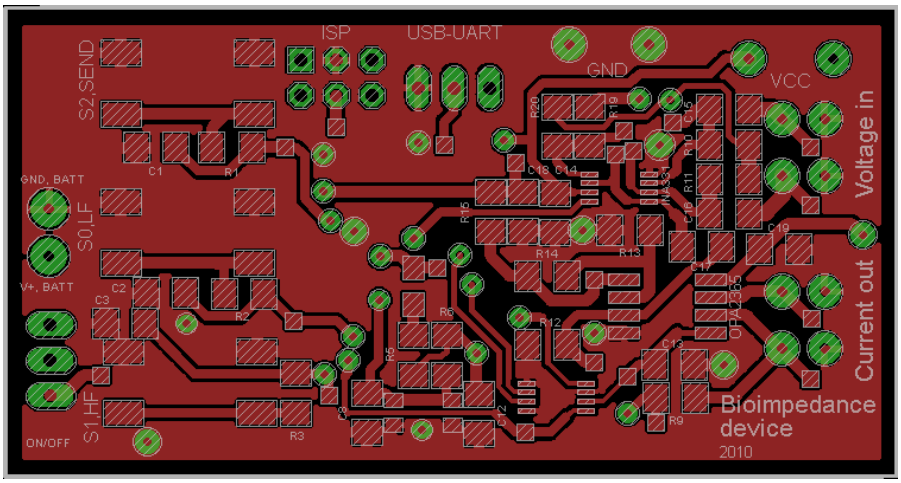

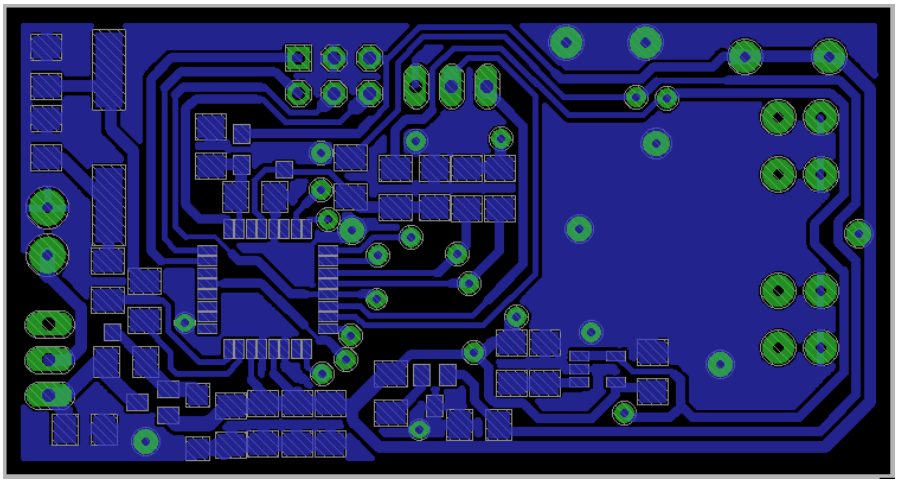

b) The top layer (red) and the bottom layer (red) of the layout of the FTDI cable. The figures are not in the actual size.

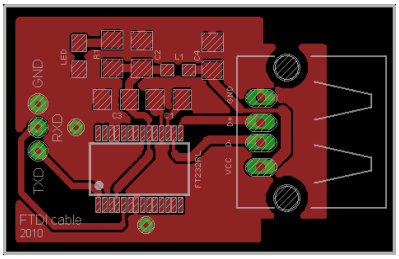

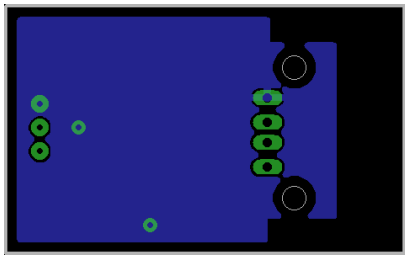

Appendix 4: External interrupt ISR flowcharts

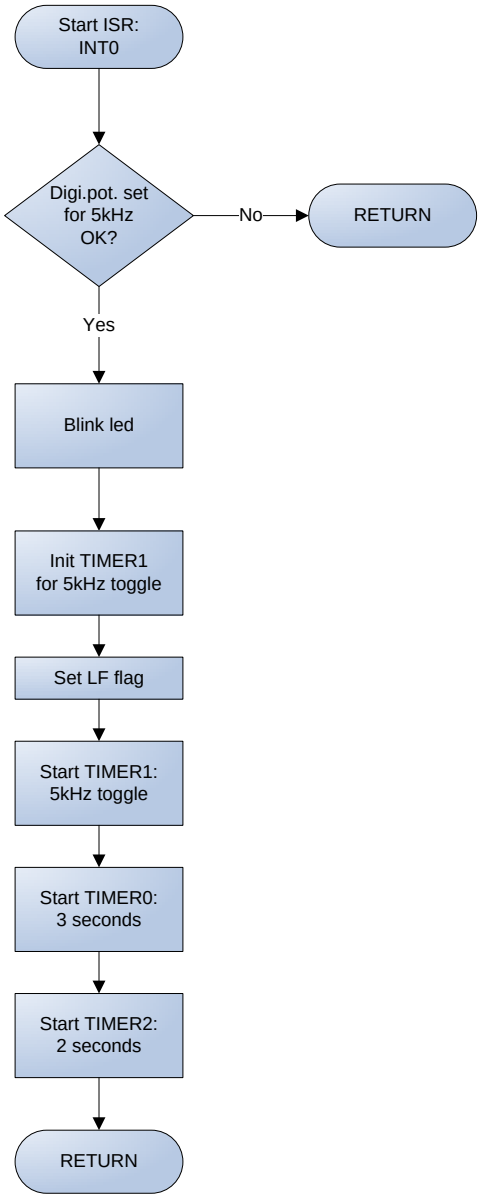

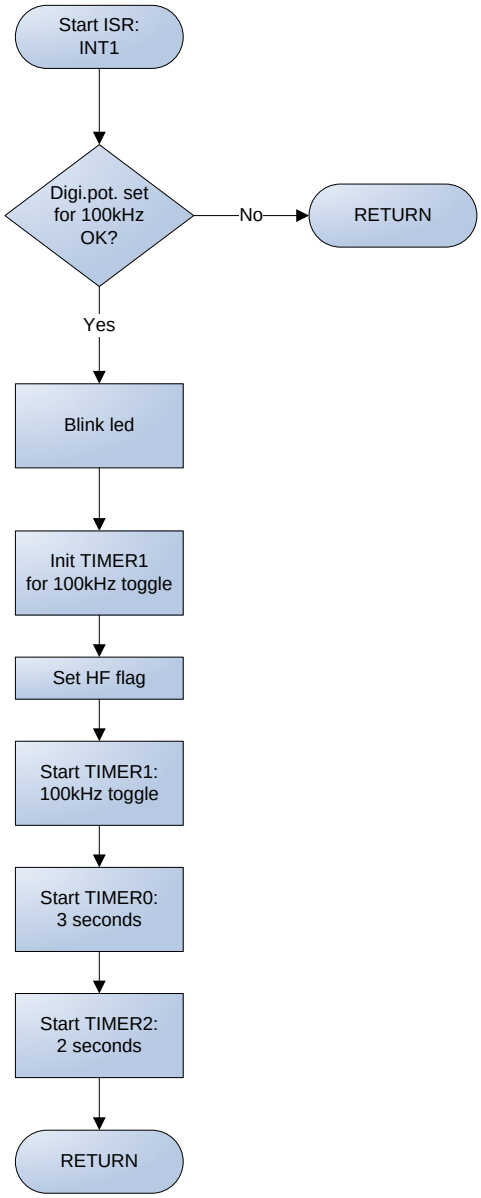

Appendix 5: Timer/counter ISR flowcharts

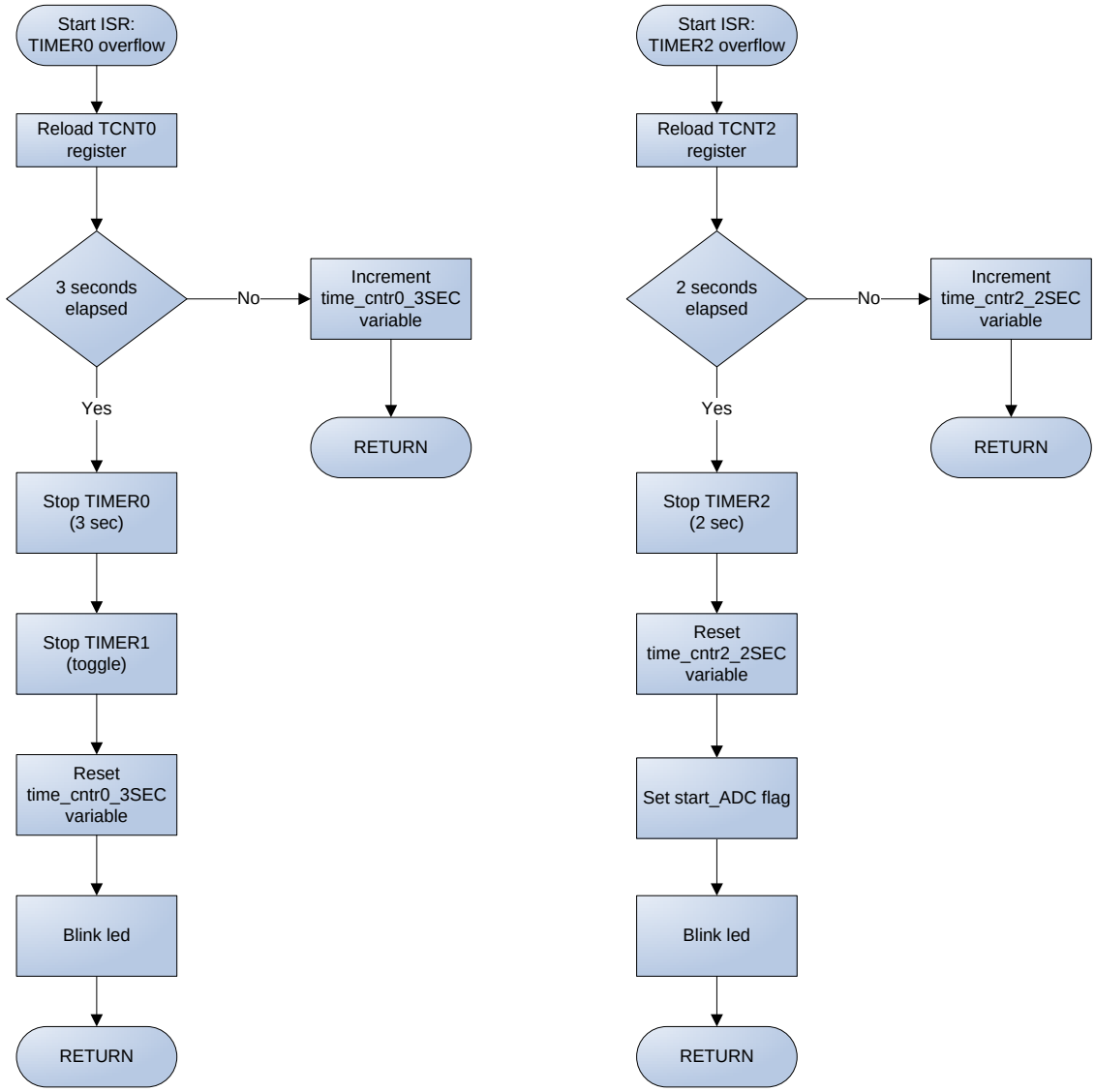

Appendix 6: The flowchart of the main function